Safety in Mines Research Advisory Committee

Final Project Report

Understanding and determining the variability of the primitive stress environment

E.J. Sellers, S.J. Coetzer, R. Kamstra

Research agency	:	Rock Engineering Programme, CSIR Division of Mining Technology
Project No	:	GAP 707
Date	:	March 2002 (Revised October 2002)
Report No	:	2002-0178

Executive summary

The primitive stress state is an important input into the design of underground excavations. However, it is well known that the stress state varies considerably from place to place. The aim of this project was to determine the main causes of the variability to be able to understand how to consider the stress state in the context of designing safer mine excavations. Furthering the *understanding* of stress variability was addressed in a review of the literature on the stress state in South Africa and its application in mine design. Descriptive summaries of the stress state in the gold and platinum mines were also provided.

A literature survey of the causes of the initial stress state and the effects that various geological structures have on the distribution of stresses is also presented. The review showed that the tectonic history is the main influence on the primitive stress state. A number of figures are presented to illustrate the effect of typical geological structures. Folds and surface topography cause rotations of the stress state. Faulting causes the major stress state to rotate towards being parallel to the fault surface. Dykes can act like faults if the contact is sheared, but may also contain residual stresses that are significantly different to the surrounding stresses. Thus, the stress state varies continuously and a single measurement cannot be considered to be representative of the complete primitive stress state within a mine or mining region.

The problem of *quantifying* the variability was addressed by firstly re-evaluating the stress measurement database provided in SIMRAC project GAP 511 to determine statistical trends and variation between the major mining regions. Methods are presented for the correct determination of the average and standard deviation of a number of stress tensors. On average, the stress measurements taken within a mining region are relatively consistent. The stress state associated with the Bushveld Igneous complex is more difficult to average as the stresses are aligned relative to the curve of the outcrop. In this case, the averages must be determined over a smaller region where the outcrop direction is more or less constant.

Improvements were made to the SIMRAC three-borehole technique. A new measuring device was developed that could measure more diameters and so provide redundant readings for the least squares estimate of the stress state and uses a set of 16 linear voltage differential transducers to obtain eight diametric regions. A statistical method was

used to determine the stress state using combinations of the eight borehole diameters and to identify errors in the measurements. Underground testing proved that the drilling technique was practical as long as the drill was set up accurately. Testing was undertaken at sites on Western Platinum Mine, Impala Platinum Mine and Tau Tona Mine. The measuring device was shown to be able to measure the borehole deformation to micron accuracy in underground tests. The measurements that appeared to be successful underground were analysed and found to contain significant deviations in the diametric changes, possibly due to the locator hitting the measuring device. Unfortunately, the testing of the measurement technique had already been considerably delayed by difficulties with the underground sites and further measurements could not be obtained within the remaining project duration.

The three-hole method was found to be highly sensitive to variations in the borehole diameter. The method is not very sensitive to changes in the stress component aligned parallel to the line connecting the centres of the three holes. The method will not be economic in lower stress regions where the CSIR and CSIRO strain cells operate well and only require a single hole for a full three dimensional stress tensor. The benefit of the method would be that only the measuring device needs to be purchased and can be used many times, whereas the strain cells are discarded after use. The three borehole technique as developed does appear to be a step towards a device that is able to make stress measurements in highly stressed ground where strain cells cannot be used due to discing of the overcore. More testing is needed and some modifications to the locator may be required. Other methods must be considered as drilling the third hole has a very small effect on the first hole and so minute deformation must be measured. The ultimate goal should be to develop an indirect measurement technique that can determine the stress field over a wide area easily and economically.

The stress state surrounding the Modderlaag thrust fault on the Western Platinum Mine was measured using CSIR strain cells from six boreholes varying in distance up to 50 m from the fault intersections. The stress state appears to be most affected by the subsequent tectonic activity and the major principal stresses are aligned in an East-West direction, sub-parallel to the outcrop of the Bushveld Igneous complex, and perpendicular to the approximately North- South trending dyke sets. Numerous attempts to measure the stresses in and near the Speckled Dyke on Tau Tona mine were hampered by quartz veins and the faulted nature of the dyke. The single reliable stress measurement indicated that the principal stress was consistent with the activation of the dyke contact as a normal fault. The three-borehole drilling technique was successfully tested at the site, but no stress measurements could be made within the project duration due to delays in drilling.

Finally, *dealing* with the variable stress distribution is the most important task from the point of view of the rock engineer. Ten measurements per borehole is the optimum number of measurements to obtain a statistically meaningful average stress. Thirty to fifty average stress tensors would be required to determine a stress field. These numbers of tests would be uneconomical for most mines. However, analysis of the stress database suggests that the stress state does have a representative mean value within a similar tectonic environment or geotechnical region. Thus, the number of measurements required to determine an average stress state would depend on the geological variability of the mine and where the mine is located in relation to the Bushveld Complex or Witwatersrand basin, the presence of large structural events such as thrust blocks, the Pilanesburg, and the relationship to dykes and faults.

The basis of a design methodology is presented that permits the formal application of variable *in situ* stress conditions in rock engineering designs within the context of risk based design procedures. The methodology describes the selection of the appropriate input data for application in analytical design formulas or numerical models to determine the probability distribution of the failure criterion as a function of the variable stress state. A simple example is given to illustrate the technique. The application of probabilistic design methods is becoming more popular, but consideration still needs to be given to selection of the appropriate confidence levels and to determine what level of risk is acceptable.

Acknowledgements

The authors gratefully acknowledge funding from SIMRAC. Mr Alan Day of Western Platinum Mine contributed considerably to the success of this project with his support, provision of a site and assistance with drilling costs. We would also like to thank Mr Greg More O'Ferrall for his help in facilitating the underground work on Western Platinum mine. The project team is grateful to Mr Shaun Murphy from Tau Tona Mine and Mr Les Gardner from Impala Platinum Mines who also provided sites for testing. We thank the mining staff of Western Platinum, Impala Platinum and Tau Tona mines for their assistance and for having to work around our drilling machines for extended lengths of time. The hard work, long hours and precision drilling provided by the various drilling crews is also appreciated.

List of contracted Enabling Outputs

NO.	ENABLING OUTPUT	MILE -STONE DATE (MM/YYYY)	MAN DAYS	TOTAL OUTPUT cost (R000's ex VAT)
1	Investigation of factors that influence in situ stress conditions near geological features and software that demonstrates the implications for mining	10/2000	32	75
2	Suggestions for establishment of the stress environment in a given area	10/2000	17	55
3	Stress measurements in up to two typical stress environments	12/2000	191	626
3.1	Modify stress measurement device			
3.2	Stress state within and near a dyke			
3.3	Stress state surrounding a normal fault			
4	Report containing updates for stress database.	01/2001	32	112

Table of contents

Page

Executive summary 2

Acknowledgements 5

List of contracted Enabling Outputs 6

List of Figures 9

List of Tables 14

1 INTRODUCTION 15

2 SA STRESS STATE AND EFFECT ON MINING 18

2.1 Importance of the *in situ* stress state 18

2.2 State of stress in the Witwatersrand basin 24

2.3 State of stress in Platinum Mines 28

3 EFFECT OF GEOLOGICAL PROCESSES ON THE VARIABILITY OF THE STRESS STATE 32

3.1 Causes of initial stress state 32

3.2 Effect of layering on stress state 35

3.3 Effect of surface topology on stress state 38

3.4 Effect of Folding on stress state 39

3.5 Effect of Faults on stress state 41

3.5.1 Theoretical studies of the change in stress state due to fault formation 41

3.5.2 Measurements of the change in stress state due to fault formation 49

3.6 Effect of Dykes on stress state 54

3.6.1 Theoretical studies of the change in stress state due to dyke formation 54

3.6.2 Measurements of the change in stress state due to dyke formation 61

3.7 Effect of Jointing on stress state 63

4 VARIABILITY OF STRESS STATE 66

4.1 Statistical description of the variability of the stress state 66

4.2 Quantification of the variability of the stress state in South Africa 74

5 THREE-BOREHOLE STRESS MEASUREMENT TECHNIQUE 78

5.1 Development of new drilling and measuring techniques 78

5.2 Underground testing and evaluation 83

6 CASE STUDIES OF STRESS VARIABILTY 91
6.1 Stress state near a fault 91
6.1.1 Site description 91
6.1.2 Analysis of results 93
6.2 Stress state near a dyke 96
6.2.1 Site description 96
6.2.2 Results 98
7 CONTROLLING FACTORS, DENSITY AND METHODOLOGY 101
8 CONCLUSIONS 109
References 113
Appendix A 121
Rock test results 121

List of Figures

Page

Figure 2.1.1 Schematic of decrease in stress level as the size of the region activated by the stress measurement technique or excavation increases (Hyett et al., 1986) ... 19

Figure 2.1.2 Graphs of the effect of depth on a) moment and b) magnitude from a DIGS models with k= 0.5 (27/54 MPa), a span of 200 m and a pillar width of 20 m. The contours of maximum expected moment are shown for k-ratios of c) 0.5 d) 1.0 and e) 2.0 for a stope with dip of 15 degrees, and discontinuity angle of 75 degrees (Dede and Handley, 1997). ... 21

Figure 2.1.3 Sensitivity of estimated seismic magnitudes to the ratio of horizontal to vertical stress k (after Ryder, 1988) ... 22

Figure 2.1.4 Schematic of the position of damage due to strain bursting when developing through a dyke (Adams and Geyser, 1999) ... 23

Figure 2.1.5 Numerical predictions of fracture patterns surrounding a stope when the principal stress plunges 60^{o} towards the East (Sellers et al. 1987) ... 23

Figure 2.2.1 Variation of major and minor k-ratios with depth below surface for some South African gold mines from data reported by Stacey and Wesseloo (1998) ... 27

Figure 2.2.2 Relationships between major (kH) and minor (kh) k-ratios for some South African gold mines from data reported by Stacey and Wesseloo (1998) ... 27

Figure 2.3.1 Variation of major and minor k-ratios with depth below surface for some South African platinum mines from data reported by Stacey and Wesseloo (1998) ... 29

Figure 2.3.2 Relationships between major (kH) and minor (kh) k-ratios for some South African gold mines from data reported by Stacey and Wesseloo (1998) ... 29

Figure 2.3.3 Variation of principal horizontal stress directions for some South African platinum mines a) from GAP 511 (Stacey and Wesseloo, 1998) and b) data collected in GAP 511 with the data measured at Western Platinum added ... 30

Figure 3.2.1 Variation in Young's modulus with confinement for two types of quartzite (Briggs, 1982) ... 37

Figure 3.3.1 Principal stresses showing a) directions and b) magnitudes in cross section of river valley (Guangyu et al. 1986) ... 38

Figure 3.3.2 Measured stress state in a mountainside (Guangyu et al. 1986) 39
Figure 3.4.1 Evolution of folding (Seilei et al, 1997) 40
Figure 3.4.2 Rotation of stress field near fold axis (Charlsson and Christianson, 1986) 40
Figure 3.5.1 Stress states at onset of faulting (after Seilei et al 1997)a) normal faulting, b) reverse faulting and c) thrust faulting 42
Figure 3.5.2 Fault formation due to various geological processes. a) gravitational sliding, b) bending of crust c) creep flow at depth d) lateral extrusion of sub strata e) rising dome f) and g) extension of ductile base h) subsiding basement i) offset along strike slip fault and j) block faulting in plan in extension environment 44
Figure 3.5.3 Major compressive principal stress trajectories due to the formation of faults by extension of a uniform layer of strain softening material (Witlox, 1986) 45
Figure 3.5.4 Finite element model of the development of a graben by application of strain with increasing magnitude and extent to the base of a layer of strain softening material (Mandl, 1988) a) model, b) $\sigma 1$ trajectories inside graben 46
Figure 3.5.5 Alteration of the distribution of plastic strain and the major principal stresses as a result of a reverse fault (Mandl, 1988) 46
Figure 3.5.6 Schematic diagram of secondary fault forming as compression forces the strata to conform to a pre-existing fault plane (Mandl, 1988) 47
Figure 3.5.7 Rotation of stress state due to fault with friction angle of 3^{o} in horizontal plane with k-ratio of 1.25 (Su and Stephannson, 1999)............ 47
Figure 3.5.8 a) stress difference as a function of friction angle on the fault and b) effect angle between the fault and the major principal stress on the stress difference across the fault. (Su and Stephannson, 1999)............... 48
Figure 3.5.9 Stress state due to a steeply dipping normal fault with slip of 10 m over 3000 m 49
Figure 3.5.10 Changes of stress due to presence of faults (Sugawara et al, 1997)........ 50
Figure 3.5.11 a) fault lines and b) horizontal stresses in Japan (Sugawara et al 1997) 51
Figure 3.5.12 Changes in a) stress direction and b) magnitude across a fault (Martna and Hansen, 1986).. 52
Figure 3.5.13 Directions of faults and principal stresses in Klerksdorp district (after Gay et al, 1984)... 52

Figure 3.5.14 a) Measurements sites in the Carletonville area b) lower hemisphere stereo plot of the stress states on either site of the Elf fault and c) schematic of two-dimensional section through the fault (after Handley, 1987) ... 53
Figure 3.6.1 Schematic of the estimated changes with time of thermal induced stresses in and near a dyke (Gay, 1979). (Initial temperatures are 300^{o}C in quartzite and 1100^{o}C in dyke, stress magnitudes given in bold type) ... 55
Figure 3.6.2 Observed and theoretical profiles of dykes plotted as normalized width and normalized distance along the fault (Peacock and Marrett, 2000) ... 56
Figure 3.6.3 Geometry of a plane strain hydrofracture (Papanastasiou, 2000) simulating a dyke intrusion process ... 57
Figure 3.6.4 Effect of a dyke on the horizontal stress state (Sengupta et al., 1997) ... 59
Figure 3.6.5 Influence of a) k-ratio and b) strike direction on rotation of horizontal stress due to emplacement (Sengupta et al, 1997) ... 60
Figure 3.6.6 Stress state due to a steeply dipping dyke with a forced opening of 10 m ... 60
Figure 3.6.7 Directions of dykes and principal stresses in the Klerksdorp district (after Gay et al, 1984) ... 61
Figure 3.6.8 (a) Dykes associated with Pilanesburg igneous event (Trusswell, 1980) and (b) dyke directions in four major mining regions (McCarthy et al, 1999). ... 62
Figure 3.6.9 Stress state measured around an intrusive orebody (Leijon, 1986) ... 62
Figure 3.6.10 The stress state measured within and nearby a dyke on Durban Deep Gold Mine (Coetzer, 1982) ... 63
Figure 3.7.1 Stress states measured by different techniques in a jointed block loaded in situ (Brown et al, 1986) ... 64
Figure 3.7.2 Stress states predicted by finite element analysis for a jointed block loaded in situ (Brown et al, 1986). a) discontinuous model and b) continuous model with varying elastic moduli ... 65
Figure 4.1.1 Schematic diagram to illustrate the concept of performing a number of tests to produce an average stress tensor at each site ... 66
Figure 4.1.2 Variability of the stress magnitude with number of tests (Leijon, 1986) ... 69
Figure 4.1.3 Variability of the stress direction with number of tests (Leijon, 1986) ... 69

Figure 4.1.4 Result of finite element model of tectonic extension followed by erosion. The localised plastic zones represent faults 71
Figure 4.1.5 Result of finite element model of tectonic extension followed by erosion showing rotation of the stress state near the faults 71
Figure 4.1.6 Result of finite element model of tectonic extension followed by erosion showing histograms of the plunge of the principal stress 72
Figure 4.1.7 The distribution of k-ratios before and after erosion event in finite element model of tectonic extension followed by erosion 72
Figure 4.1.8 Schematic of plan of shaft geological structure showing sequence of structural events applied in the DIGS model.. 73
Figure 4.1.9 Results of DIGS model indicating the variability of the stress state induced by geological features over the extent of a single shaft............... 74
Figure 4.2.1 Variability of the major k-ratio for different regions in South Africa 76
Figure 4.2.2 Variability of the minor k-ratio for different regions in South Africa 76
Figure 4.2.3 Variability of the bearing of the major principal horizontal stress for different mining regions in South Africa. Angle represents the angle of the stress clockwise from North.. 77
Figure 5.1.1 Locator developed for the diamond drilling method 79
Figure 5.1.2 Laser measuring system 80
Figure 5.1.3 Schematic of new LVDT based measuring system................................. 80
Figure 5.1.4 Photograph of the LVDTs assembled in pairs to measure diameters 81
Figure 5.1.5 Photograph of the disassembled LVDT assembly showing the inner and outer tubes 81
Figure 5.1.6 Photograph of the relay unit 82
Figure 5.1.7 Photograph of the data acquisition unit 83
Figure 5.2.1 Schematic of three-borehole technique with measuring device and cut-away locator 84
Figure 5.2.2 Photograph of site at Western Platinum Mine 85
Figure 5.2.3 Photograph of locator and measuring device 85
Figure 5.2.4 Photograph of data acquisition system underground............................... 86
Figure 5.2.5 Photograph of drilling of third borehole past the measuring device during testing at Impala Platinum mine... 88
Figure 5.2.6 Data acquisition system in use on the site at Impala platinum mine 88
Figure 5.2.7 Schematic of three borehole technique showing how the locator was diverted by a joint aligned sub – parallel to the third borehole causing the locator to rotate and hit the measuring device (not to scale).............. 89

Figure 5.2.8 Diameter deformation measurements for test 2 at Impala platinum mine ... 89
Figure 5.2.9 Diameter deformation measurements for test 3 at Impala platinum mine ... 90
Figure 6.1.1 Plan of the site near a fault at Western Platinum Mine ... 91
Figure 6.1.2 Photograph of the shear zone and the layer of pink Mottled Anorthosite. ... 92
Figure 6.1.3 Photograph of borehole breakout in the vicinity of the tunnel ... 93
Figure 6.1.4 Perspective view of principal stresses near Modderlaag shear ... 95
Figure 6.1.5 Vertical view of principal stresses relative to the Modderlaag shear ... 95
Figure 6.1.6 Plan view of the site showing the direction of the most compressive horizontal principal stresses (thick lines) relative to the boreholes (marked by a dot at the collar and a thin line), the shear plane intersection (dotted line) and haulage (thin rectangle) ... 96
Figure 6.2.1 Plan of the site on 83 Level at Tau Tona ... 97
Figure 6.2.2 Visualization of the stress state measured at Tau Tona Mine looking west ... 99
Figure 6.2.3 Visualization of the stress state measured at Tau Tona Mine in plan, looking down ... 100
Figure 6.2.4 Visualization of the stress state measured at Tau Tona Mine looking South-West ... 100
Figure 7.1.1 Flowchart of methodology for stress measurement programme ... 107
Figure 7.1.2 Flowchart of methodology for risk based design methodology incorporating variability of the stress state ... 108

List of Tables

Page

Table 3.2.1 Ratio of horizontal to vertical stress k in an isotropic elastic material for a range of Poisson's ratios 35

Table 3.5.1 Stress states and k-ratios in Klerksdorp mines (Gay et al, 1984). 52

Table 3.6.1 Thermal penetration distance with time for quartzite based on Muller and Pollard (1986) and diffusivity $k=2.5x10^{-6}$ (Tucker, 1968) 59

Table 4.2.1 Mean and standard deviation of major k-ratio, minor k-ratio and bearing of different regions in South Africa 75

Table 5.2.1 Diametric deformations measured at Western Platinum 84

Table 5.2.2 Activity log for tests at Impala Platinum Mine 87

Table 5.2.3 Diametric deformations measured at Impala Platinum in test 2 90

Table 5.2.4 Diametric deformations measured at Impala Platinum in test 3. 90

Table 6.1.1 Stress state near Modderlaag shear in West, South Down coordinate system 94

Table 6.1.2 Principal stress state near Modderlaag shear. Bearing is clockwise in degrees from North and dip is in degrees and positive down from horizontal. An asterisk denotes a dubious reading 94

Table 6.2.1 Stress state measured in the Speckled dyke on Tau Tona Mine in West, South Down coordinate system 99

Table 6.2.2 Principal stress state in Speckled dyke on Tau Tona Mine 99

Table 7.1.1 Confidence coefficients for normal distribution (Harr, 1987) 103

Table 7.1.2 Values of means and standard deviation of k-ratio and unconfined strength assumed for the minor k-ratio and UCS in the example 105

Table 7.1.3 Calculation of Point estimates for example 105

Table 7.1.4 Expected values and variance for the RCF in the example 105

Table 7.1.5 Calculated probabilities of failure. 106

1 INTRODUCTION

In situ stress is one of the most important and least well defined parameters for input into mine design. All numerical models rely on an input of the overall stress state and any conclusions regarding the safety of a particular mine-layout will be dependent on the stress state. Evaluation criteria such as ERR and ESS that are used to estimate the seismic hazard depend strongly on the initial stress state. Newer numerical models that include non-linear effects such as rock fracture, failure and time dependency will be even more influenced by the primitive stress state. A preliminary study of the implications of the selection of the initial stress state on the results of numerical models was completed as part of GAP 029. The studies showed that the horizontal stresses are dissimilar due to historical tectonic activity and that faults can rotate the major stress direction from the vertical. Modelling of rock fracture processes in GAP 332 has shown that the geology and initial stress state can alter the fracture zone. For example, mining in the direction of the plunge of the principal stress can lead to flat fractures in the hangingwall and the formation of large blocks that are difficult to identify and support. These blocks are a potential rock fall hazard.

However, the stress state is difficult and costly to determine with current technology. SIMRAC have supported a number of studies to consider stress measurement techniques for application in deep mines. GAP 220 reported on the different techniques and suggested the application of the three-borehole method that was later developed as part of GAP 314. A database was built up from measurements on South African Mines as part of GAP 511 and indicated that there is a great need for more information about the stress state.

This project aimed to synthesize the current knowledge on the variability of the stress state into a document that will be useful for rock engineers to determine if the stress state at a particular site needs to be investigated further, how many measurements would be required and to consider assumptions that may be needed for numerical modelling of mining sequences. This was to be achieved with a revised look at the available data to characterize the variations in stress state surrounding geological structures. The SIMRAC three-borehole stress measurement technique, developed as part of GAP 314, needed to be improved to become robust and able to be applied regularly underground. The project would then focus on evaluating the viability of the new technique for undertaking stress measurements in difficult conditions. The spatial variation in stress would then be considered by performing stress measurements in and near a dyke, and near a fault. The use of the three-borehole method should allow many measurements to be undertaken in a single hole, but needed to be compared with conventional stress measurement techniques.

The focus of the project altered slightly as the work progressed. The use of percussion drilling in the original design for the three-borehole method meant that the drilling could be performed economically by non-specialised drill crews with standard equipment. However, the measurement accuracy required for the stresses in hard rock implied that damage to the rock surrounding the borehole led to overestimates of the deformation. It was decided to prove the technique using diamond drilling. A new measuring device was required that could measure more diameters and so provide redundant readings for the least squares estimate of the stress state. In addition, there were too few measurements in South Africa that could provide a good understanding of the way that the stress changed near geological features. Delays on site and the manufacture of the new instrument meant that fewer measurements were performed at the two sites than anticipated.

The project work was therefore refocused on three main issues for the rock engineer with regard to the variability of the *in situ* stress state. Firstly, the project was to provide an *understanding* of the importance of the stress state and relationship between various geological features and the observed variability. Secondly, the problem of *quantifying* the variability needed to be addressed. Finally, *dealing* with the variable stress distribution is the most important task from the point of view of the rock engineer.

Furthering the *understanding* is addressed in the first section of the report by reviewing the literature on the stress state in South Africa and its application in mine design. The section discusses the effect of the *in situ* stress state on mine excavations and numerical models. Subsequently, descriptive summaries of the stress state in the gold and platinum mines are given. The background to understanding of variability in the stress state is then revealed by a literature survey of the causes of the initial stress state and the effects that various geological structures have on the distribution of stresses. Theoretical studies are compared with published observations and measurements.

The problem of *quantifying* the variability is addressed by firstly re-evaluating the stress measurement database to determine statistical trends and variation between the major mining regions. Secondly, improvements were made to the SIMRAC three-borehole technique and these are described along with the results of underground testing. Thirdly, as the stress measurement database is focused on the virgin stress conditions away from the disturbance by geological features, stress measurements were undertaken at two sites where the effect of the geological structures could be measured directly. The stress state surrounding the Modderlaag thrust fault on the Western Platinum Mine is discussed and attempts were made to measure the stresses in and near the Speckled Dyke on Tau Tona mine.

Finally, *dealing* with the variability implies the need to incorporate statistical distributions into standard design procedures. In the final section, comments are made regarding the required number of stress measurements on a mine and a methodology is presented that permits the formal application of variable *in situ* stress conditions in rock engineering designs within the context of risk based design procedures.

2 SA STRESS STATE AND EFFECT ON MINING

2.1 Importance of the *in situ* stress state

The safety of mining activities is influenced significantly by the *in situ* stress fields. The changes in the initial stress state, because of mining activities, lead to extensive fracturing around excavations, and may cause slip events on potentially active faults. Important factors in the design of mining excavations include the pre-mining state of stress, the strength and elastic properties of the individual rock types, the relative differences in competence between the strata, the degree of stratification, and the occurrence of faults, joints, dykes, and sills (Gay and Jager, 1986). The principal stresses are known to control the orientation of fracturing and, hence, the rock mass conditions will depend on the relative directions of mining and associated stresses (Sellers *et al*, 1997). In addition, boxhole and orepass stability conditions are influenced by the *in situ* stresses. Stress variations can have a big influence in planning layouts, and an error in layout can cause major financial loss. A detailed knowledge of the magnitude and direction of the *in situ* stress state is, therefore, a crucial factor in the planning of appropriate mine layouts that reduce the potential risk of rockfalls and rockbursts (Durrheim *et al*, 1998). Design procedures have been developed for pillar systems (e.g. York *et al*, 1998, 1999, Joughin *et al*, 2000, Day and Godden, 2000, Martin and Maybee, 2000) that also emphasize the importance of considering the correct *in situ* stress state.

A significant proportion of rockbursts in South African gold mines are associated with geological structures such as faults and dykes. For instance, in the Carletonville district, 40% of mining is found to take place within 20 m of a geological structure and results in 60% of the rockburst activity (Gay, 1986). Similar conclusions can be drawn from the Klerksdorp (More O'Ferrall, 1986) and Orange Free State (Potgieter and Roering, 1984; Ortlepp *et al*., 1986) regions. The prediction of the response of a rockmass to a planned mining excavation can be undertaken using numerical analyses. However, the interpretation of the numerical results should take into account that the rock is subject to an initial stress state. The magnitude of this in-situ stress is to some extent controlled by the gravitational loading of the rock, and also by the geological processes to which the rock has been subjected.

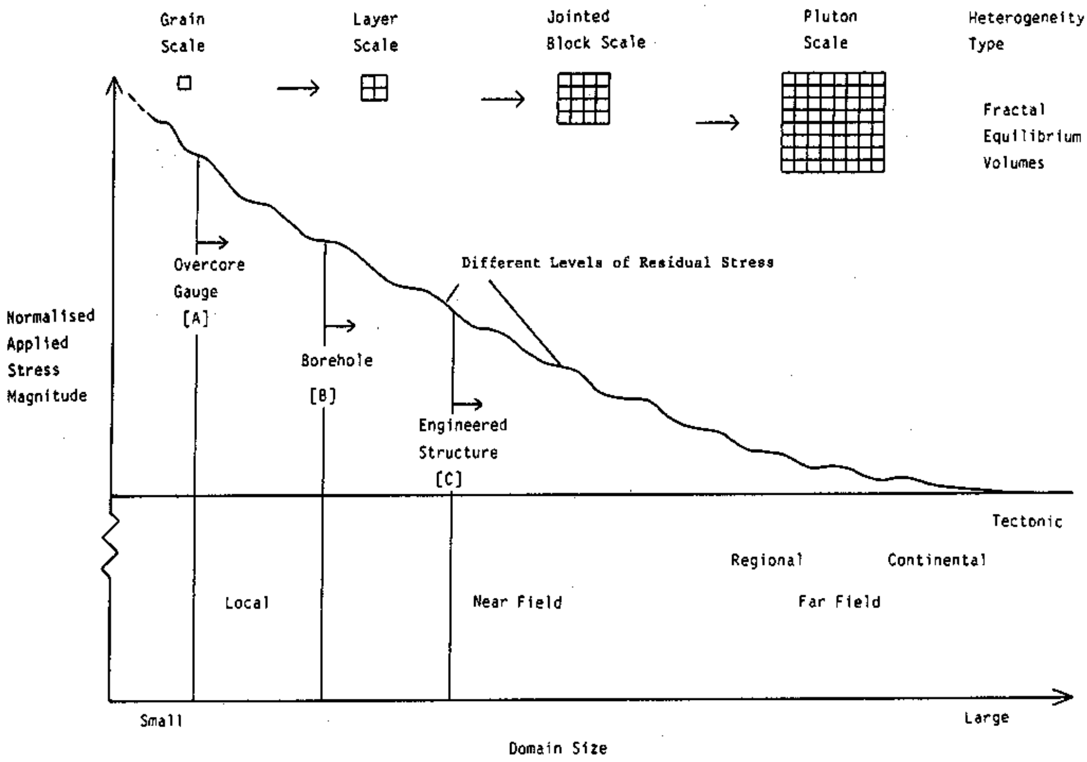

Figure 2.1.1 Schematic of decrease in stress level as the size of the region activated by the stress measurement technique or excavation increases (Hyett et al., 1986)

Tectonic movements, deposition of overlying sediments and volcanic rocks, folding, faulting, dyke intrusion and metamorphism, can all alter the in-situ stress state. However, these changes are difficult to quantify, and consequently, in-situ measurement is the best way of obtaining the stress state at a particular site for numerical analyses (Brady and Brown, 1993). In many cases, direct measurement is not feasible and the in-situ stress state must be estimated. The most commonly used stress state is a uniformly increasing vertical stress proportional to the rock density and then the selection of the horizontal stress as being some fraction of the vertical stress.

The virgin stress ratio (k-ratio) is conventionally obtained when the horizontal virgin stress is divided by the vertical virgin stress. The k-ratio may vary with direction if the horizontal stresses have been disturbed by tectonic action and if the major principal stress is not vertical. In general, the major principal stress in not vertical in South Africa (Gay, 1975) indicating that significant tectonic actions have altered the stress state. In many cases, the ratio of horizontal to vertical stress is selected to be 0.5. The selection of the in-situ state for a numerical analysis can, however, make a significant difference to the results and thus requires careful consideration. For example, measurements of the k-ratio prior to a shaft pillar extraction in a South African mine suggested that the values of k were higher than in regions undisturbed by mining (Smallbone *et al*., 1993). Subsequent numerical analyses identified a need for increased support in the stress state with a higher k ratio.

Dede and Handley (1997) used numerical modelling to consider the theoretical maximum seismic events associated with a mining layout and showed that the *in situ* stress state has a considerable influence on the possible seismic events. The addition of a discontinuity in the form of a fault can increase the maximum event further. The throw on the fault, induced by the previous tectonic events will also alter the event magnitude. Throws of over 100 m can increase the expected moment by orders of magnitude.

The effect of an increase in depth is to increase the vertical stress (Dede and Handley, 1997). As the depth increases, the largest expected seismic moment increases, as shown in Figure 2.1.2a, and therefore the corresponding magnitude increases as shown in Figure 2.1.2b. The influence of excavation geometry in relation to the *in situ* stress state is demonstrated by the increased hazard of the stope with a higher dip. The stability of regional pillars is most affected by the k-ratio. Figure 2.1.2 shows a plot of contours of maximum magnitude for various pillar sizes and mining spans. The low k-ratio of 0.5 (Figure 2.1.2c) has a potential maximum magnitude of 3.6 for the worst case of high spans and small pillar dimensions. When the k-ratio is 1.0 (Figure 2.1.2d), the maximum event magnitude is slightly reduced to 3.0. If the k-ratio is increased to 2.0 (Figure 2.1.2e), the maximum event size is significantly reduced to about 1.0. Thus, the relatively low horizontal stress can lead to an increased seismic hazard, whereas horizontal stresses that are higher than the overburden stress may cause buckling failure of stope hangingwalls. The maximum expected moment would differ, depending on the angle of dip between the fault plane and the stope as shown in Figure 2.1.3 (Ryder, 1988).

Other effects of high stresses would be to increase time dependent closure in stopes (Malan, 1997). In tunnels, squeezing effects become prominent at greater depths (Malan and Basson, 1998). Increased incidents of “dog-earing” and failure in the sidewalls of tunnels could also be expected (e.g. Ortlepp, 1997). Thus, the orientation of tunnels and excavations should be altered to take into account the effect of the initial stress state (Haile and Jager, 1995). The relatively high horizontal stresses observed in Bushveld mines leads to breakout in the roof of tunnels and the tunnels have a characteristic “Gothic Arch” shape (de Maar and Holder, 1994, Haile, Wojno, Jager, 1995).

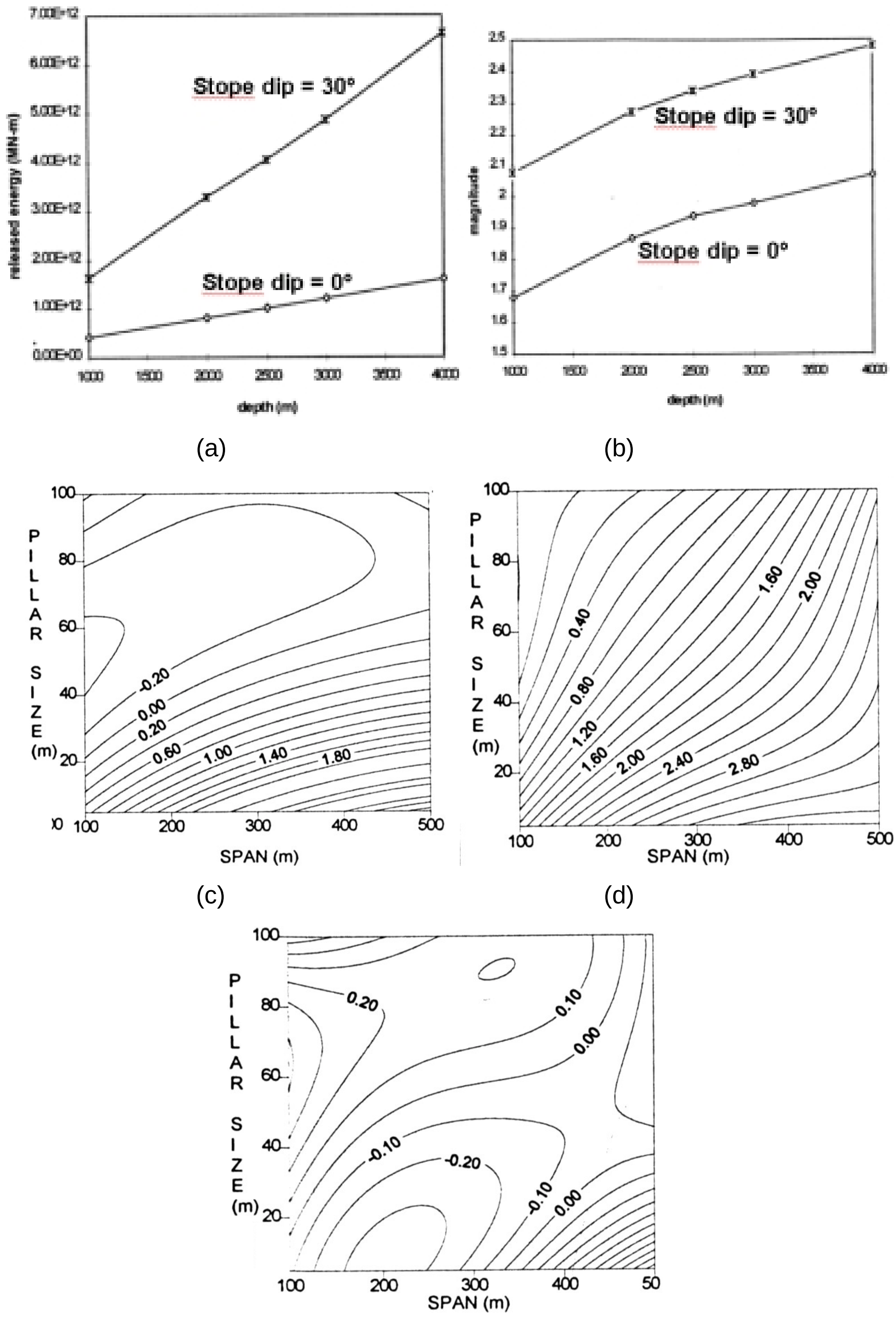

Figure 2.1.2 Graphs of the effect of depth on a) moment and b) magnitude from a DIGS models with k= 0.5 (27/54 MPa), a span of 200 m and a pillar width of 20 m. The contours of maximum expected moment are shown for k-ratios of c) 0.5 d) 1.0 and e) 2.0 for a stope with dip of 15 degrees, and discontinuity angle of 75 degrees (Dede and Handley, 1997).

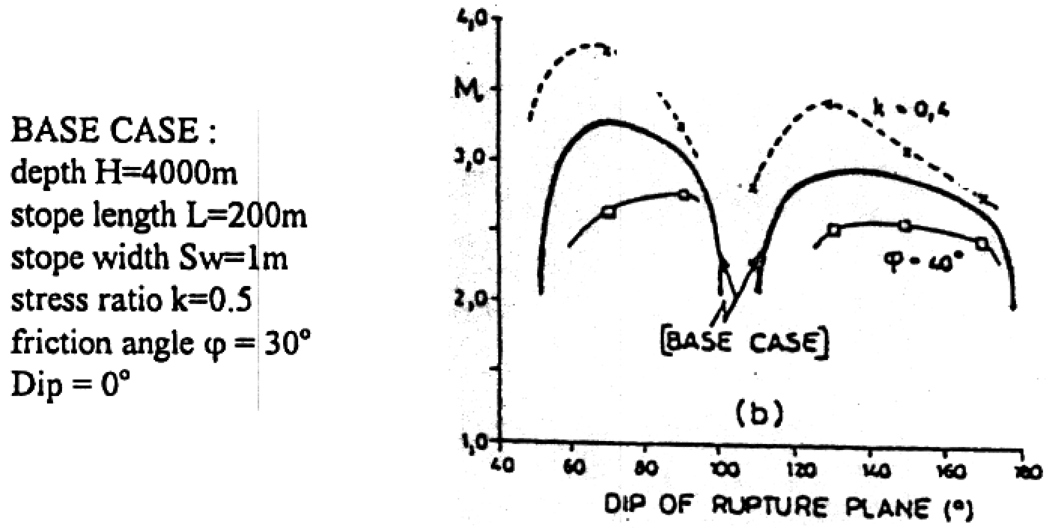

Figure 2.1.3 Sensitivity of estimated seismic magnitudes to the ratio of horizontal to vertical stress k (after Ryder, 1988)

Mining through different rock types will produce different responses in the rock mass as the stress state may be different. De Maar and Holder (1994) noted that Anorthosites experienced more damage than Pyroxenites. Even if the stress state is the same, the weaker rock may fail under a stress state for which the stronger one remains stable. Overstoping of tunnels will cause different extents of fracturing depending on the stress environment. This will affect the tunnel support requirements (Roberts *et al*, 1999). Overstoping will also cause the reduction in vertical clamping stresses on sub horizontal thrust faults e.g. the faults associated with the Merensky reef. Horizontal movements on the faults associated with the reduction in vertical stresses may result in seismic events.

Development through a dyke poses a number of potential hazards (Adams and Geyser, 1999). The dyke formation processes may have resulted in joint sets that are aligned parallel and perpendicular to the trend of the dyke. The dyke may have a strength that is different to that of the surrounding rock. High residual stresses remaining in the dyke may then lead to strain bursting when a tunnel is developed into the dyke material (Figure 2.1.4). In the case study considered by Adams and Geyser (1999), it was suggested that the observed strain bursting occurred because the dyke was weaker than the surrounding rock and contained high residual stresses.

Numerical simulations of the fracturing induced by tabular stopes mining through a jointed rockmass with a non-vertical principal stress were studied by Sellers *et al*. (1987). These studies showed that the fracture directions are altered depending on the relationship of the mining direction to the plunge of the principal stress. Steeper fractures occur when the mining is away from the plunge of the major stress. Flatter fractures are induced when mining with the direction of the principal stress (Figure 2.1.5). These flatter factures would be more likely to produce large flat slabs in the hangingwall that could go unnoticed and result in an increased rockfall hazard.

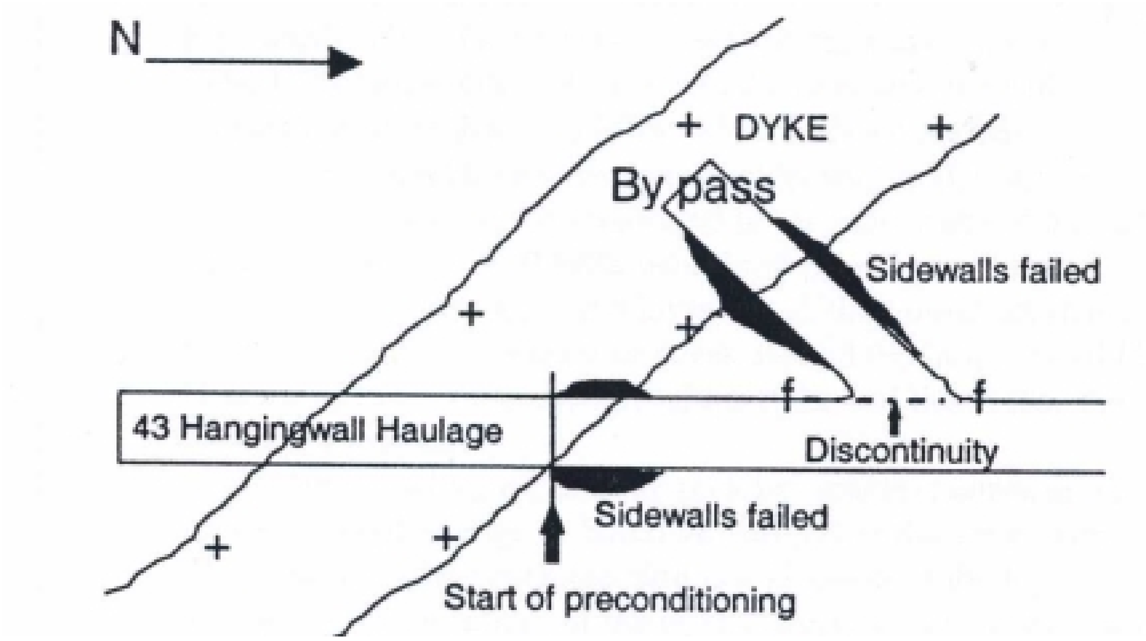

Figure 2.1.4 Schematic of the position of damage due to strain bursting when developing through a dyke (Adams and Geyser, 1999)

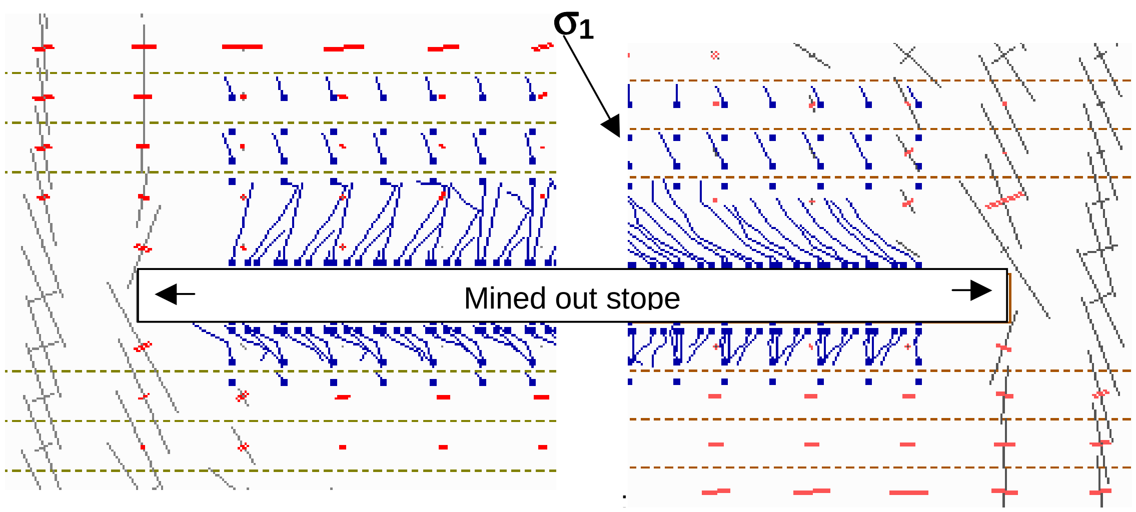

Figure 2.1.5 Numerical predictions of fracture patterns surrounding a stope when the principal stress plunges 60^{o} towards the East (Sellers et al. 1987)

Tunnels and orepasses driven in high stress conditions experience spalling of the sidewalls that cause the excavation width to extend in a direction perpendicular to the maximum compression (Jager and Ryder, 2000).

2.2 State of stress in the Witwatersrand basin

The Witwatersrand basin has been subjected to a complex series of geological processes through the course of time (Truswell, 1970, Tankard *et al*., 1982, amongst others). These will have changed the stress state many times and caused variations between various parts of the basin. Some of these are discussed by McCarthy *et al*, 1989 and summarized by Sellers (1995). The sediments of the Witwatersrand Supergroup were deposited in a basin starting 3000 million years ago. The extent of the basin and amount of deposition has varied with time as shown by the contours of constant sediment thickness of the strata (Truswell, 1970). The long axis of the basin was aligned in a NE-SW direction and migrated towards the NW during the formation processes. The addition of sediments has caused deepening of the basin and led to the formation of a series of faults around the perimeter of the basin.

The stress state in these rocks will have been altered by metamorphism due to burial at pressures of 20 to 60 MPa and temperatures of 250^{o}C (Tankard, 1982) at depths of 10-15 km. Subsequent erosion of 5 to 7 km of overburden may have induced residual stresses. The calculation of the residual stresses depends on the amount of erosion, and the magnitude of subsequent relaxation due to creep, both of which are difficult to determine. The stresses introduced into the crust by the weight of overlying sediments have caused extension faulting in the basement rocks permitting the extrusion of the Ventersdorp lavas (Tankard, 1982). The outpouring of the Ventersdorp lavas contributed to the higher-grade metamorphism, and to the alteration of the rock properties and the in-situ stress state close to the feeder dykes.

The intrusion of the Bushveld Complex caused some dykes to intrude into the Witwatersrand basin and may have altered the in-situ state in the Witwatersrand rocks. The dyke swarms, originating from the Pilanesberg complex, are oriented in a North South direction. The direction of dyke propagation will tend to follow the maximum stress (Muller and Pollard, 1970) and so these dykes provide further evidence that the maximum horizontal principal in-situ stress in the region is oriented in a North - South direction. McCarthy *et al*., 1990 studied dyke directions for four regions of the Witwatersrand basin and inferred that the directions of the principal stresses are consistent over wide areas of the basin. Local alterations of the stress state due to the emplacement of these dykes remain unknown. The intrusion of the Vredefort dome has had a major influence on the Witwatersrand basin, caused overturning and faulting in the southern parts of the basin and will have considerably altered the stress state (McCarthy *et al*., 1989). Further disturbances to the stress state will have been caused by the subsequent tectonic collisions, which led to the formation of the Kaapvaal and Kalahari cratons.

The virgin stress ratio (k-ratio) is defined to be the horizontal virgin stress in a given direction to the vertical virgin stress. This implicitly assumes that the vertical stress is a principal stress direction although this may not be true, particularly in the Witwatersrand basin where a number of, very different, tectonic events have occurred though time. It is believed that this virgin stress ratio tends to decrease with depth, from quite high values (>1) at shallow depths, to relatively low values (<0.5) in the deepest mines. The virgin stress ratio is the most common data required to specify the stresses or stress fields around mine sites and in different geological environments. Schweitzer and Johnson (1997) stated that geological features largely control the deformation mechanisms associated with Witwatersrand orebodies and reviewed the relevance of geotechnical information to mining associated with the Witwatersrand Basin. This information is necessary for the modelling of excavations and the planning of mine-layouts. In addition, a knowledge of the *in situ* stress state is necessary to design appropriate regional support systems, particularly bracket pillars, for different geological environments. In the design of local support systems, the initial stress affects a number of parameters such as the likelihood of seismicity, the magnitude of clamping stresses in the hangingwall and the stress induced fracture patterns. Thus, the *in situ* stress fields in which the mining operations are carried out govern to a large degree the stability of these operations, and hence the safety and mining efficiency.

Gay (1975) and McGarr and Gay (1978) have shown that the maximum principal stresses are generally orientated within 30 degrees of the vertical, and that the intermediate and minimum principal stresses are orientated at less than 30 degrees to the horizontal plane. Gay and Jager (1986) stated that the principal stresses differ in magnitude resulting in shear stresses. Their results show that the magnitude of the shear stress varies for the different regions, being small in the shallow Evander mines and largest in the deep Carletonville and Central Rand mines. Stacey and Wesseloo (1998) suggested that the horizontal principal stresses tend to be aligned approximately in the north-west/south-east or north-east/south-west directions in South Africa. However, the principal horizontal stress orientations in the Klerksdorp area are significantly different from the Carletonville and Free State regions. The stress measurements of Gay, Spencer, Van Wyk and Van der Heever (1984) indicated the presence of relatively large horizontal components of stress acting in a north-west to south-east direction over most of the mining area in the Klerksdorp goldfield. This regional stress acts at approximately right angles to the major fault planes. In addition, they stated that a large horizontal stress anisotropy exists in the region. Thus, inherent deviatoric stresses, capable of causing movement along a fault or dyke exist throughout the region. Relationships between the tectonic activities and the stress states in the basin were reviewed in more detail by Sellers (1995)

Stacey and Wesseloo (1998) considered most of the stress measurements in the Witwatersrand basin and stated that the major horizontal stress values are equal to or greater than the vertical stresses. The k-ratio data are shown in Figure 2.2.1 for some South African gold mines in the Carletonville, Klerksdorp and Free State areas.

Brown and Hoek (1978) present an analysis of the *in situ* stress state worldwide, including data points from Southern Africa, and provide an equation for the k-ratio. They suggest that the k-ratios vary between

$$k = \frac{100}{z} + 0.3 \text{ and } k = \frac{1500}{z} + 0.5 \qquad (2.2.1)$$

where z is the depth below surface.

There is a difference in the k-ratios related to the minor and major horizontal principal stresses. The major and minor k-ratios for stress measurements in some South African Gold mines are shown in Figure 2.2.2. The minor stress ratio, k_3, ranges from about 0.3 to 0.9 and the major k-ratio ranges from 0.5 to 1.7. Thus, an average value of about 0.5 is often assumed. However, the common assumption of an average horizontal to vertical stress ratio of 0.5 is not valid, and a value of 0.9 may be more realistic. It is remarkable that the measurements for the Klerksdorp region are so well correlated, possibly due to the similar tectonic environment.

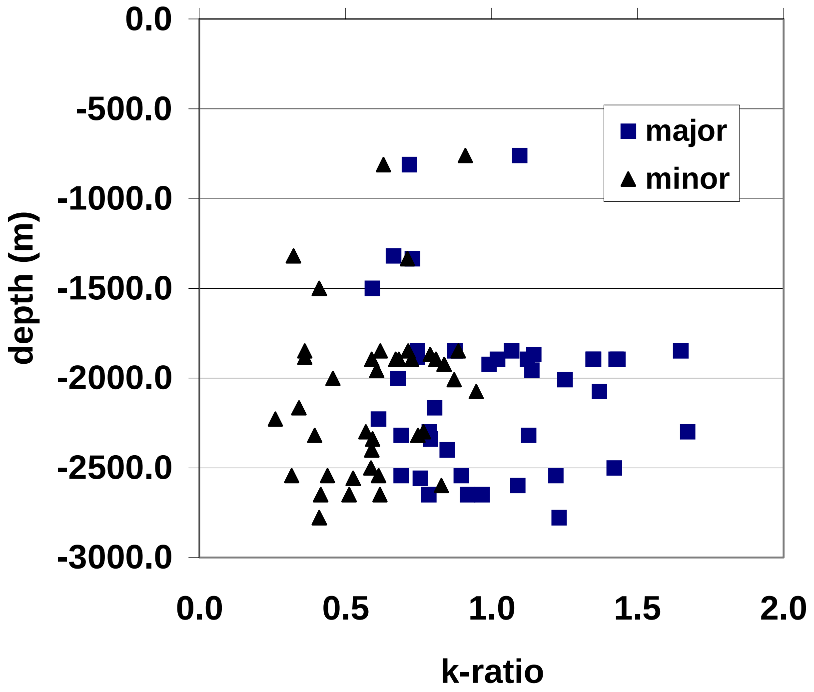

Figure 2.2.1 Variation of major and minor k-ratios with depth below surface for some South African gold mines from data reported by Stacey and Wesseloo (1998)

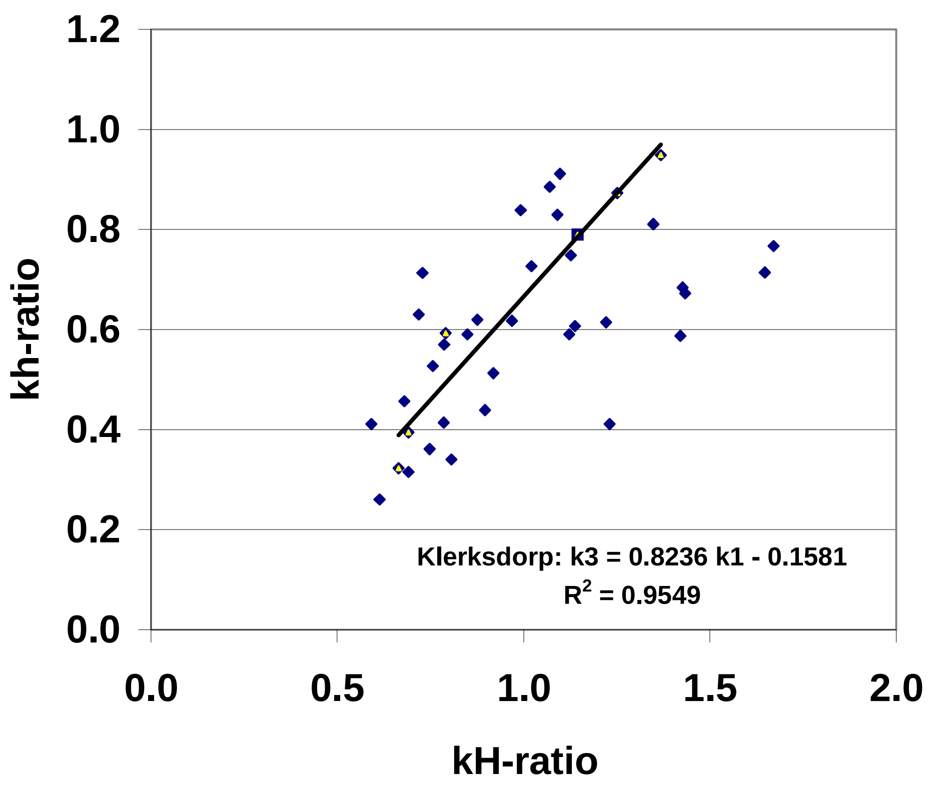

Figure 2.2.2 Relationships between major (kH) and minor (kh) k-ratios for some South African gold mines from data reported by Stacey and Wesseloo (1998)

2.3 State of stress in Platinum Mines

There has been considerable discussion regarding the initiation of the processes of formation of the Bushveld Complex (Vermaak and Van Gruenewalt, 1986, Schweitzer and Berlenbach, 1995). The Bushveld Complex intruded into and extruded onto the sedimentary rock of the upper Transvaal sequence 2061 million years ago. The intrusion was rapid in geological times taking place over 7 million years. The intrusions occurred in an extensional tectonic environment and slumping of the basin due to the weight of lava would have caused the observed flat dipping thrust faults and the division of the succession into a variety of "stress compartments" (Vermaak and Van Gruenewalt, 1986) with different vertical stresses by sub vertical reverse faults (de Maar and Holder, 1994). Granitic domes intruded 2054 million years ago and terminated the Bushveld sequence. These domes would have also had an effect on the stress state, but this has not yet been quantified (Schweitzer and Berlenbach, 1995). Vermaak and Van Gruenewalt (1986) note that the intrusion process can be simulated using fluid dynamic experiments and so the stresses would have initially been determined by the hydrodynamics of the intrusion process and then altered as the melted rock cooled.

The Pilanesburg Alkaline Complex subsequently intruded into the rocks of the Bushveld complex and the resulting dyke swarm was oriented in a North West - South East direction that would have increased the horizontal stresses in the perpendicular direction. Rock layers in the Bushveld sequence would have buckled leading to changes in strike of the layers and further stress variations. Lamprophyre dykes trending in the East-West direction are related to Kimberlite intrusions occurring 1000 to 1500 million years ago. These dykes are possibly associated with high horizontal stresses in the north south direction (de Maar and Holder, 1994).

Figure 2.3.1 shows how the measured k-ratio changes with depth. The data, collated for SIMRAC project GAP 511 (Stacey and Wesseloo, 1998), indicates that the k-ratio tends to decrease with depth. There is a marked difference between the minor and major horizontal stresses. The major horizontal principal stress has been observed to be as high as 7 times the vertical stress. The minor stress varies from about half to about twice the vertical stress. The relationship between the horizontal principal stresses is shown in Figure 2.3.2.

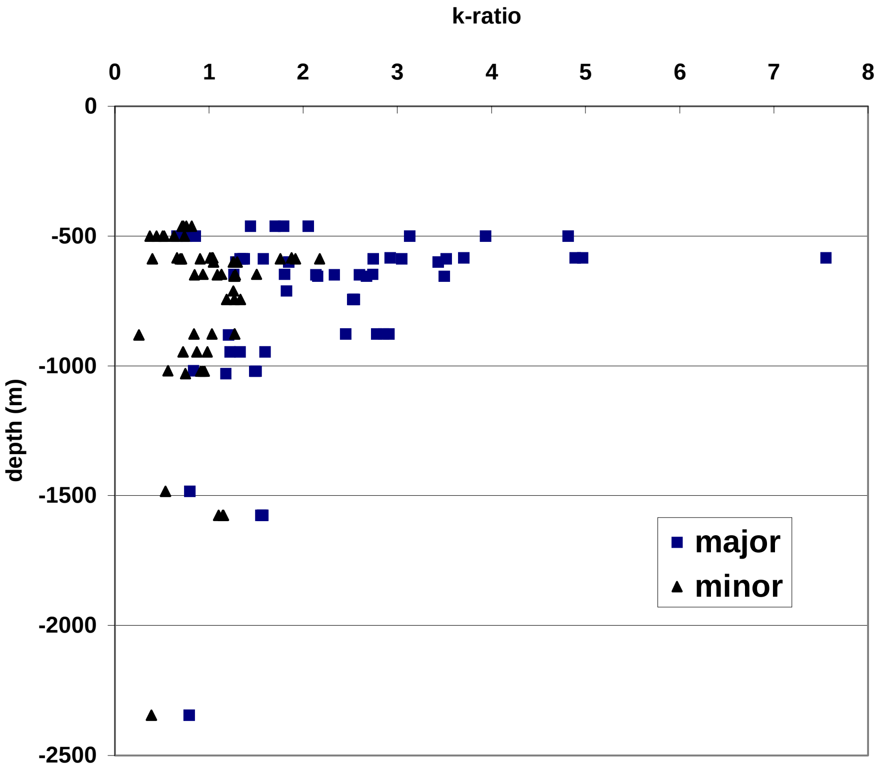

Figure 2.3.1 Variation of major and minor k-ratios with depth below surface for some South African platinum mines from data reported by Stacey and Wesseloo (1998)

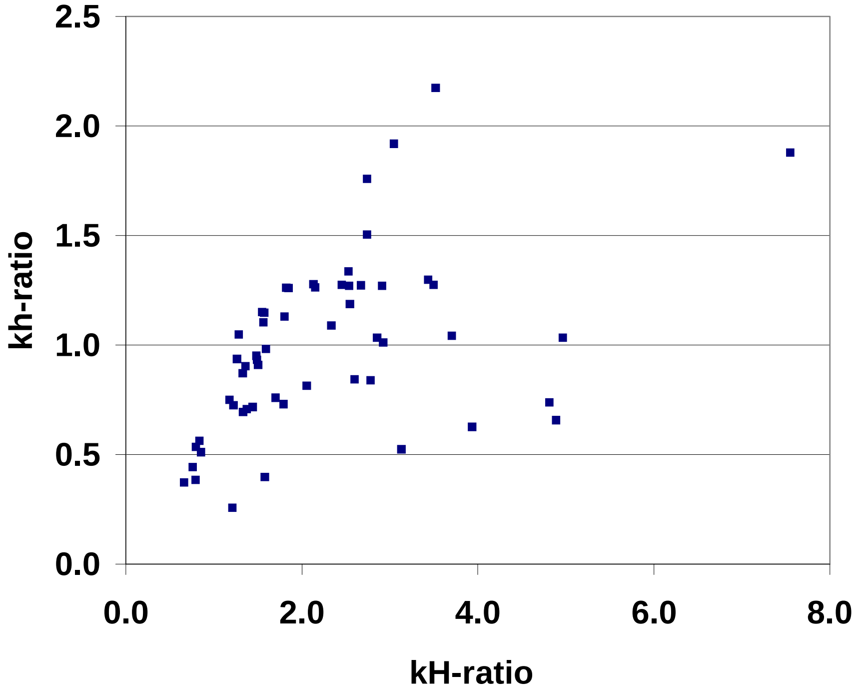

Figure 2.3.2 Relationships between major (kH) and minor (kh) k-ratios for some South African gold mines from data reported by Stacey and Wesseloo (1998)

Figure 2.3.3 shows the principal horizontal stress directions for the measurements compiled in SIMRAC project GAP 511 (Stacey and Wessellloo, 1998). The figure also shows the outcrop of the Merensky reef and indicates that the horizontal stresses tend to be either parallel or perpendicular to the reef outcrop. Thus, the stress state is influenced by the Bushveld complex. The intrusion of the Pilanesburg complex just north of Rustenburg caused dykes to be intruded in a North-South direction, and these probably account for the increased East-West alignment of horizontal stresses near Rustenburg.

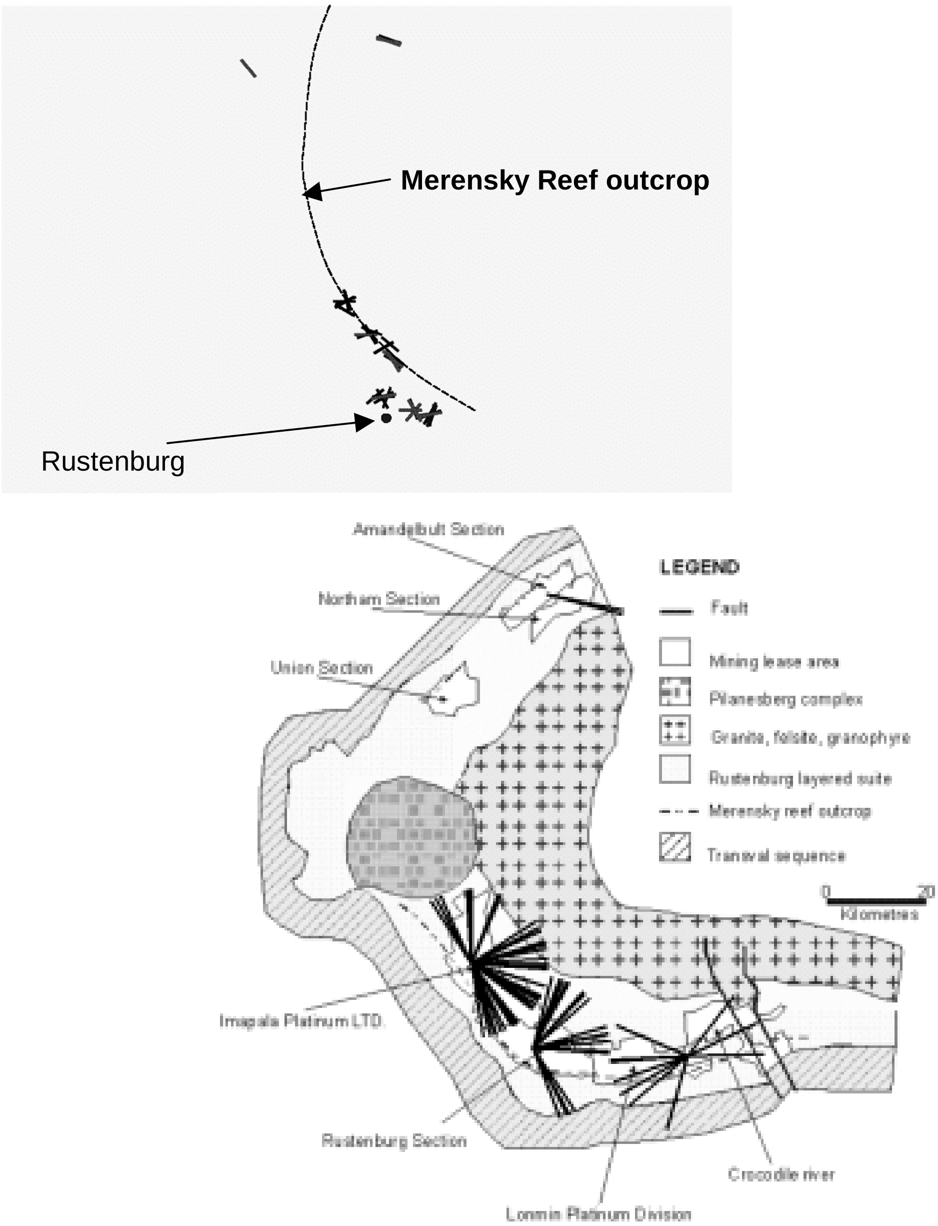

Figure 2.3.3 Variation of principal horizontal stress directions for some South African platinum mines a) from GAP 511 (Stacey and Wesseloo, 1998) and b) data collected in GAP 511 with the data measured at Western Platinum added

The results of a number of stress measurements on Rustenburg Platinum mines are summarized by de Maar and Holder (1994). These measurements and the observations of the rock response were summarized by de Maar and Holder (1994) as follows:

1. off-reef, the stress has a relatively high east-west horizontal component oriented approximately on strike
2. there are large disparities in horizontal stresses off-reef
3. off-reef stresses change due to geological disturbances and between layers
4. potholes affect the stress direction
5. on-reef vertical stresses are higher than the overburden
6. the on-reef k-ratio is 0.65 in contrast to the k-ratio of 1.5 off reef
7. off-reef vertical stresses are less than the overburden weight
8. on-reef, the north-south and east-west components are equal.

The presence of such different stress states is attributed to the variety of geological processes (de Maar and Holder, 1994), but differences in the vertical stress may be due to measurement inaccuracies or to the choice of the *in situ* Young's modulus.

York *et al* (1998) found that high horizontal stresses played a role in causing panel span collapses in Bushveld Complex Mines. The horizontal stresses tend to clamp vertical joints, but destabilize discontinuities that dip at a low angle. The relatively high horizontal stress states were often associated with the presence of potholes. The rock strength tends to be anisotropic, probably because of the intrusion processes, and has a tensile stress that is relatively low in the horizontal direction.

3 EFFECT OF GEOLOGICAL PROCESSES ON THE VARIABILITY OF THE STRESS STATE

3.1 Causes of initial stress state

The in-situ stress state is the result of complex interactions within the Earth's crust. Gravitational loading, tectonic forces, thermal energy variations and physico-chemical processes, such as recrystallisation, absorption and pore pressures all contribute to the final stress state (Hyett *et al.*, 1986). The simplest model for the in-situ stress state within the earth is to assume that the vertical stresses are due only to gravitational loading of the rock. In this case, the vertical stress is given by

$$\sigma_{\mathrm{v}} = \rho g \mathrm{z} \tag{3.1.1}$$

where ρ is the density of the rock, g is the gravitational constant and z is the depth below the surface. The horizontal stress is calculated by assuming that the rock can be modelled as an isotropic linear elastic material and that the rock forms in a state of complete lateral restraint (i.e. with zero horizontal strain) (Jaeger and Cook, 1979). Then, the horizontal stress becomes

$$\sigma_{\mathrm{h}} = \frac{\nu}{(1-\nu)}\sigma_{\mathrm{v}}, \tag{3.1.2}$$

where ν is the Poisson's ratio. The stress magnitude will be related to the variation of the elastic properties with depth. The shear modulus is expected to increase to a depth of 2 or 3 km and then remain constant (Leary, 1985).

If the rock is assumed to be viscoelastic, the material will creep and Heim's rule states that the stress state will tend to become lithostatic (equal horizontal and vertical stresses) with time (Jaeger and Cook, 1979). The rock is described by a linear elastic model in hydrostatic compression with shear modulus G and bulk modulus K and by a Maxwell substance in shear with elastic modulus k and viscosity η. Then, applying a vertical stress S along the z axis and assuming complete lateral restraint, the vertical and horizontal stresses become

$$\sigma_v = S = \rho g z \text{ and } \sigma_h = \sigma_x = \sigma_y = S - \frac{6k\eta S}{(3K+4k)\eta} e^{-t/t_1} \tag{3.1.3}$$

respectively. Thus, as the time *t* approaches the characteristic time t_1 the second term in the expression for the horizontal stress diminishes and the in-situ stress state tends to become lithostatic. The amount of time required for this process to occur depends on the elastic moduli K and k, and the viscosity η through the expression for the time constant $t_1 = (3K + 4k)\eta / 3Kk$. Haxby and Turcotte (1976) suggest that the crust remains elastic for a stress range of up to 100 MPa over a time period of 1 to 10 million years and at temperatures of less than 300°C.

The *in situ* stress state derived from either the elastic assumption or Heim's rule does not fit the observed data (Gay, 1975). Improved estimates can be obtained by including the curvature of the Earth (McCrutchen, 1982) and by assuming an initial stress state and then unloading the material under conditions of lateral restraint to simulate surface erosion - Voight's model (Gay, 1975).

Reduction of the overburden pressure under conditions of horizontal restraint will cause an increase in the horizontal stress relative to the vertical stress (Gay, 1980). The magnitude of the change in stress depends on how the process is modelled. The assumption of a one-dimensional change and linear elastic rock leads to a change $\Delta\sigma_h = -[\nu/(1-\nu)]\Delta\sigma_v$ in the horizontal stress. When the curvature of the earth is included by assuming that the uplift occurs on a spherical surface, a horizontal tensile stress is superimposed on the compressive stress caused by gravitational loading. The ratio of horizontal to vertical stress becomes

$$\frac{\sigma_h}{\sigma_v} = \frac{[(\sigma_h/\sigma_v)_i - [(1+\nu)/2(1-\nu)]\Delta\sigma_v/\sigma_{vi}]}{1-\Delta\sigma_v/\sigma_{vi}} \tag{3.1.4}$$

where *i* refers to the initial state. Tensile thermal stresses may be induced by erosion processes. The magnitude of the thermal stresses is calculated from

$$\sigma_\theta = \alpha E \Delta T/(1-\nu) \tag{3.1.5}$$

and can be in the range of 15 MPa to 30 MPa for the removal of 1 km of rock in a region with a geothermal gradient of 25° C/km. This magnitude of stress would cause tensile fracturing within the material (Gay, 1980). Haxby and Turcotte (1976) agree that the stress state due to erosion may be due to stresses caused by the reduction of the overburden, and stresses due to uplift and thermal stresses. The thermal stresses can be high enough to exceed the stresses induced by the other effects. Stress variability is therefore strongly dependent on erosion depths. Since the history is very difficult to determine accurately and the depth of erosion is expected to vary considerably with position, it is almost impossible to calculate the magnitude of the residual stresses.

The assumption of elastic material response assumes that the in-situ stresses will increase indefinitely. However, in practice, the constitutive response of the rock is non-linear and the stress state will be controlled by the rock strength. If the loading causes the stress to exceed the material strength, the material will experience inelastic deformation, faults will form and the in-situ stress state will change (Rummel, 1986). Analysis of the stress state with the Coulomb criterion suggests that faults with no cohesion and a friction angle ϕ will become unstable when

$$\frac{\sigma_3}{\sigma_1} = \frac{1-\sin\phi}{1+\sin\phi}. \tag{3.1.6}$$

Thus, for a friction angle of ϕ=30^o any k ratio below k=0.33, or above 3.0, will result in fault formation. The k-ratio will also alter the potential for seismic events to occur near a mining excavation as indicated by the Excess Shear Stress (ESS) criterion (Ryder, 1988). Figure 2.1.3 shows the sensitivity of the event magnitudes estimated for seismic events to variations in the k ratio, as determined from the ESS lobes around a 200 m long horizontal stope at 4000 m depth. The lower value of the stress ratio induces higher seismic moments.

Brace and Kohlstedt (1980) consider that the behaviour of rock at great depths is determined by the frictional strength of the material since most deformation will occur along joints. The strength can be characterised by Byerlee’s law of frictional sliding which states that the shear strength is related to the normal stress by a bilinear relation, which is independent of rock type and temperature. In terms of principal stresses, the law states that frictional sliding occurs (Brace and Kohlstedt, 1980) when

$$\begin{aligned} &\sigma_1 \approx 5\sigma_3 \,\mathrm{for}\, \sigma_3 < 110 \text{ MPa} \\ &\sigma_1 \approx 3.1\sigma_3 + 210 \,\mathrm{for}\, \sigma_3 > 110 \text{ MPa}. \end{aligned}$$

At depths of 4 km below the surface, plastic deformation acts to reduce the rock strength, which is dependent on the strain rate and the temperature (above 500°C). The lithosphere can be shown to have negligible strength below 25 km if the plastic deformation is characterised by considering the rock having the properties of Quartzite. If, however, the rock is modelled as Olivine then the rock shear strength falls to zero at a depth of 50 km.

3.2 Effect of layering on stress state

Equation 3.1.2, implies that the horizontal stress depends on the elastic properties of the rock mass. Thus, in a layered stratigraphy, it can be expected that the horizontal stress will also vary between layers. In the case that the rock is layered, the stresses are calculated for each layer and summed. Thus, for N layers each of thickness h^i,

$$\sigma_{\mathrm{v}} = \sum_{i=1}^{N} \rho g \mathrm{h}^i \,\text{and}\, \sigma_{\mathrm{h}} = \left(\frac{\nu^i}{1-\nu^i} \right) \sigma_{\mathrm{v}} . \tag{3.2.1}$$

The ratios of horizontal stress to vertical stress $\mathrm{k} = \dfrac{\nu}{(1-\nu)}$ predicted by elastic theory are given in Table 3.2.1 for a range of Poisson's ratios.

Table 3.2.1 Ratio of horizontal to vertical stress k in an isotropic elastic material for a range of Poisson's ratios

Poisson's ratio ν	Stress ratio k
0	0
0.1	0.11
0.2	0.25
0.3	0.43
0.4	0.67
0.5	1.0

The in-situ stress state can be altered considerably if the rock is layered and aniostropic (Savage *et al*., 1986; Amadei *et al*., 1988; Amadei and Pan, 1992). In an orthotropic rockmass, the material is described by twelve elastic constants, E_x, E_y, E_z, G_{xy}, G_{yz}, G_{xz}, ν_{xy}, ν_{yz}, ν_{xz} ν_{yx}, ν_{zy}, and ν_{zx}. Then, assuming a condition of no lateral strain, the in-situ stresses, which satisfy the thermodynamic constraints, equilibrium and compatibility requirements and the boundary conditions at the surface, are found (Savage *et al.*, 1986) to be

$$\sigma_{\mathrm{z}} = \rho g\mathrm{z} \;\; \sigma_{\mathrm{x}} = \rho g\mathrm{z}\frac{(\nu_{xz} + \nu_{yz}\nu_{xy})}{1-\nu_{yx}\nu_{xy}} \text{and} \, \sigma_{\mathrm{y}} = \rho g\mathrm{z}\frac{(\nu_{yz} + \nu_{yx}\nu_{xz})}{1-\nu_{yx}\nu_{xy}} \tag{3.2.2}$$

and thus unequal horizontal stresses can be induced by gravity. If the rock is transversely isotropic in planes parallel to the surface, then $E_x = E_y = E$, $E_z = E'$, $G_{xy} = G$, $G_{xz} = G_{yz} = G'$, $\nu_{xy} = \nu_{yx} = \nu$, and $\nu_{zx} = \nu_{zy} = \nu'$, $\nu_{xz} = \nu_{yz} = \nu' E/E'$. There is no difference in the horizontal stresses and then

$$\sigma_{\mathrm{z}} = \rho g\mathrm{z} \;\; \sigma_{\mathrm{x}} = \rho g\mathrm{z}\frac{\nu_{xz}}{1-\nu} = \sigma_{\mathrm{y}} \, . \tag{3.2.3}$$

If, however, the plane of isotropy is vertical, the elastic constants can be re-expressed as $E_z = E_y = E$, $E_x = E'$, $G_{yz} = G$, $G_{xy} = G_{xz} = G'$, $\nu_{yz} = \nu_{zy} = \nu$, $\nu_{xy} = \nu_{xz} = \nu'$, $\nu_{yx} = \nu_{zx} = \nu' E/E'$. In this case, the horizontal stresses are not equal and are given by

$$\sigma_{\mathrm{z}} = \rho g\mathrm{z} \;\; \sigma_{\mathrm{x}} = \rho g\mathrm{z}\frac{\nu'(1+\nu)}{1-\frac{E}{E'}\nu'^2}, \text{and} \, \sigma_{\mathrm{y}} = \rho g\mathrm{z}\frac{(\nu + \frac{E}{E'}\nu'^2)}{1-\frac{E}{E'}\nu'^2} \, . \tag{3.2.4}$$

When the rockmass can be described as a series of transversely isotropic layers with different elastic properties and densities, the vertical stress in a layer R is the sum of the contributions from the layers above, and the horizontal stresses depend only on the properties of the layer, R. Then,

$$\sigma_z^R = \rho^R g\mathrm{z} + \sum_{j=1}^{R}(\rho^j - \rho^R)g\mathrm{h}^j \text{and} \, \sigma^R = \frac{\nu^R E^R}{E'^R(1-\nu^R)}\sigma_{\mathrm{zR}} \tag{3.2.5}$$

Assuming that the vertical compressibility decreases with depth such that $E/E'^R = 1 + E/(a + bz_R)$, where a and b are constants, produces a distribution of ratios of vertical to horizontal stress that approximates the experimental observations, and suggests that rock stiffening may play a major part in the in-situ stress distribution (Savage *et al.*, 1986). There is evidence from triaxial laboratory tests (Briggs, 1982) that the compressibility of the Witwatersrand Quartzites decreases slightly with depth. The measured increase in Young's modulus with confinement is presented in Figure 3.2.1 for 90% and 70% quartzites, along with the result of a linear regression for each rock type. Of more importance, will be variations in the moduli of the different rock layers, which will invalidate the approximation of the continuous increase of the Young's modulus with depth, suggest by Savage *et al* (1986). For a special case of layered rock consisting of alternating thick, isotropic elastic, and thin, transversely isotropic, layers of rock, and assuming that the transverse isotropy reduces with depth as before, the ratio of horizontal to vertical stress will remain constant with increasing depth in the thick layers. The k ratio in the thin layers will be considerably greater than in the thicker layers, but will reduce with depth (Amadei *et al*., 1988).

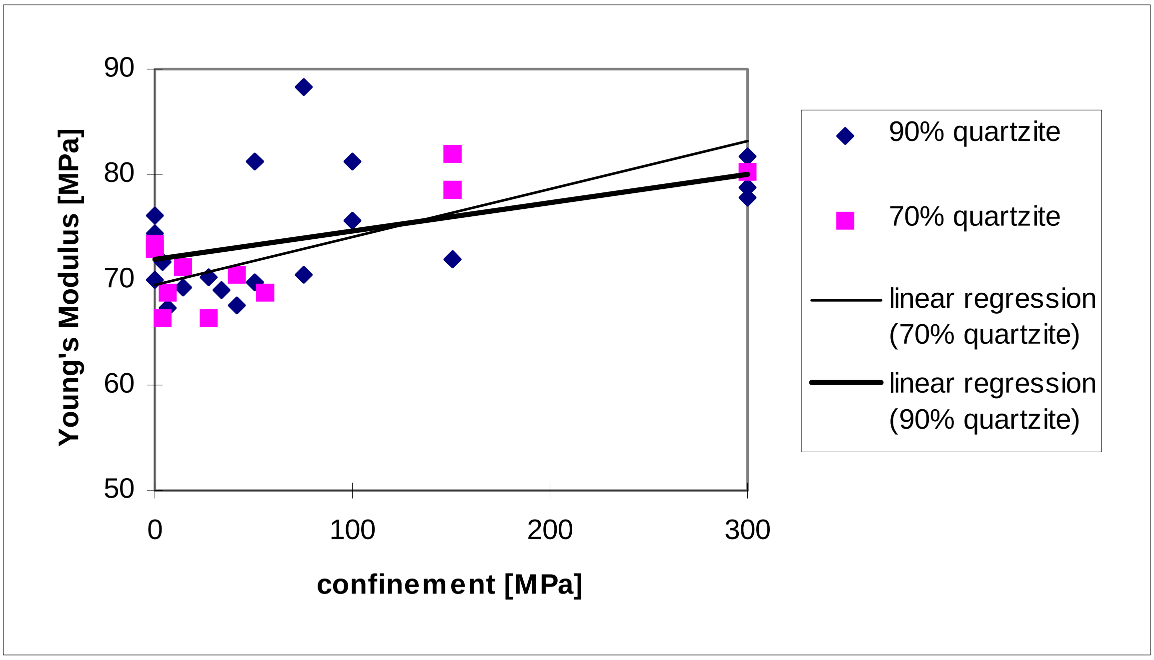

Figure 3.2.1 Variation in Young's modulus with confinement for two types of quartzite (Briggs, 1982)

When the rockmass is completely anisotropic, the vertical stress is always a principal stress and the horizontal stresses are unequal. The direction of the horizontal stresses depends on the type and degree of the anisotropy. If the rock consists of layers of transversely isotropic material with dipping strata, the horizontal stresses parallel to the strike and dip directions are principal values and differ in magnitude depending on the elastic properties. Theoretically, tensile stresses can be induced by gravity in dipping strata, depending on the elastic properties of the rock, leading to the possibility of gravity induced fracture formation (Amadei and Pan, 1992).

3.3 Effect of surface topology on stress state

Surface topology is probably not a significant effect in deep level gold or platinum mines, but a few examples are provided for completeness and to indicate another way in which geological factors can alter the stress state. In deep level mines the prehistoric topology may have affected the stress state in a similar manner and there is no way of determining how subsequent depositional or magmatic events may have locked in, or altered the stress state.

The state of stress with depth from surface was measured in a number of tunnels extending into the mountainsides forming a river valley by Guangyu *et al* (1986). The results are shown in Figure 3.3.1 and Figure 3.3.2. Both sites indicate that the principal stress direction is sub-parallel to the mountainside at shallow depths and then becomes steeper further away from the valley. The principal stresses beneath the river at the bottom of the valley were aligned almost horizontally and vertically with the horizontal component being the highest. The magnitudes are also affected by the valley and there is a region of higher stress concentration a short distance into the valley sides.

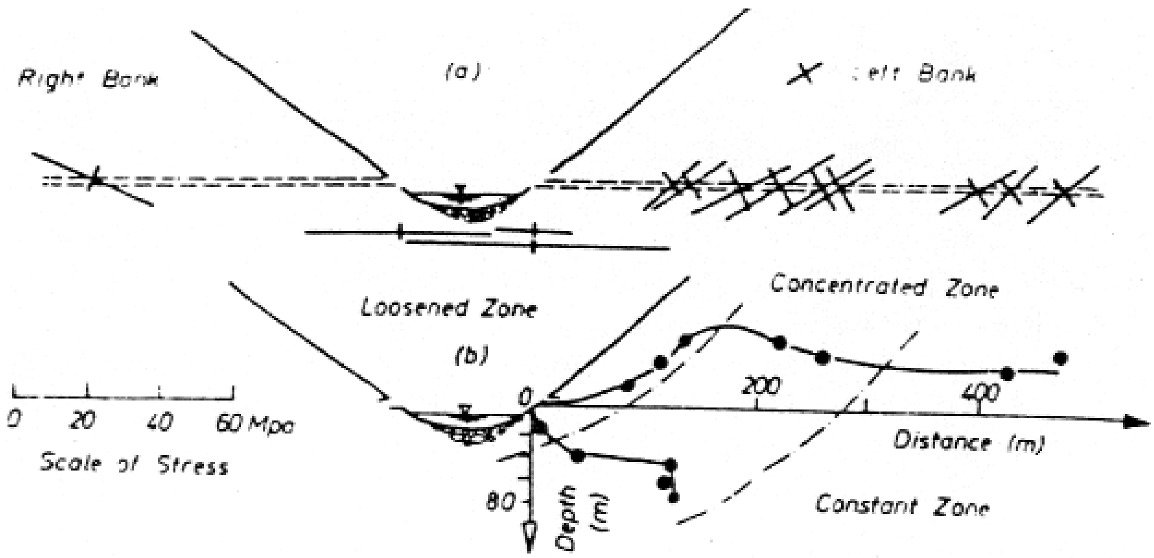

Figure 3.3.1 Principal stresses showing a) directions and b) magnitudes in cross section of river valley (Guangyu et al. 1986)

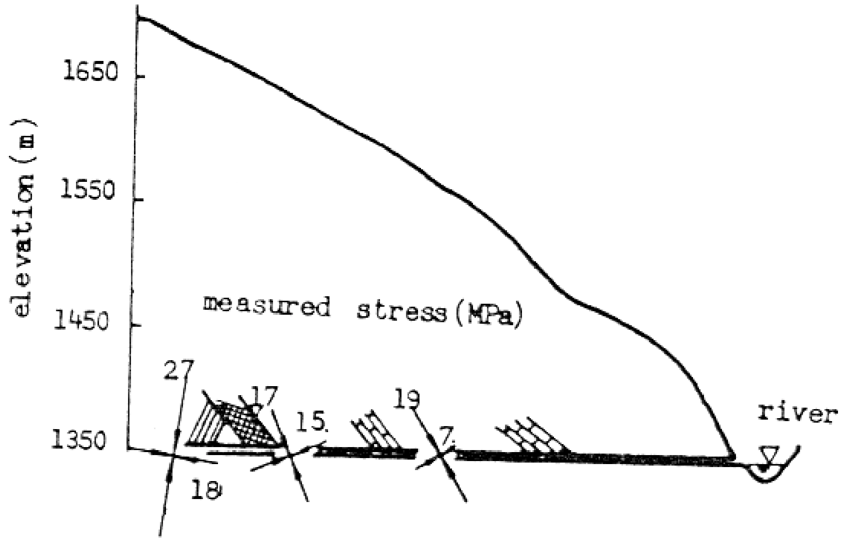

Figure 3.3.2 Measured stress state in a mountainside (Guangyu et al. 1986)

3.4 Effect of Folding on stress state

The effect of folding of the rock mass is to alter the stress state through the thickness of the layers. The layers act as beams with the axial stress varying from tension, on the side that is stretched, to compression within the layer, depending on the position relative to the fold. A number of microstructural indicators such as crystal, grain and oolite deformations are used in structural geology to determine the strain in the layer (e.g. Hobbs, *et al*, 1976, Weijermars, 1992). However, in conditions of folding, the long-term nature of the process implies that the rock is effectively viscous and flows like a fluid. In this case, the stress is proportional to the strain rate, and not to the strain as in an elastic-plastic material. Thus, the principal directions of the stresses and strains will be different. The same fold shape will also have different stresses if it formed at a different rate (Hobbs *et al*., 1976).

The evolution of folding in a brittle material can be seen in Figure 3.4.1 (Seilei *et al*, 1997). Excessive deformation results in faulting and the stress state will be affected as discussed in the section on faulting. The type of faults will depend on the tectonic loading.

The numerical modelling of folding processes is usually aimed at predicting the actual shape of the folds rather than determining the effect of folding on the in-situ stress state. Lan and Wang (1987) present a finite element model for the formation of an overturned fold by describing the rock as a viscous incompressible Newtonian fluid. Lan and

Huddleston (1990) consider the rock to be a visco-elastic material with a power law relationship between the strain rate and the stress. The finite element simulation is able to predict the development of the shape of buckle folds. Mülhaus *et al*. (1994) model the process of folding as a buckling instability in a plate of elastic or viscous material embedded in a viscous medium.

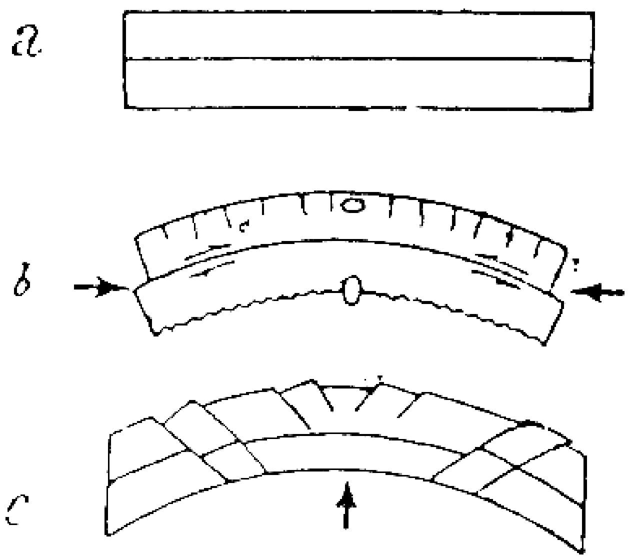

Fig. 2 Evolution of folding

Figure 3.4.1 Evolution of folding (Seilei et al, 1997)

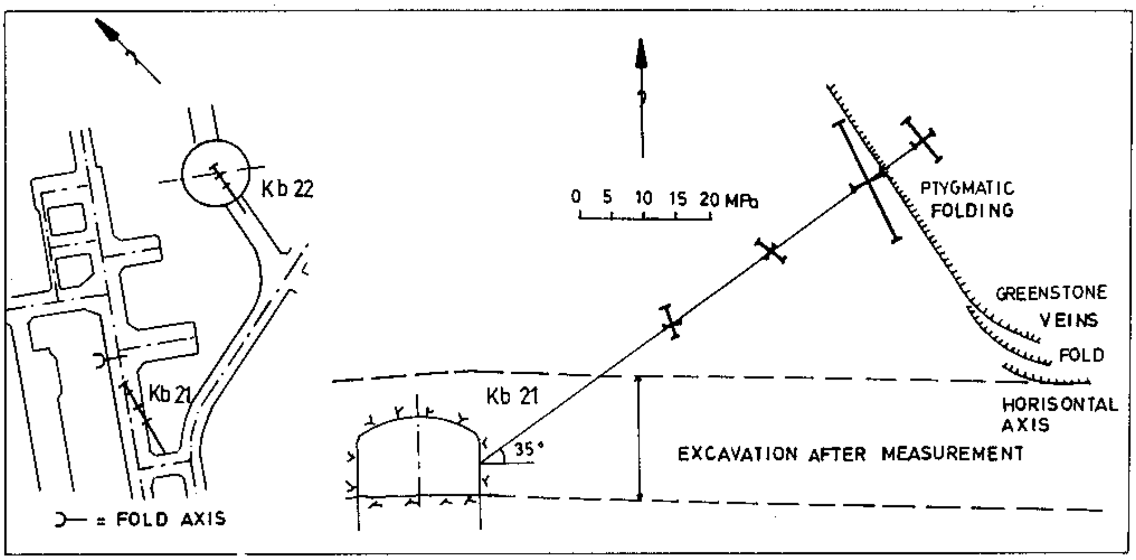

Figure 3.4.2 Rotation of stress field near fold axis (Charlsson and Christianson, 1986)

In situ measurements show how folding can affect the stress state. Higher stresses were found near a folded vein by Carlsson and Christianson (1986) as shown in Figure 3.4.2. Tensile principal stresses were observed some distance away from the fold. Gale (1986) showed that the stress states in Australian coal mines were closely related to the folding. The major principal stress was found to be horizontal and oriented in the direction normal to the trend of the fold axis.

3.5 Effect of Faults on stress state

3.5.1 Theoretical studies of the change in stress state due to fault formation

Faults may arise because of a variety of geological processes (Mandl, 1988). Classical analysis (Price, 1966, Jaeger and Cook, 1979) considers fault formation in terms of the Mohr Coulomb strength criterion. The fractures form as conjugate planes parallel to the direction of the intermediate principal stress and are aligned at an angle of between 17^o and 30^o to the major principal stress direction. As depicted in Figure 3.5.1, normal faults form when the major principal stress is vertical and the minor stress is horizontal and thus occur in extensional tectonic regimes. Strike-slip (wrench) faulting initiates when the major principal stress is horizontal and the intermediate principal stress is vertical. When the minor stress is vertical and the major stress horizontal, thrust faulting can occur. In three dimensional stress states with changing stress conditions, more than two fault sets may be required to accommodate the strain changes (Mandl, 1988). If the rock has some pre-existing fabric or strength anisotropy, the direction of faulting may be altered and the angle of faulting will depend on the angle between the major principal stress direction and the fabric orientation (Mandl, 1988). The stress state in the rock mass will be altered by the formation processes, secondary fault formation and the slip sequences on the fault set.

The stress state around faults, joints and dykes may be inferred from analytical solutions of cracks in an elastic medium (Price, 1976; Pollard and Segal, 1987). Joints and solution surfaces may be characterized as mode I (opening) cracks under tension and compression respectively. Joints may form perpendicular to bedding planes in layered rock to relieve built-in horizontal stresses or shear stresses applied to the layer interface (Pollard and Segal, 1987). The redistribution of stress resulting from the introduction of a tensile crack into the layer can be shown to cause tensile stresses to rise with distance from the crack. At a distance of approximately the height of the layer, the tensile stresses are sufficiently high to initiate another fracture.

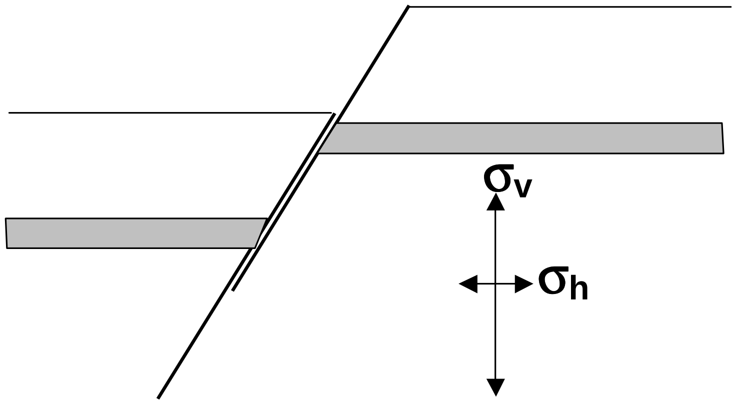

(a)

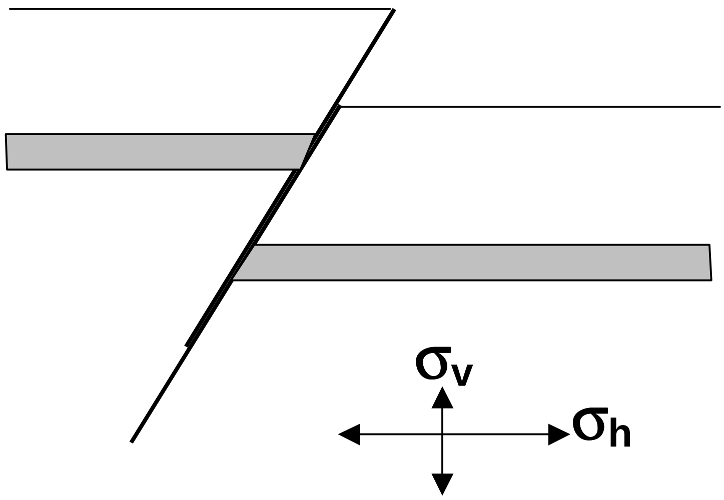

(b)

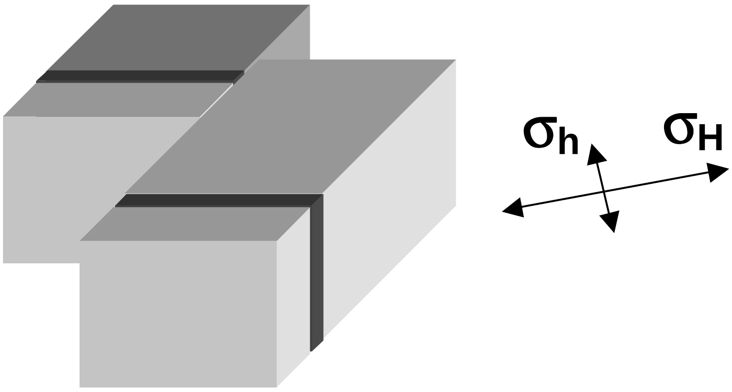

(c)

Figure 3.5.1 Stress states at onset of faulting (after Seilei et al 1997)a) normal faulting, b) reverse faulting and c) thrust faulting

The mechanism of sliding on faults requires that they be considered as mode II or mode III cracks (Pollard and Segal, 1987). However, the selection of the fracture mode of a particular fault requires information regarding the opening, sliding, separation, slip and the direction of the fault motion. The stress distribution around the faults can then be determined by considering the effect of a driving shear stress on the crack. The magnitude of the shear stress is estimated to be approximately one hundredth of the shear modulus of the host rock.

The deformation of rock can be expressed in terms of a state diagram to represent the phases of material behaviour under different conditions of pressure, temperature, grain-size, time and strain rate (Handy, 1989). Strain localization of the material into shear bands or ductile fault zones will result from transitions between different material phases in the state diagram. The strain localization occurs at boundaries between rock types, at high stress regions and at the transition from brittle to viscous creep behaviour. Alternatively, changes in the geothermal state can cause chemical reactions which result in recrystallisation of the material or alteration of the amount of water in the rock which in turn lead to localised shear deformations in the rock.

Faulting can result from inelastic deformation in the lithosphere due to the interaction between tectonic processes, and a number of examples are depicted in Figure 3.5.2 (Mandl, 1988). Each case will induce different stress states. The primary mechanisms of fault formation are the result of the strain softening behaviour of the rock during deformation. In an extensional environment, as shown in the examples of Figure 3.5.2, and as currently acting in South Africa, the major principal stress tends to be vertical. As a results of tectonic stresses, the rock mass will fail and localize into fault planes, which will cause the stress to be redistributed. The major principal stress vector will tend to be rotated normal to the fault plane.

Subsidence and differential uplift is another cause of fault formation and the resulting fault patterns are shown in Figure 3.5.2h and Figure 3.5.2e, respectively. Joints can also form due to the relative motion of rocks of different properties under the action of tectonic forces. These processes, named ‘simple-shear tectonics’ (Mandl, 1988) can occur when weaker rock is sheared by adjacent layers of strong rock, or by basement induced wrenching in which shearing is applied to the crustal rocks by deformations within the basement rock. In each case, the principal stress axes are rotated from the vertical towards the direction of the normal to the developing fault.

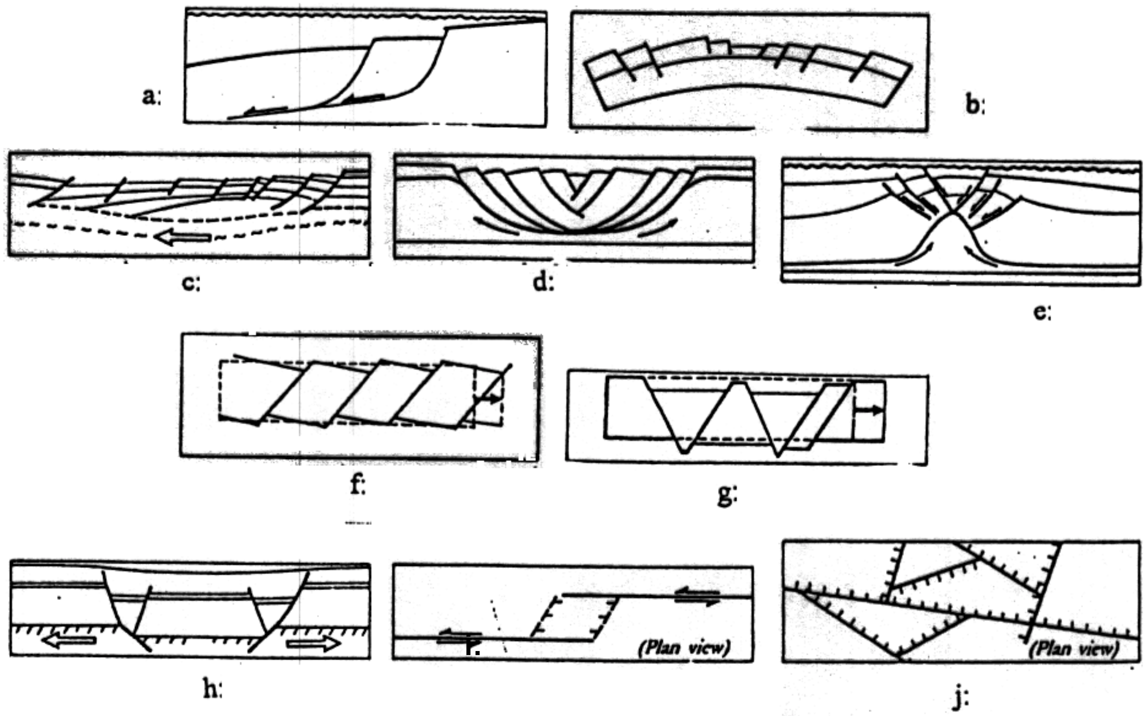

Figure 3.5.2 Fault formation due to various geological processes. a) gravitational sliding, b) bending of crust c) creep flow at depth d) lateral extrusion of sub strata e) rising dome f) and g) extension of ductile base h) subsiding basement i) offset along strike slip fault and j) block faulting in plan in extension environment

As shown in Figure 3.5.3, finite element analyses of a uniform layer of strain softening material on a frictional, rigid base which is loaded by a uniform horizontal strain along the base of the layer, indicate that the extension or compression of plates will result in sets of conjugate shear planes (Witlox, 1986). In the analysis, the rock is described by a Drucker-Prager plasticity model with a non-linear softening law to characterise the evolution of the cohesion and friction angle. A notch in the surface of the model is used as an initial non-uniformity to initiate the first fault, although the angle of the faulting is found to be independent of the type of non-uniformity. The spacing of the faults is strongly dependent on the layer thickness and the parameters of the softening law. The final pattern of fracturing under an extension stress is shown in Figure 3.5.3. Originally, the stress direction is vertical and the stresses tend to rotate to become perpendicular to the fault plane. The distance from the fault over which the rotation occurs will depend on the rock properties, the fault length and thickness, and the stress levels.

When the layer is considered to be resting on a frictionless surface and has a uniform deformation applied to the base, the material localises into two normal faults forming a graben structure as shown Figure 3.5.4. Graben formation can also be a result of the application of a region of extension strain along the base of the layer, which increases in magnitude and extent with time. The fault pattern will depend on the rate of growth of the strained region. The trajectories of the major principal stress are deflected from their initial vertical state and the major principal stress vectors are rotated towards the normal to the fault. In the case of a reverse fault, the stress is also rotated close to the fault as shown in Figure 3.5.5. In this case, the rotation causes the major stresses to deviate from the horizontal direction.

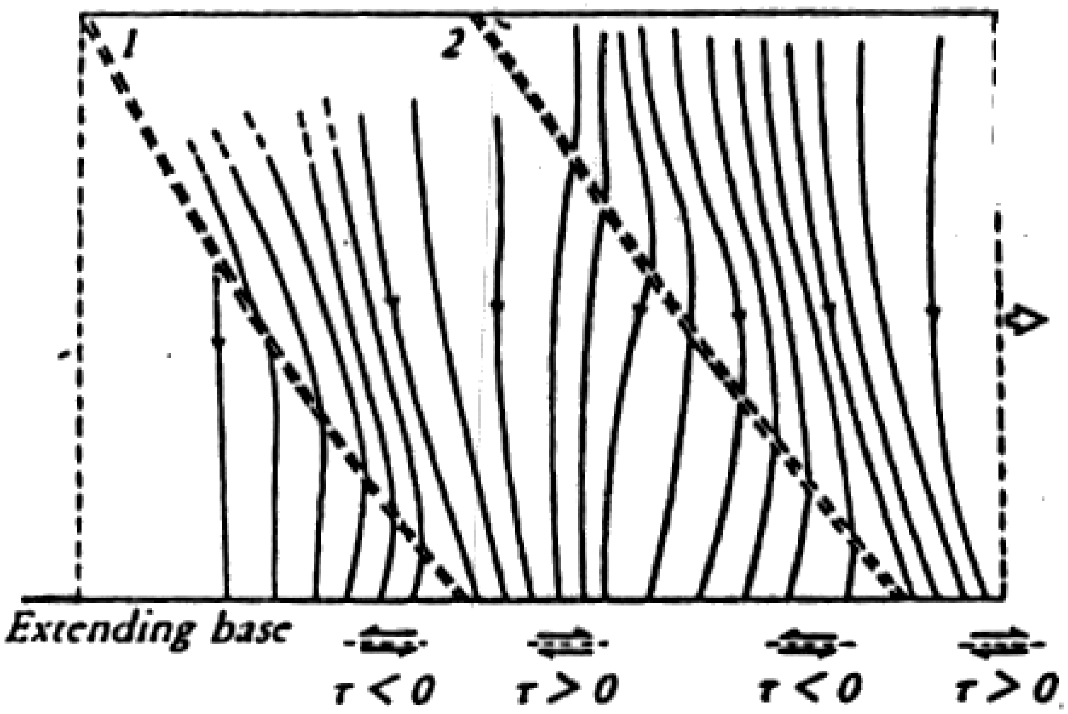

Figure 3.5.3 Major compressive principal stress trajectories due to the formation of faults by extension of a uniform layer of strain softening material (Witlox, 1986)

Secondary fault formation is an important mechanism that can only be considered with strain softening material models because of the redistribution of stresses that arises after fault formation. The main mechanism of secondary fault formation is the constraint on the deformation of the rock provided by the geometry of existing faults. For example, continued rotation of rock on one side of a curved fault will lead to reverse faulting as the rock is forced to conform to the shape of the curved fault as shown in Figure 3.5.6. Continued loading of a fault plane can lead to changes in the stress trajectories and hence to secondary fault development on either side of the main fault move relative to each other.

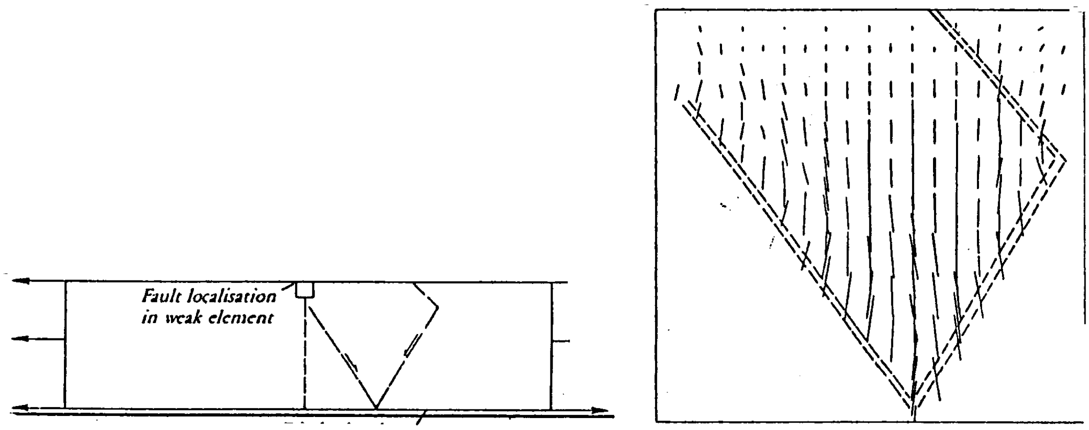

(a) (b)

Figure 3.5.4 Finite element model of the development of a graben by application of strain with increasing magnitude and extent to the base of a layer of strain softening material (Mandl, 1988) a) model, b) σ1 trajectories inside graben

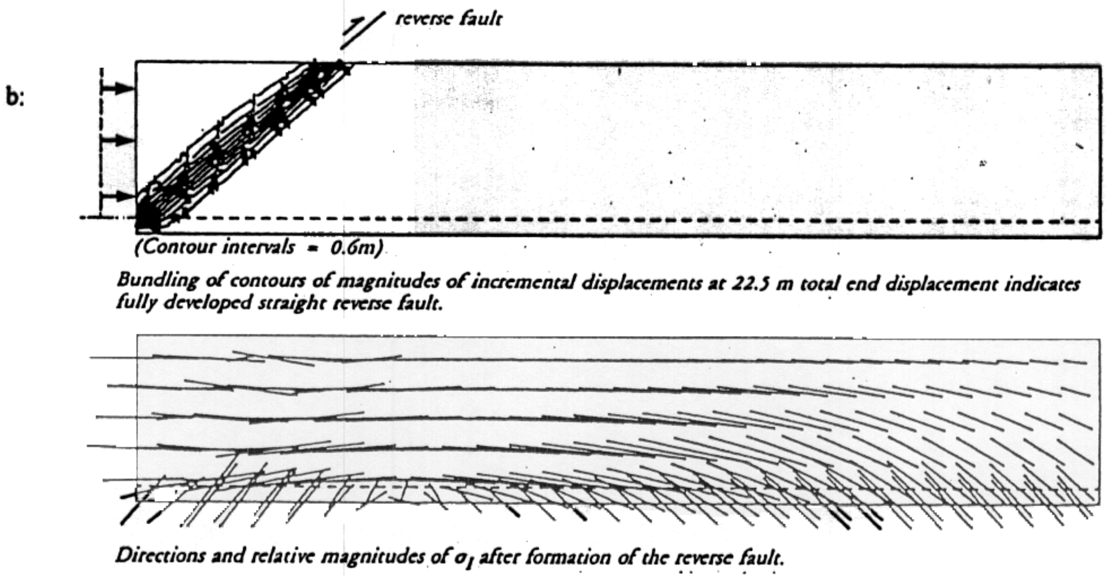

Figure 3.5.5 Alteration of the distribution of plastic strain and the major principal stresses as a result of a reverse fault (Mandl, 1988)

A few authors have used numerical modelling to investigate how faults can cause rotation of the stress field. Sengupta *et al*. (1997) and Su and Stephansson (1999) have both studied the effect of thrust faults on the stress state. An example result is shown in Figure 3.5.7 to demonstrate how the principal stress directions rotate to become nearly perpendicular to the fault plane.

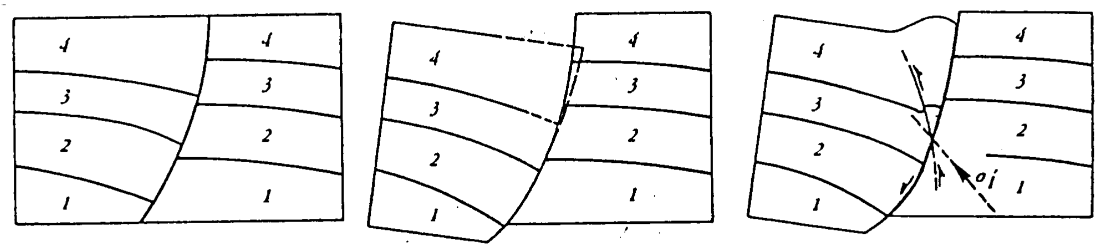

Figure 3.5.6 Schematic diagram of secondary fault forming as compression forces the strata to conform to a pre-existing fault plane (Mandl, 1988)

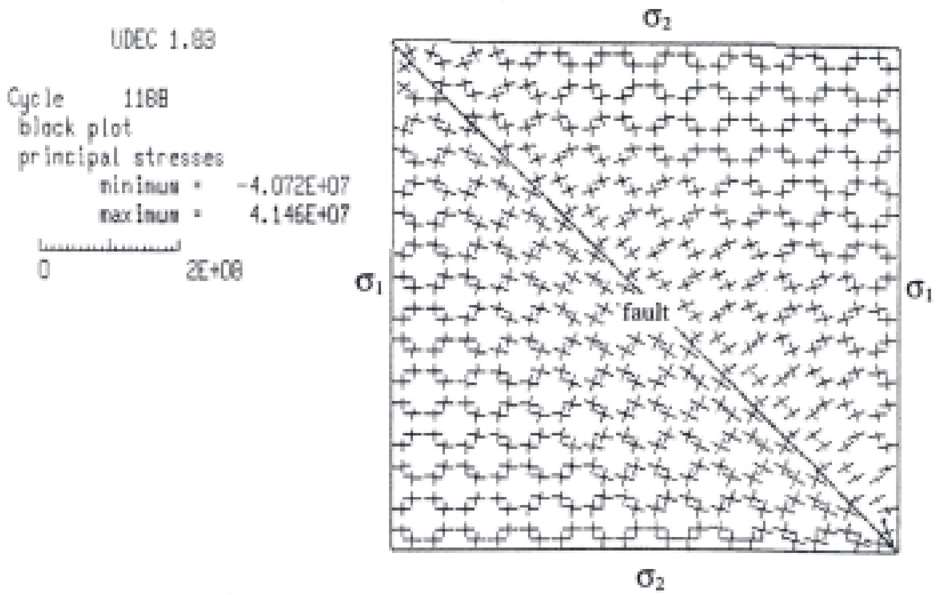

Figure 3.5.7 Rotation of stress state due to fault with friction angle of 3° in horizontal plane with k-ratio of 1.25 (Su and Stephannson, 1999)

An estimate of the amount of stress rotation that occurs after faulting can be obtained from a simple formula by assuming that the σ_2 axis remains parallel to the fault plane, is either horizontal or vertical, and the normal stress on the fault remains the same (Yin and Rogers, 1995). Then, the change in the angle α of the σ_1 axis is a function of the ratio of the stress drop to the initial shear stress, the angle between the principal stress axis and the fault plane, the dip of the fault, and the direction of the slip vector. The friction angle of the fault will also affect the magnitude of the change in stress associated with fault slip, as shown in Figure 3.5.8a. The graph in Figure 3.5.8b shows how the principal stress difference depends on the angle between the major principal stress and the fault, and the k-ratio.

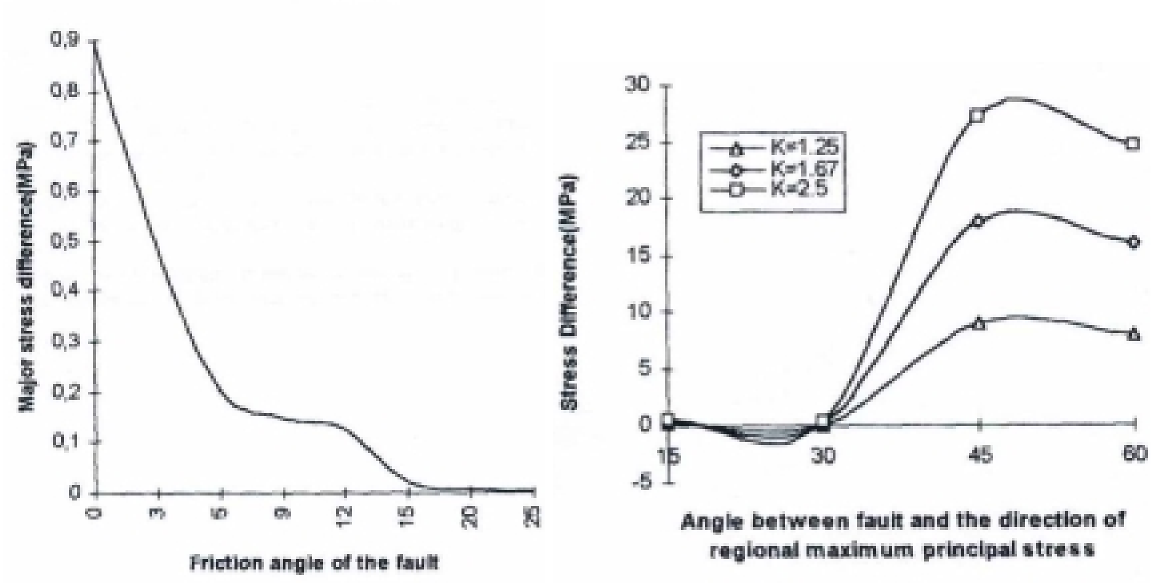

(a) (b)

Figure 3.5.8 a) stress difference as a function of friction angle on the fault and b) effect angle between the fault and the major principal stress on the stress difference across the fault. (Su and Stephannson, 1999)

A DIGS model was constructed to investigate the effect of a steeply dipping normal fault that is more common in the South African mining environment. The fault extends to a depth of 3000 m and the ground surface extends 10 000 m in each direction. The change in stress state due to a constant slip of 10 m imposed on the fault is shown in Figure 3.5.9. The figure indicates the high stress concentration at the lower edge of the fault. The magnitude of the stress concentrating effect will depend on the slip profile and the rock mass strength. An induced tension exists in the footwall of the fault at the lower end. This could induce secondary fault formation in a manner analogous to the wing crack development predicted for flaws in a brittle material (see e.g. Dyskin *et al*, 1995). It may be expected that the three-dimensional shape of the fault could be as complex as the three-dimensional fractures observed in laboratory tests (see e.g. Dyskin *et al*, 1995). If more than one fault occurred, the stress state would also be affected by shielding, local failure and joint formation and other complex growth interactions that make it practically impossible to predict the final stress state.

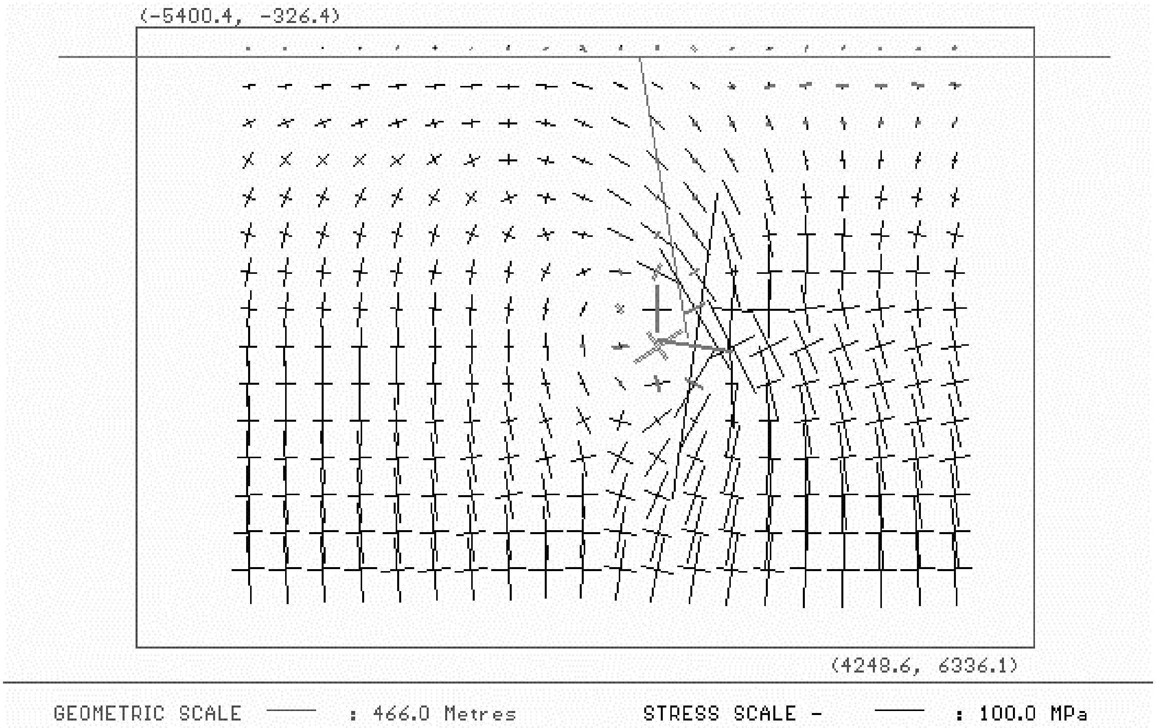

Figure 3.5.9 Stress state due to a steeply dipping normal fault with slip of 10 m over 3000 m

3.5.2 Measurements of the change in stress state due to fault formation

Measurements of the stress across faults in Japan (Sugawara *et al*., 1997) showed that the stress state varied significantly with distance from the fault. The stress was also discontinuous across the fault, as shown in Figure 3.5.10. In section, the stresses rotate to become orthogonal to the fault. The plan view also indicates stress rotation and a discontinuity in stress magnitude across the fault. Thus, there is a three-dimensional rotation of the stress state and the magnitude and direction are determined by the actual slip direction on the fault. Figure 3.5.11 provides an example from Japan (Sugawara *et al*, 1997), which indicates that the direction of the maximum horizontal stress is altered by faulting and may be discontinuous across plates boundaries. Adjacent regions may have completely different stress states if they are composed from different tectonic plates. Similar rotations were observed by Martna and Hanssen (1986) in Sweden, where faults with throws of 1 m to 35 m affected the stress state to distances of at least 50 m. Figure 3.5.12 shows that the major stress strikes parallel to the fault in the hangingwall and both the vertical and horizontal stresses decrease near the fault. There is an increase in stress and a rotation away from the strike of the fault with increasing depth into the footwall. In contrast, Mills *et al*. (1986) noted that the stress states found in New Zealand coal mines was similar to those expected for formation of the faults and hence there must have been little alteration of the stress directions.

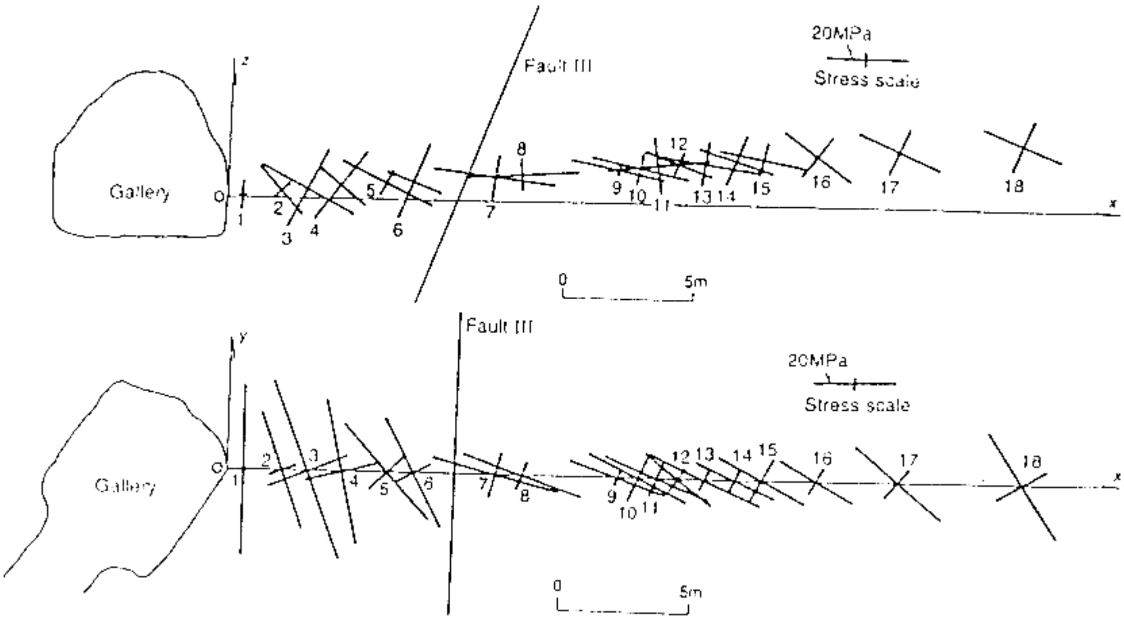

Figure 3.5.10 Changes of stress due to presence of faults (Sugawara et al, 1997)

A South African example of the effect of faults on the stress state was produced by Gay *et al*, (1984). The comparison of measured stresses with the fault direction data for the Klerksdorp region is shown in Figure 3.5.13. The stress measurement sites had different relationships to nearby geological structures. The Hartebeesfontein site (labelled H) was undisturbed, the Vaal Reefs site (labelled V) was near two faults, and the Buffelsfontein sites (labelled B) were near dykes and faults. The undisturbed sites show an almost vertical major principal stress whereas the site affected by two faults at the Vaal Reefs site shows that the major and intermediate stresses are almost normal to the average fault plane orientations. At all sites the major horizontal stress strikes in a North Westerly direction, indicating that the faulting is associated with an anisotropic distribution of the horizontal stresses. The stress is increased normal to the faults. Even though the stress is rotated, the k-ratio is not significantly affected by the faulting as can be seen by comparing the major and minor k-ratios for Hartebeesfontein (unfaulted) and Vaal Reefs (faulted) in Table 3.5.1.

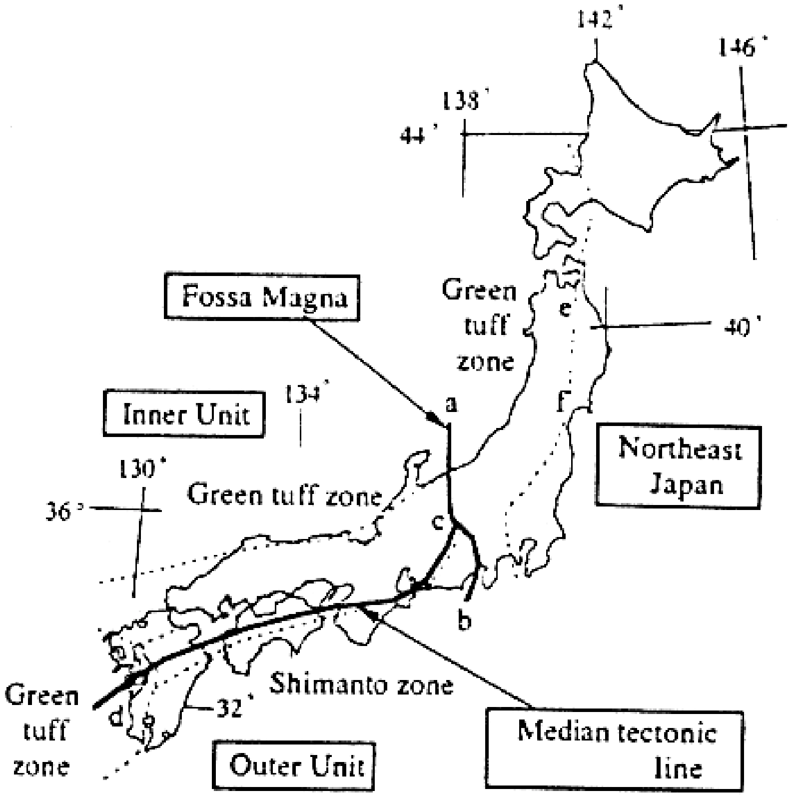

(a)

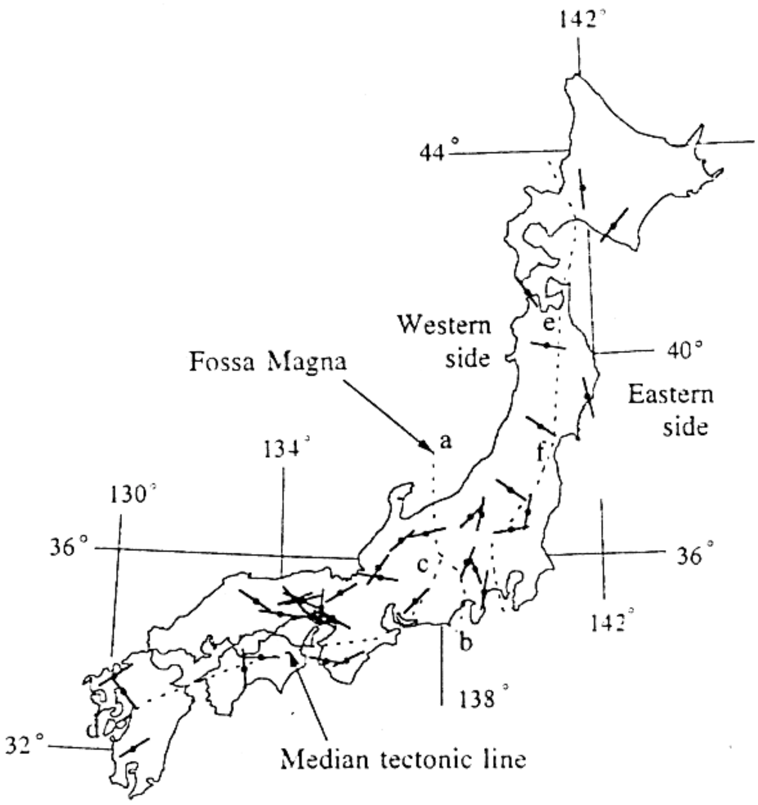

(b)

Figure 3.5.11 a) fault lines and b) horizontal stresses in Japan (Sugawara et al 1997)

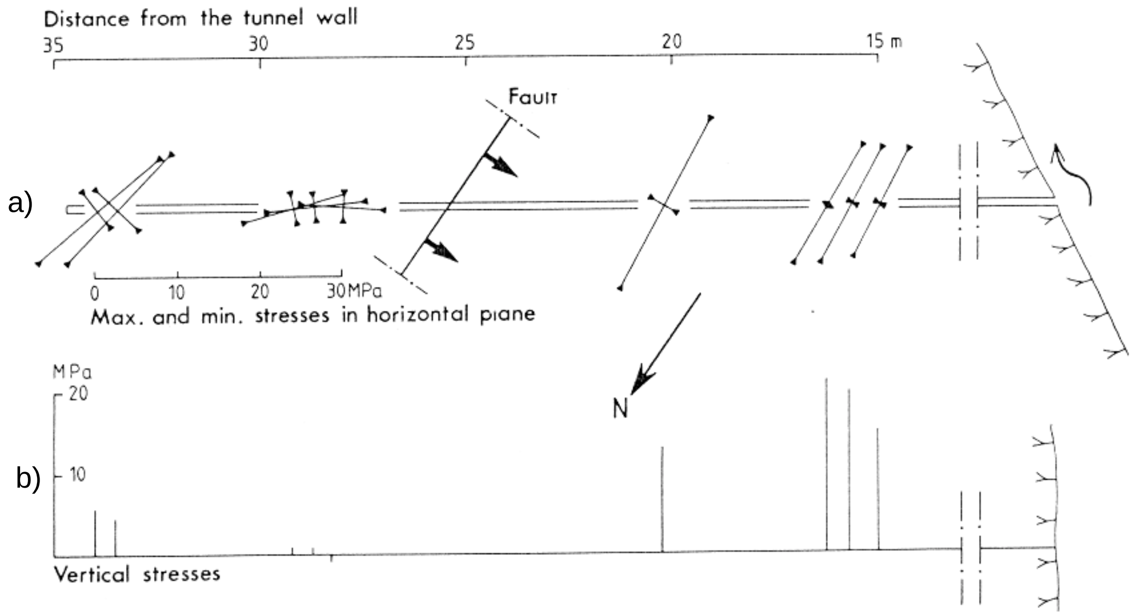

Figure 3.5.12 Changes in a) stress direction and b) magnitude across a fault (Martna and Hansen, 1986)

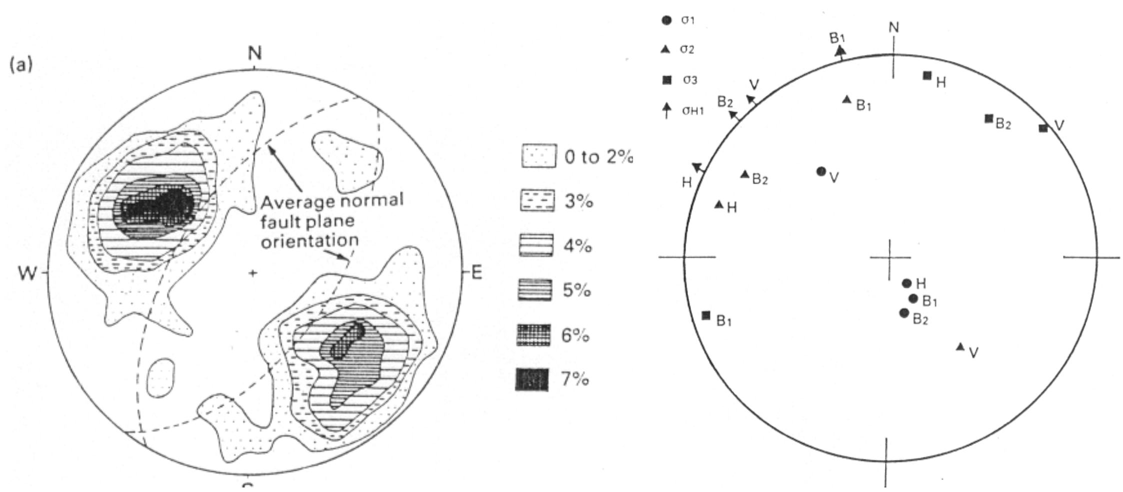

Figure 3.5.13 Directions of faults and principal stresses in Klerksdorp district (after Gay et al, 1984)

Table 3.5.1 Stress states and k-ratios in Klerksdorp mines (Gay et al, 1984).

	σV	σH	σh	kH	kh
Vaal Reefs 1868m	53	53	39	1.00	0.74
Buffelsfontein 2166m	67	56	26	0.84	0.39
Hartebeesfontein 2340m	66	53	40	0.80	0.61
Buffelsfontein 2560m	62	48	34	0.77	0.55

Handley (1987) monitored the stress state across the Elf fault as it was approached by mining. The fault is a steeply dipping reverse fault with a strike of 30 degrees East of North and a dip of 75 degrees to the South East. The fault was observed to have a down throw of 36 m to 40 m to the West. The South West Dyke, striking parallel to the fault was observed about 60 m to the West of the fault. The strata are displaced by the Elf fault and intruded by the South West Dyke. The Georgette Dyke, striking about 15 degrees south of East, with a down throw of 24 m to the north, intersects these features about 300 m to the North East of the monitoring site. The initial stress state was determined from measurements from two different researchers, each measurement site being about 3 km on either side of the fault. The measured stress states and the fault plane are shown in Figure 3.5.14.

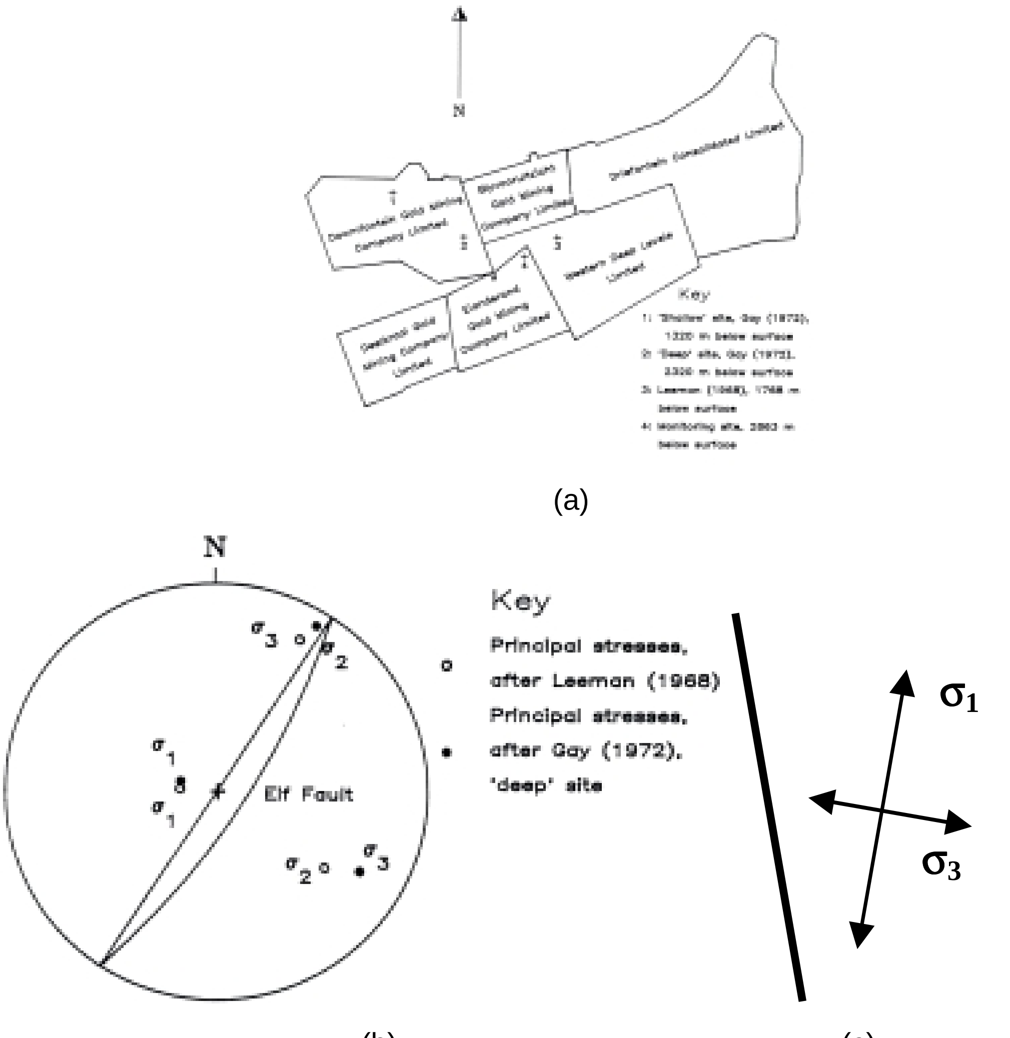

Figure 3.5.14 a) Measurements sites in the Carletonville area b) lower hemisphere stereo plot of the stress states on either site of the Elf fault and c) schematic of two-dimensional section through the fault (after Handley, 1987)

The intermediate principal stresses from the deeper site are aligned along the strike of the fault plane. This agrees well with the Mohr Coulomb theory of normal fault development (e.g. Price 1966). The fault is steeply dipping and the major principal stress has rotated in the opposite direction to the dip of the fault. This is expected from the numerical analyses shown in Section 3.5.1. The plunge of the principal stress is approximately the same magnitude as the dip of the fault, but is in the opposite direction. The minor principal stress is almost perpendicular to the fault. The relative position of the minor and intermediate principal stresses is swapped around between the two sets of data. This is probably due to the orthogonality of the two major structural trends (See Figure 3.5.14b) and/or due to the different positions relative to the fault, as demonstrated in the numerical model shown in Figure 3.5.9. Measurements of the change in stress state due to mining towards this fault indicated that the stress increased, but did not cause the fault to slip. The induced stresses were transmitted across the fault.

3.6 Effect of Dykes on stress state

3.6.1 Theoretical studies of the change in stress state due to dyke formation

A simple model for the effect of thermal stress and overburden pressure on the formation of residual stresses in a Dyke was presented by Gay (1976). To obtain stresses parallel to the dyke plane, the dyke - host rock system is modelled as a three layer plate, assuming that the rocks are homogeneous, isotropic linear elastic materials, and that the thermal properties are independent of temperature, there is no lateral restraint of the plates and the temperature only varies perpendicular to the dyke plane. Thermal stresses parallel to the dyke are calculated to be $\sigma_{th} = \alpha E \Delta T / (1 - \nu)$. Tensile thermal stresses, shown schematically in Figure 3.6.1, are induced in both the dyke and the host rock by cooling of the dyke material. The magnitudes of the tensile stresses are greater than the rock strength, which implies that joint sets are expected, and observed, parallel and perpendicular to the plane of the dyke in both the dyke and the host rock. The state of the dyke margin is important in determining the transfer of stresses from the hot dyke to the surrounding rock. If slip occurs on the margin then the stresses in the surrounding rock will be less affected by the dyke.

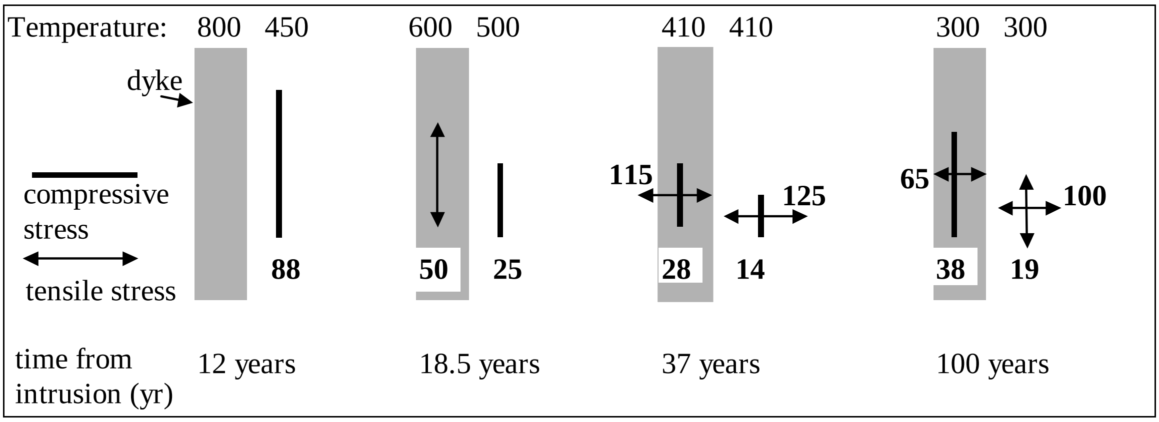

Figure 3.6.1 Schematic of the estimated changes with time of thermal induced stresses in and near a dyke (Gay, 1979). (Initial temperatures are 300°C in quartzite and 1100°C in dyke, stress magnitudes given in bold type)

Delaney *et al*. (1986) discuss a series of simple models for dyke intrusion, based on a pressurised mode I crack in an elastic medium. The magma pressure P_m is assumed to depend on the relative magnitudes of the major, s_H and minor s_h horizontal stresses. Thus, if $s_h = s_H$ then P_m is greater than the overburden stress (ρgz). Otherwise, if $0.5\ \rho gz < s_h < \rho gz$ and $\rho gz < s_H < 1.5\ \rho gz$ then the magma pressure is between the two horizontal stress magnitudes. The stresses induced ahead of an advancing tip are shown to generate joints in the host rock ahead of the advancing dyke tip and parallel to the direction of growth. The dyke advances when the high stress concentration at the dyke tip creates a tension crack, which bisects the region between the joints ahead of the dyke. This process will alter the in-situ stress state around the dyke and could result in a jointed or fractured dyke interface, which can allow relative displacements between the dyke and the country rock. Assuming that joint formation occurs at a specific tensile stress T, the pressurised crack model predicts a distance of potential jointing r_f such that

$$r_f / a \leq \tfrac{1}{2}[(P_m - S_h)/(T - S_h)]^2 , \qquad (3.6.1)$$

where a is the half-length of the dyke. If pressure gradients exist in the magma due to viscous flow, the driving stress and hence the distance of potential jointing will be reduced. This distance will be altered by flow gradients within the magma. The joint set ahead of the dyke is equivalent to the fracture process zone around a conventional crack.

Peacock and Marret (2000) investigated a number of dyke profiles in the USA and found, as shown in Figure 3.6.2, that they seldom resemble the shape of an ideal open crack as assumed by Delaney *et al* (1986). The stress state, therefore, would be expected to vary from the ideal distribution predicted by the model. Modelling of a dyke as a pressurised crack also suggests that once the crack contains a critical volume of fluid, it will rise towards the surface (Weertman, 1980). The crack surfaces will close behind the rising crack, so that the crack length remains constant. This model of Weertman (1980) apparently does not account for the volume and stiffness of the magma intruded into the crack.

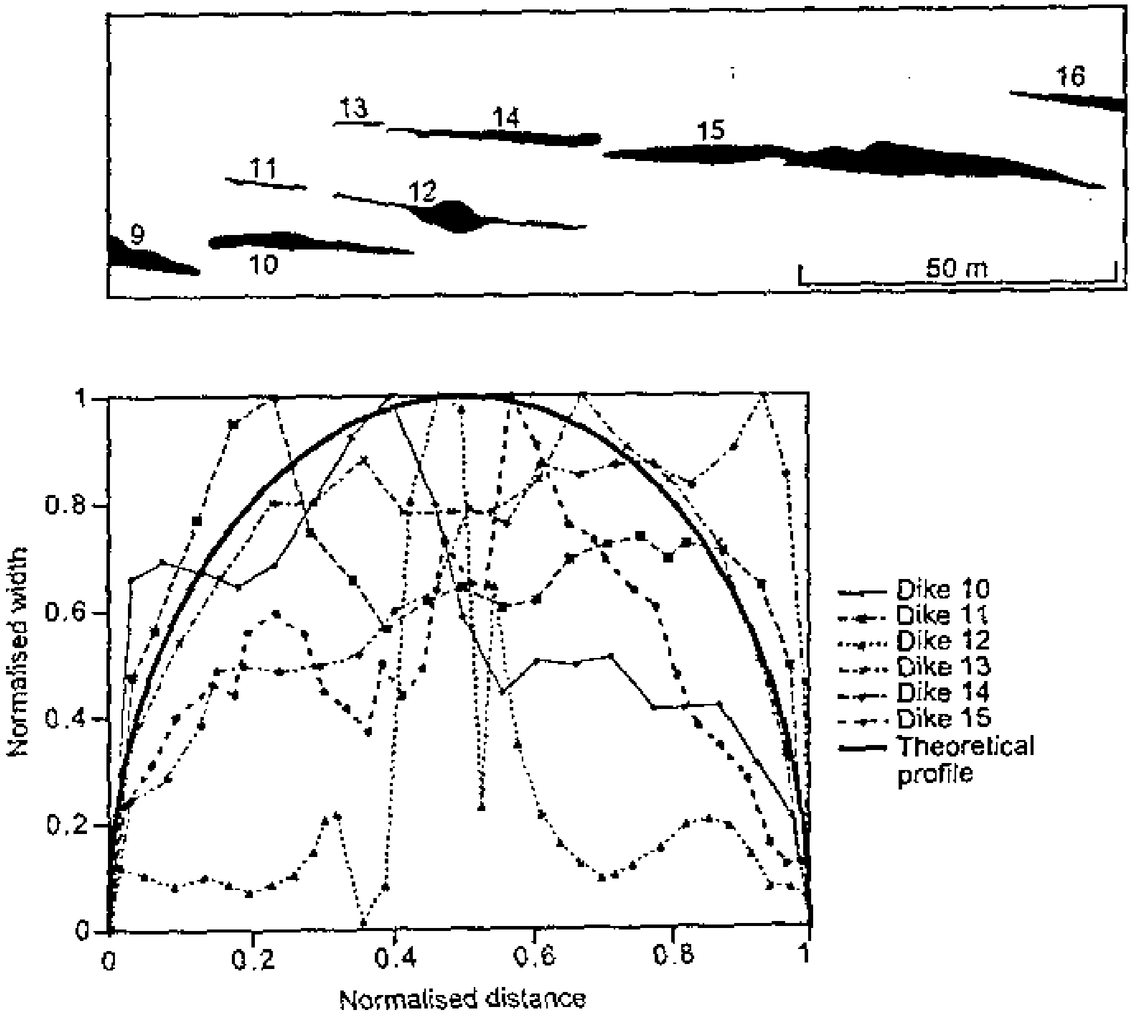

Figure 3.6.2 Observed and theoretical profiles of dykes plotted as normalized width and normalized distance along the fault (Peacock and Marrett, 2000)

A model that could be used to describe the dyke formation processes is that of a hydrofracture containing a proppant material (e.g. Papanastatiou, 2000). The proppant would prevent closing of the crack and would simulate the solidifying magma that prevents total closure of the crack. A plastic damage zone extends to the side of the developing dyke, as shown in Figure 3.6.3. The extent of the damage zone corresponds to the zone of rock affected by the dyke intrusion. The stress in the plastic zone would be essentially constant and equal to the yield stress of the rock mass. The extent of the zone will depend on the deviatoric stress, the rock strength, the elastic properties and the propagation pressure. These parameters are generally not well constrained and will vary in any specific situation so it is infeasible to produce a more general model of dyke-induced stresses.

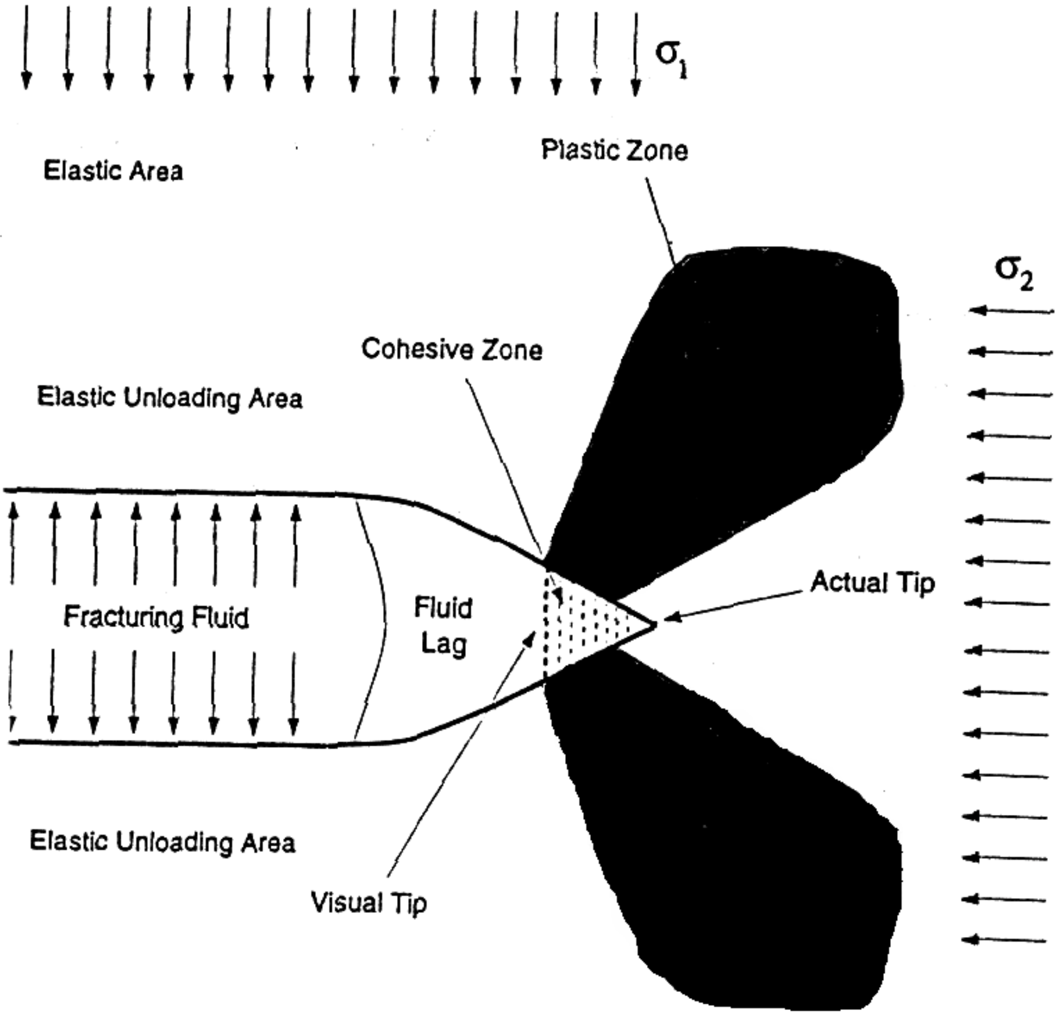

Figure 3.6.3 Geometry of a plane strain hydrofracture (Papanastasiou, 2000) simulating a dyke intrusion process

The intrusion mechanism of a particular dyke can be postulated from geological maps (Delaney *et al*., 1986), because dykes tend to strike parallel to the least principal compressive stress at the time of intrusion. If dykes in a particular area are of the same age and different strikes, either the formation process was insensitive to the direction of least principal stress or the stress state was nearly homogeneous at the time of emplacement. Dykes of similar strike can be assumed to have invaded a joint set, which provided planes of weakness in the rock fabric. When adjacent joints, and dyke-parallel regional joints, are absent, it can be assumed that the dyke created it's own fracture. In this case, the path of the dyke intrusion will be perpendicular to the original least compressive principal stress. Interpretation of the present in-situ stress from the dyke directions presents problems because the dyke intrusion will have altered the initial stress state.

Significant stresses are induced by the temperature differences, but these only affect a narrow region adjacent to the dyke. Whilst the magma is fluid, all heat transfer to the country rock occurs by conduction and the thermal penetration depth is calculated to be $x_1^T = 2.3(kt)^{1/2}$ where k is the thermal diffusivity and t is time. For Witwatersrand Quartzite, an average value of $k=2.5x10^{-6}$ m^2/s (Tucker, 1968). The thermal penetration distance with time is given in Table 3.6.1. Delaney *et al*. (1986) suggest that the magma will only remain fluid for about 10 hours resulting in a thermal penetration to 0.7 m. Pore pressure increases in water trapped within the rock can also lead to hydraulic fracturing adjacent to the dyke. In this case, the affected distance is estimated as $x_1^p = 2.3(wt)^{1/2}$ where w is the hydraulic diffusivity. Hydraulic fracturing due to intrusion of the lava affects a larger area than thermal fracturing, and was estimated to be about 40 m.

Muller and Pollard (1977) modelled a dyke in plan, as a pressurised cylindrical hole in an elastic plate. A nearby mountain range, which forms an interplate zone, was modelled as a rigid boundary. The deformation near the dyke was considered to be non-linear and governed by thermal effects. However, the elastic assumption was accepted as an approximation to permit calculation of the stresses at some distance from the dyke, assuming the stress is uniform over regions of about 1 km. The analysis demonstrated that the directions of the dyke swarm extending away from the main dyke follow the trajectories of the maximum horizontal principal stress.

The stresses induced within a dyke during cooling can be interpreted by analogy to the manufacture of glass. Cooling will occur from the surface inwards and the core will deform plastically to conform to the solidifying surface (Almen and Black, 1963).

Subsequent cooling of the core will induce a residual stress distribution within the dyke. Thus, there will be a distribution of residual stresses across the width of the dyke, but the resultant stress will be in equilibrium with the external loading. The different cooling rates can lead to a variation in grain size within the dyke, with finer grained rock in the dyke margin, which cools most rapidly (Jeffery, 1975). Disturbance of the applied stress state by a mining excavation could result in failure of the dyke material in a manner which would be completely different from that predicted in a numerical analysis in which the formation processes were neglected.

Table 3.6.1 Thermal penetration distance with time for quartzite based on Muller and Pollard (1986) and diffusivity $k=2.5x10^{-6}$ (Tucker, 1968)

Time after intrusion	Thermal penetration distance
1 hr	0.22 m
5 hr	0.48 m
10 hr	0.69 m
100 hr	2.18 m
1 year	20.48 m

A discrete element model was used to investigate the effect of dyke emplacement on the stress field in the horizontal plane by Sengupta *et al*. (1997) and a result is shown in Figure 3.6.4. The magnitude of the rotation of the angle of the principal stress was found to depend on the k-ratio (as shown in Figure 3.6.5a) and the angle of the major *in situ* principal stress to the dyke (as shown in Figure 3.6.5b).

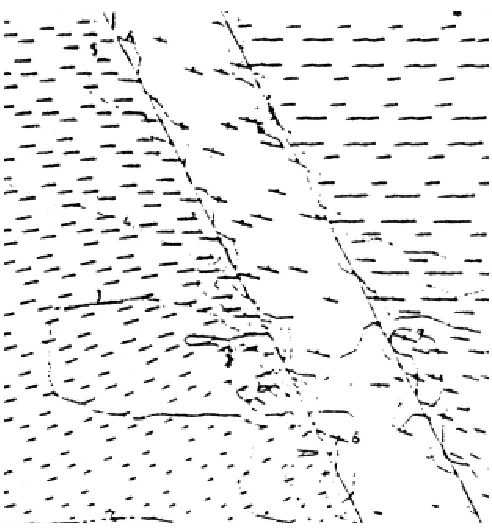

Figure 3.6.4 Effect of a dyke on the horizontal stress state (Sengupta et al., 1997)

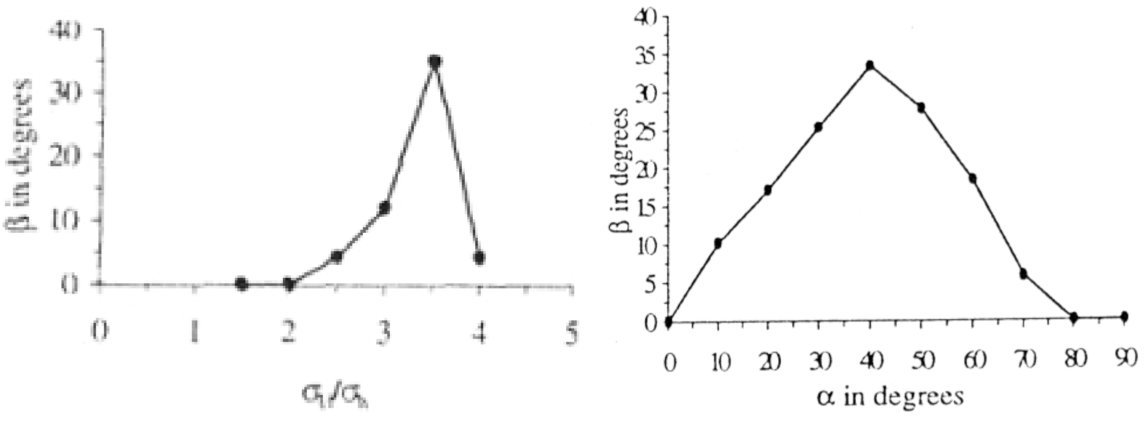

(a) (b)

Figure 3.6.5 Influence of a) k-ratio and b) strike direction on rotation of horizontal stress due to emplacement (Sengupta et al, 1997)

No modelling has been done locally for the extensile tectonic environment existing in South Africa. Thus, for this project, the DIGS program was used to develop a model of the stress state induced by a dyke that dips at a steep angle of 80 degrees. The dyke expansion causes an increase in stresses close to the dyke and the dip of the dyke causes rotation of the major principal stress (assumed to be initially vertical), as shown in Figure 3.6.6. The stress concentration at the lower portion of the dyke can be expected to be reduced due to failure and melting of the rock mass.

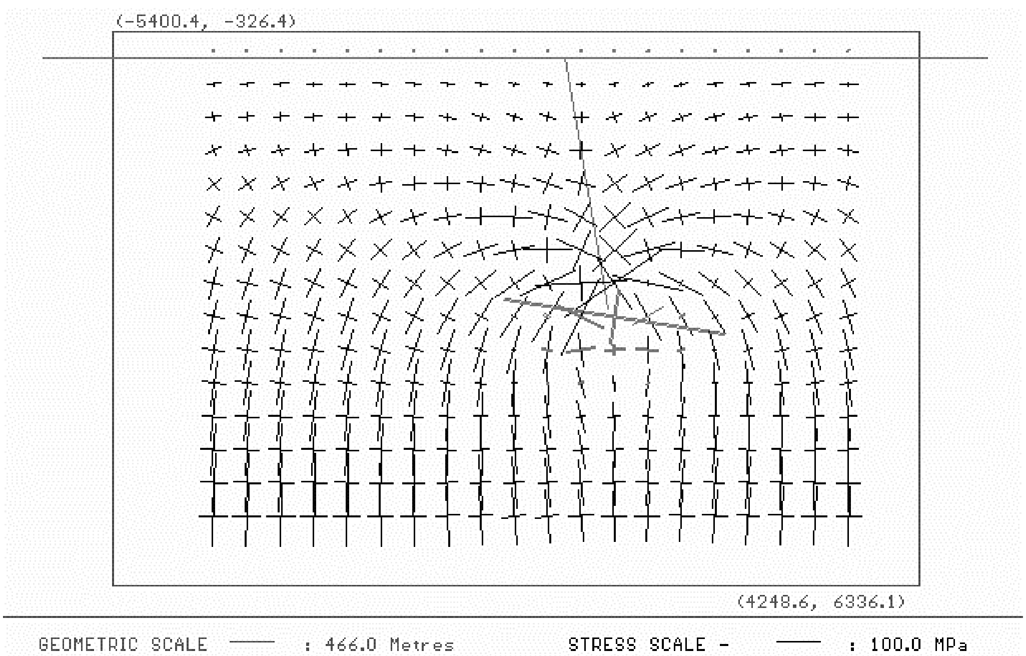

Figure 3.6.6 Stress state due to a steeply dipping dyke with a forced opening of 10 m

3.6.2 Measurements of the change in stress state due to dyke formation

The requirement to measure the stress state in completely virgin ground conditions to provide input information for numerical modelling implies that there has been very little work done on measuring the stresses within and near dykes. Gay (1980) studied a dyke.

A comparison of the stereoplot of dyke directions with a set of four measurements in the Klerksdorp region is shown in Figure 3.6.7. The dyke directions do not appear to correlate with the stress directions. The theory suggests that the dykes will be emplaced in the direction that is along the direction of the intermediate principal stress and perpendicular to the minor principal stress. The two sites that are reported to be associated with dykes indicate that the intermediate principal stress is sub-perpendicular to the majority of the dykes. This is either due to the dykes in question not being part of the main group, or more likely that the stress state has altered since emplacement. The intrusion of the dykes may well have increased the stress normal to the dyke to such an extent that it became the intermediate principal stress. This effect could be compounded by stress relief due to erosion. Dyke cooling could also have altered the stress state.

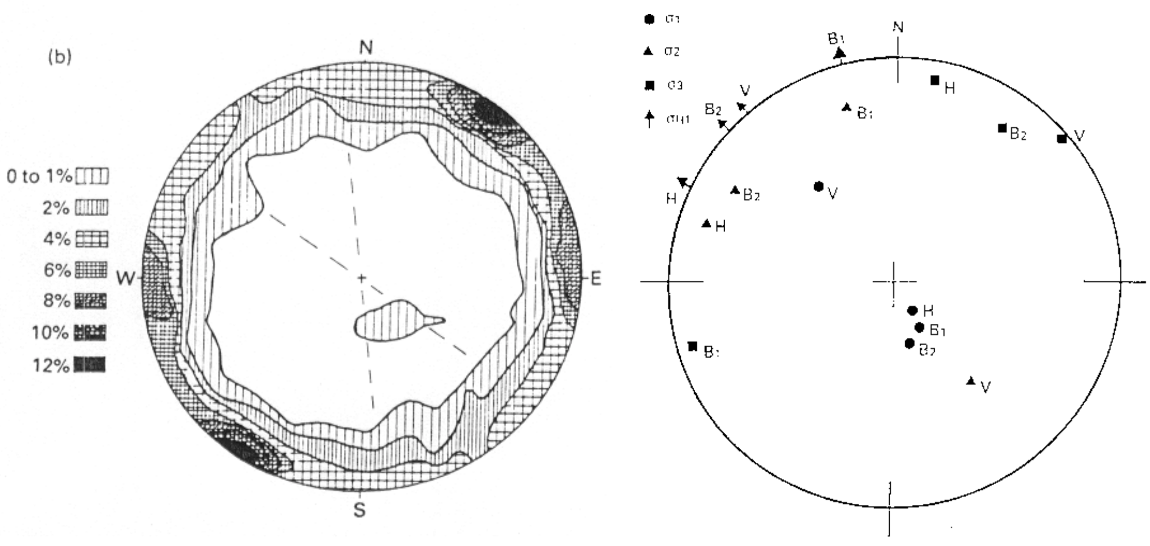

Figure 3.6.7 Directions of dykes and principal stresses in the Klerksdorp district (after Gay et al, 1984)

A study of the dyke directions in the main mining areas in South Africa was undertaken by McCarthy *et al*. (1999). The results are shown in Figure 3.6.8b. The correlation with direction of dykes intruded during the Pilanesburg era can be observed by comparing the stereoplots with the main dyke directions, shown in Figure 3.6.8.a, and described by Trusswell (1980).

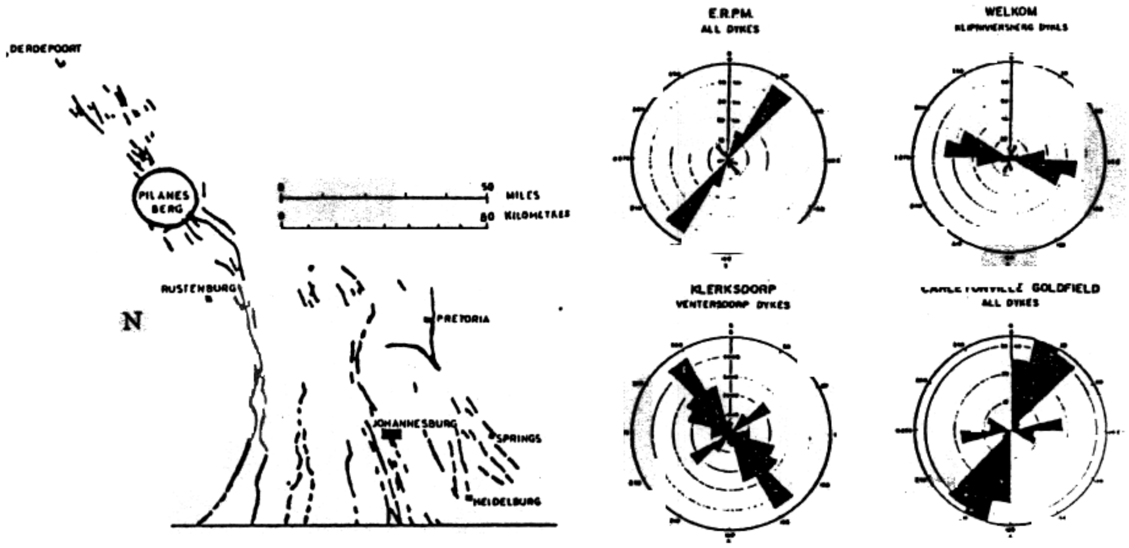

(a) (b)

Figure 3.6.8 (a) Dykes associated with Pilanesburg igneous event (Trusswell, 1980) and (b) dyke directions in four major mining regions (McCarthy et al, 1999).

An intrusive ore-body is not common for South African gold or platinum mines, but is a common feature overseas. Such an ore-body can also be considered as a dyke in terms of the changes to the stress state. A case study was performed by Leijon (1986) to investigate how the stress varies around such an orebody. The results are shown as stereoplots superimposed on the plan view of the orebody in Figure 3.6.9.

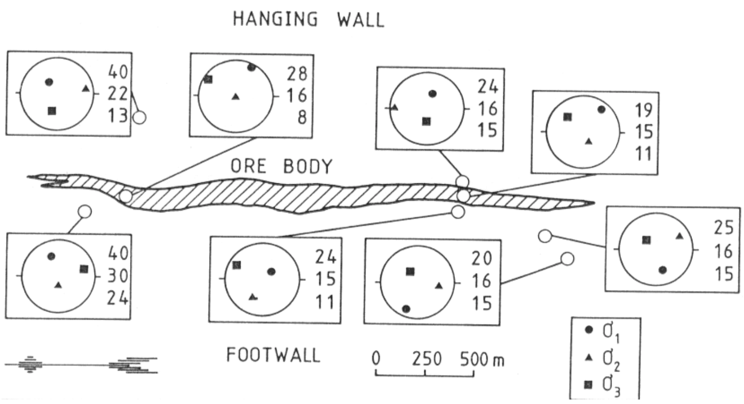

Figure 3.6.9 Stress state measured around an intrusive orebody (Leijon, 1986)

A local study investigated the stress near a dyke (Coetzer, 1972). The data was reported in the collation of stress measurements by Stacey and Wesselloo (1998). Detailed analysis of this case study is not possible due to the lack of information about the exact positions of the measurements relative to the dyke. It would appear however, that the stress in the dyke was relatively high in comparison to the stress in the neighbouring quartzite. Considerable difficulty was experienced in obtaining solid core for good measurements, due to the fractured nature of the rock, and discing of the extracted core. A plot of all the measurements for each of the three holes using the CSIR INSITU visualization software is shown in Figure 3.6.10. There is reasonable agreement in magnitude and direction between the measurements in each borehole. This provides some evidence that the differences in magnitude relate to the stress state and not to test procedures. The quartzite is assigned a very high modulus of 104 GPa. As this is an upper bound for most quartzites, it can only be anticipated that any errors would reduce the stress outside the dyke relative to the stress inside the dyke.

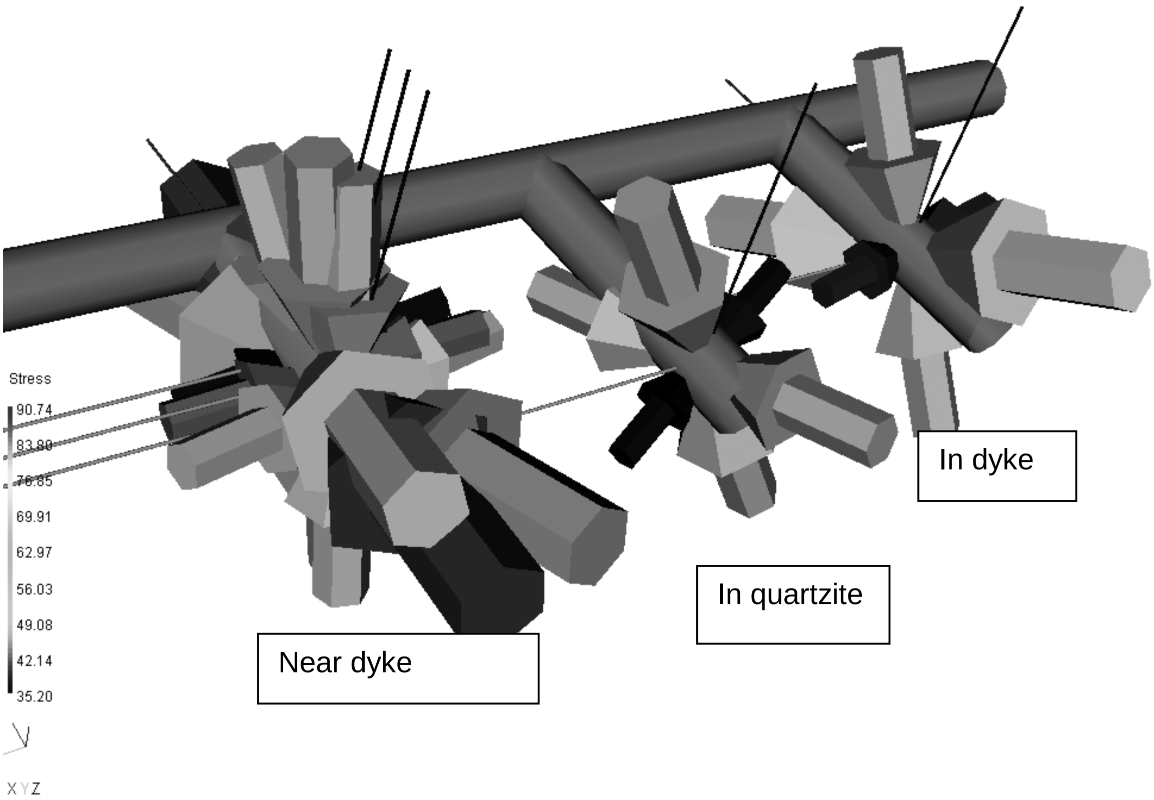

Figure 3.6.10 The stress state measured within and nearby a dyke on Durban Deep Gold Mine (Coetzer, 1982)

3.7 Effect of Jointing on stress state

The presence of jointing can significantly affect the stress state in a block of rock. A detailed study was performed by Brown *et al*. (1986) by cutting vertical slots into a jointed rock mass to separate a block of side length 2.5 m. A known pressure was applied to the surfaces of the block by inserting flatjacks into the slots. The stress state in the block was measured at a number of different points using two methods, namely, the USBM borehole deformation gauges and the Lulea Strain gauge. The methods produced similar stress states, as shown in Figure 3.7.1, but indicated that there were considerable rotations of stress within the block. Deviation in stress were also noted thorough the vertical thickness of the block. On average, the directions were consistent with the applied loads. The differences in stress at points in the block tended to decrease with increasing load, suggesting that the joints locked-up and that the material became more homogeneous. Models of the blocks were developed using finite element analysis to compare with the measured stresses. The numerical results were only partially comparable (see Figure 3.7.2), but indicated that the joints, joint model, variations in rock stiffness within the block and additional joints that formed decoupled blocks were all contributing factors to the stress state variations. *In situ* stress measurements nearby the block test site showed considerable variation in the stress due to jointing (Richardson *et al*., 1986). The standard deviation of measurements was almost the same as the mean of the stresses.

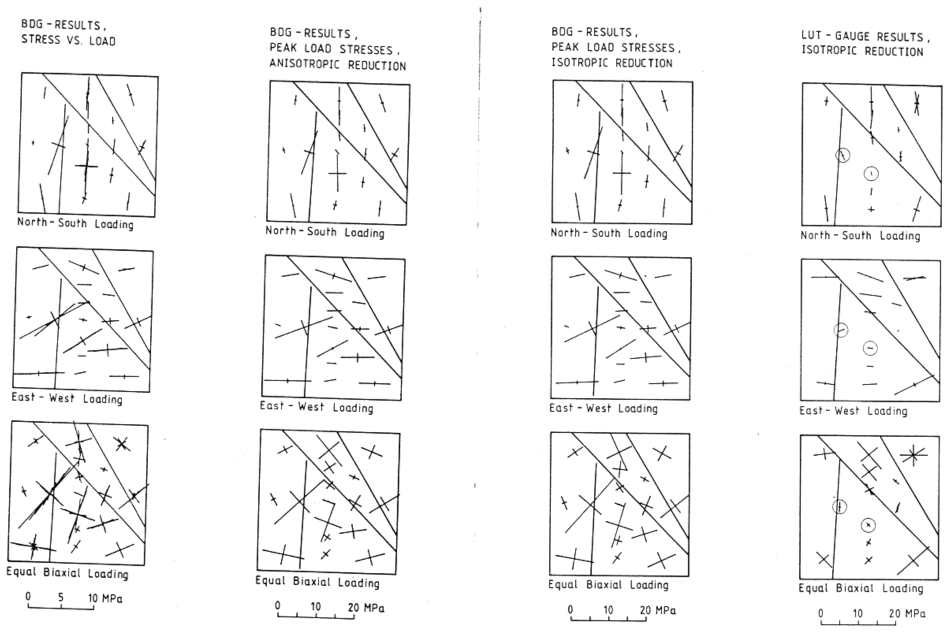

Figure 3.7.1 Stress states measured by different techniques in a jointed block loaded in situ (Brown et al, 1986)

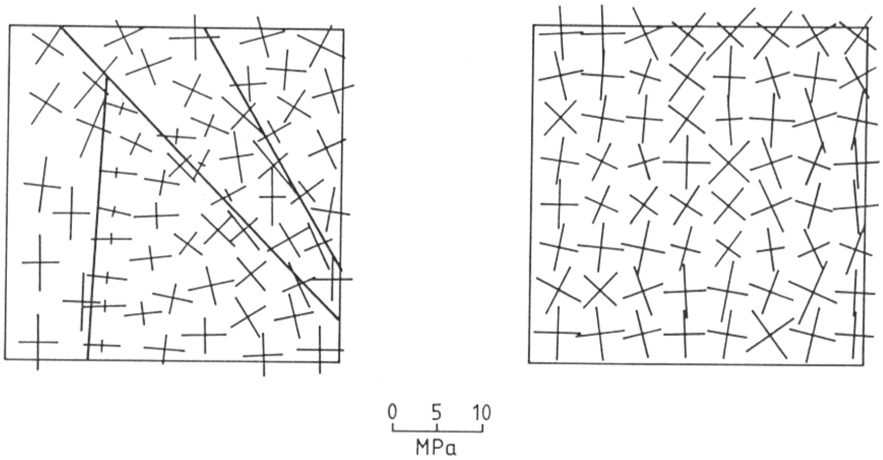

Figure 3.7.2 Stress states predicted by finite element analysis for a jointed block loaded in situ (Brown et al, 1986). a) discontinuous model and b) continuous model with varying elastic moduli

Lang *et al*, (1986) performed measurements at the URL test site in Canada and showed that the major horizontal stress direction was parallel to the strike of the most prominent fracture set at the site. Leijohn (1989) suggests that measurements of stress in jointed rock will tend to be over-estimates of the *in situ* stress state due to the loss of measurements in poor ground. The variability of the stress state should decrease with depth as consolidation of the rock mass should close the joints. Studies of numerous stress measurement results indicate that the relative standard deviation of measurements remains approximately constant with depth.

4 VARIABILITY OF STRESS STATE

4.1 Statistical description of the variability of the stress state

There are two main problems in providing a proper statistical analysis of the stress state in any particular mine. The first is that the stress is a tensor variable and must be treated differently from most standard statistical analyses where the data is scalar valued. Secondly, there is often very little data available due to the high cost and difficulty of obtaining measurements.

Normally, the stress is measured at a number of sites on a mine. As shown in Figure 4.1.1, each site will consist of a number of stress measurement tests. For a 3-D stress cell, such as the CSIR or CSIRO cell all these tests will be performed in a single borehole. For 2-D stress measurement techniques such as the doorstopper, hydraulic fracturing or three-borehole technique, a set of three non-parallel boreholes is required. The stresses measured in each test are then averaged to produce an average stress measurement for the site. The statistical interpretation of the results should be done for each test, for each site and for the large scale i.e. the mine or shaft (Leijon, 1986).

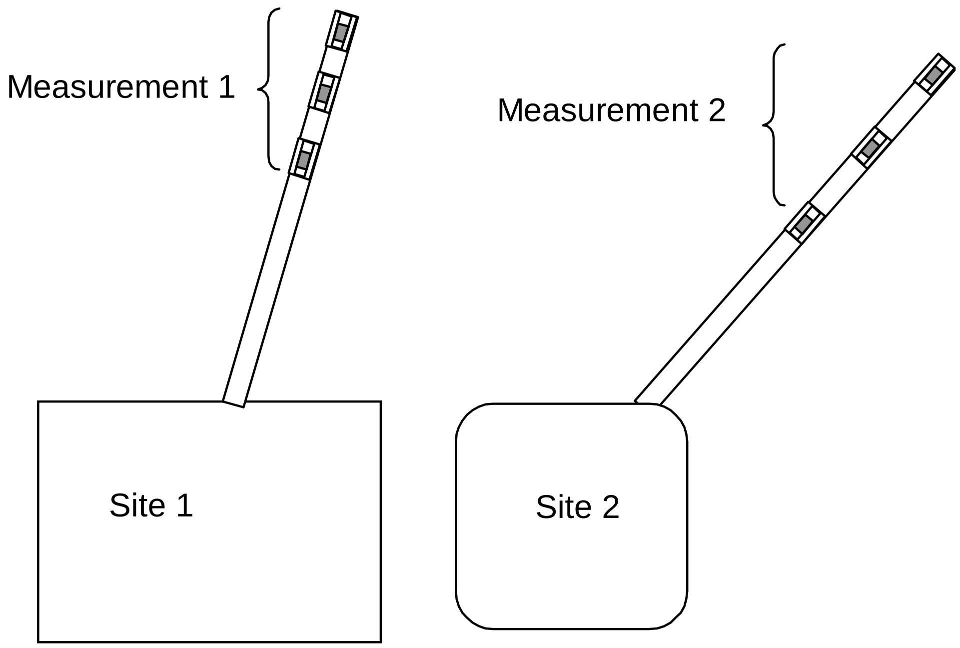

Figure 4.1.1 Schematic diagram to illustrate the concept of performing a number of tests to produce an average stress tensor at each site

At the scale of the individual test, a variety of errors can be introduced during the measurement process. Most cells provide redundant measurements and calculate the stress tensor based on a least squares process (e.g. Panek, 1966, Leeman, 1968). Experience suggests that the variation in stresses between individual tests is more often due to different rock conditions than procedural errors. Measurements of the borehole direction can also introduce errors. Often "wild outliers" may occur due to strain gauges that did not bond or wires that were broken. These are not rejected by simple statistical approaches and may be removed by an experienced practitioner with due consideration of the effects (Leijon, 1986). A single measurement error can cause a huge variation in the stress tensor. For example, Chambon and Revala (1986) report that the removal of one reading out of twenty doubled the stress tensor.

The error depends on the measurement technique (Hiramatssu and Ota, 1968). Leeman (1968) performed 10 tests in a single borehole and found that four were suspect. The mean value of vertical stress from all the reliable tests corresponded well to the expected overburden stress, but the standard deviation was of the order of thirty percent. Gray and Toews (1973) found that 89 readings had to be rejected out of a total of 783 measurements for their analysis of the stress state using a modified borehole deformation meter.

Each test measurement should be subjected to an equilibrium check that determines if the vertical stress is approximately equal to the overburden stress (Richardson *et al*, 1986). Unfortunately, there is no similar check for the horizontal stresses, but they can be considered with respect to measurements taken nearby.

The averaging procedure to obtain a mean stress at the site is given as follows (Hyett, *et al*., 1986) for n tests

1) Rotate all test measurements into a single global coordinate system (e.g. North, East, Down).
2) Sum the values of each individual stress component σ_{ij}^{k} from all the tests and divide by the number of tests, n.
3) The mean stress tensor is then given by:

$$
\sigma_{ij}^{AVE} = \begin{bmatrix} \sigma_{NN}^{AVE} = \left(\sum_{k=1,n} \sigma_{NN}^{k} \right) / n & \sigma_{NE}^{AVE} = \left(\sum_{k=1,n} \sigma_{NE}^{k} \right) / n & \sigma_{ND}^{AVE} = \left(\sum_{k=1,n} \sigma_{ND}^{k} \right) / n \\ & \sigma_{EE}^{AVE} = \left(\sum_{k=1,n} \sigma_{NN}^{k} \right) / n & \sigma_{ED}^{AVE} = \left(\sum_{k=1,n} \sigma_{ED}^{k} \right) / n \\ sym & & \sigma_{DD}^{AVE} = \left(\sum_{k=1,n} \sigma_{DD}^{k} \right) / n \end{bmatrix}
$$

4) The average principal stress and direction are calculated by calculating the principal stresses and directions of the mean stress tensor σ_{ij}^{AVE} using the standard eigenvalue calculation (see e.g. Hoek and Brown, 1980).
5) Investigate the distribution of the stress state by plotting the principal directions of all tests on an equal area stereoplot and contouring the distribution of directions (Vreede, 1982).

For this procedure, it is important to know the number of tests that are required to provide a given confidence level (Leijon, 1986). Vreede (1982) suggests that between 10 and 30 measurements are required to characterize the stress at a point and provide confidence in the variance of the results. In South Africa up to three tests are usually performed in each hole to limit the cost. The literature review indicated that in other countries, up to 10 tests are usually performed in each hole (Leijon, 1986, 1989, Richardson *et al*, 1986). Figure 4.1.2 shows the increase in confidence level obtained by increasing the number of tests. To do this, all tests were considered to be an independent sample of the normal distribution. A sequence of mean values for the borehole was obtained by including another stress reading. The 90% confidence levels for each distribution were obtained from Student's t-distribution. The mean and confidence levels are then plotted against the number of tests (or the distance along the hole). For the case shown in Figure 4.1.2, about 5 tests were required to obtain 14% accuracy and no further decrease in accuracy was obtained with further testing. The confidence levels of the angle of principal stress indicated considerably more variation (See Figure 4.1.3). These results agree with the findings of Wiles and Kaiser for a set of stress measurements in Canada. A statistical analysis of the data indicated little benefit in performing more than 10 tests at a site. In contrast, there was a very low confidence in the mean value for less than 5 tests.

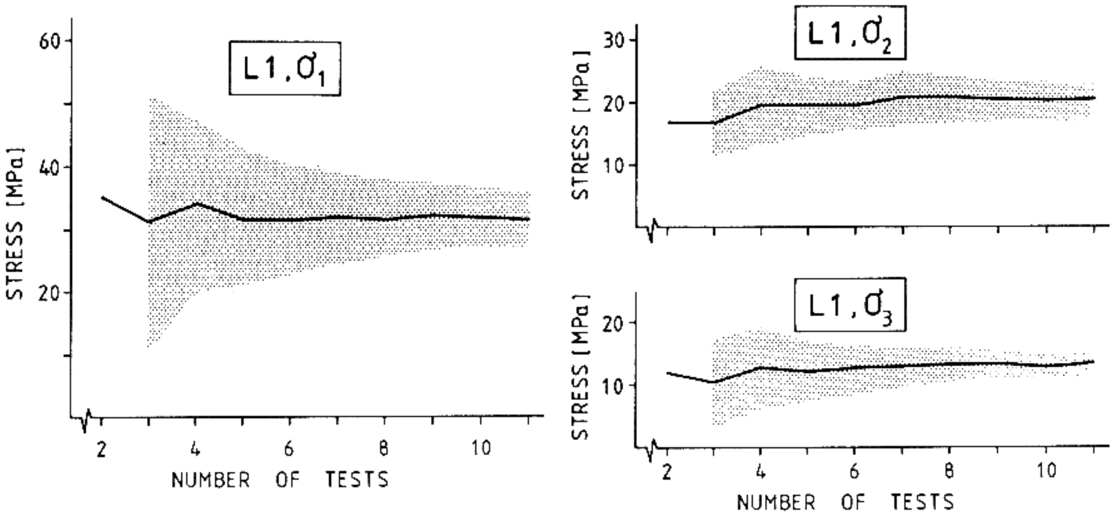

Figure 4.1.2 Variability of the stress magnitude with number of tests (Leijon, 1986)

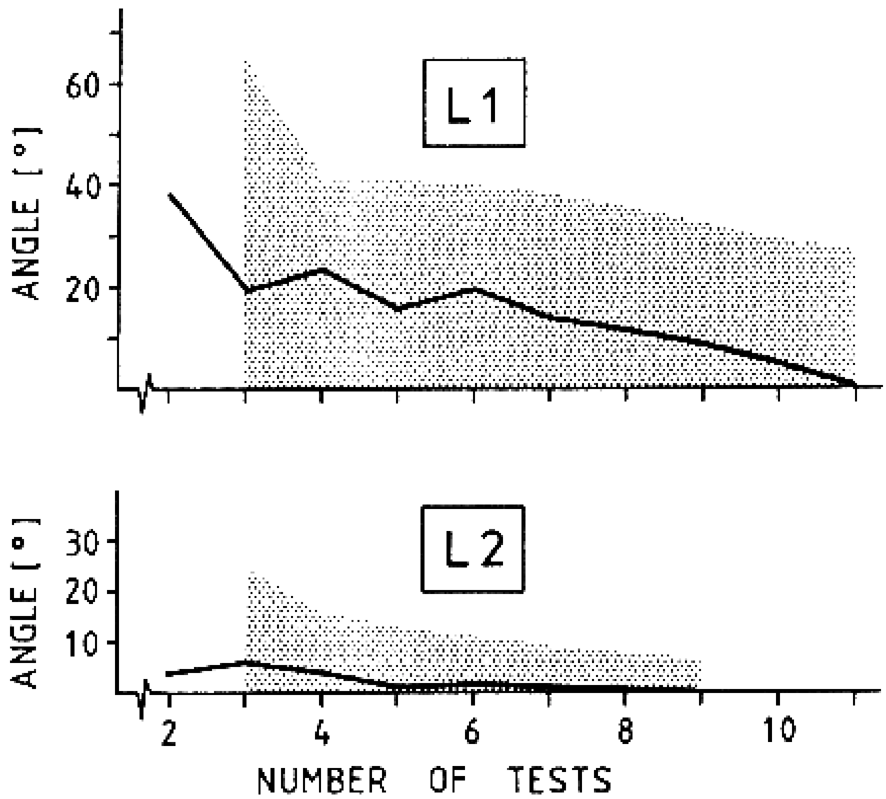

Figure 4.1.3 Variability of the stress direction with number of tests (Leijon, 1986)

It is important to determine whether the measurements are approaching a similar value or are describing a trend e.g. the stress concentration around the opening. This can be done by plotting the stresses against the distance from the hole. If the trend varies about a mean then the tests can be considered as samples of the *in situ* stress value. If the trend continually decreases, a stress concentration effect was most likely the cause and the trend can be extrapolated to a constant value (Leijon, 1989, Richardson *et al*, 1986). If the trend increases, changes in the geological structure should be investigated (Leijon, 1989). A statistical method for determining if the results are indicating a trend is to plot each value against the previous value in a scatter plot. If the results form an ellipse, there is a general trend and the angle of the major axis of the ellipse indicates the direction of the trend (Leijon, 1989).

Large-scale variations can then be evaluated by considering the mean stresses determined for each site. Leijon (1986) is of the opinion that no single stress tensor can be extracted to represent the stress state in a mine, or even on a single level. Extrapolation of measured stress states to new areas of the mine is considered to be dangerous. Measurements should be done close to critical excavations (Leijon, 1986).

Hansen and Moore (1990) proposed a statistical method for fitting a smoothed function to stress data to interpolate stress contours and trajectories over a large area. A compromise must be reached between the smoothness of the data and the agreement with the data points by selection of an input parameter. The method is very sensitive to the weighting functions used. The method shows promise, but requires large amounts of data. Two examples were given using borehole breakout data in the horizontal plane and considered 48 data points for the Californian case and 154 data points in the Canadian example. A further example, using the directions of 426 Dyke segments, was used to determine stress trajectories in the Spanish Peaks district of Colorado.

To investigate how the stress will vary within a similar tectonic environment, a finite element model was constructed of a section of the earth’s crust. The model was initially 20 km high by 150 km long. The layer was assumed to be composed of a strain softening material and contained a number of weaker patches to trigger faulting. Gravity was applied and then an extensional tectonic environment was simulated by extending the layer along the base. A complex normal fault structure formed when the plastic strains localized after sufficient extension. The top 5 km of the layer was then removed to simulate an erosion process and to investigate how the stress pattern would be altered. The final plastic strain pattern is shown in Figure 4.1.4.

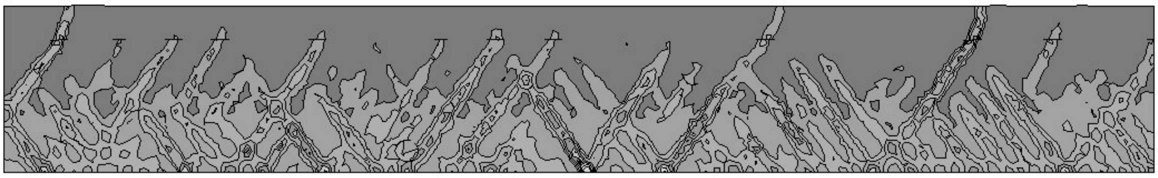

Figure 4.1.4 Result of finite element model of tectonic extension followed by erosion. The localised plastic zones represent faults

Figure 4.1.5 shows a section of the model and the associated principal stress state. The stresses have rotated away from the faults, as discussed in Section 3.5. As expected for a tectonic environment with normal faulting, the plunges of the principal stresses are distributed about the vertical, as shown in Figure 4.1.6. The erosion process causes additional rotation. The distribution of the k-ratio (ratio of horizontal to vertical stress) is shown in Figure 4.1.7. Initially, the distribution has a minimum at about 0.5 and most values are clustered near the minimum. After erosion, the vertical stress is reduced and so the minimum k-ratio increases. The variation in the values of the k-ratio also increases.

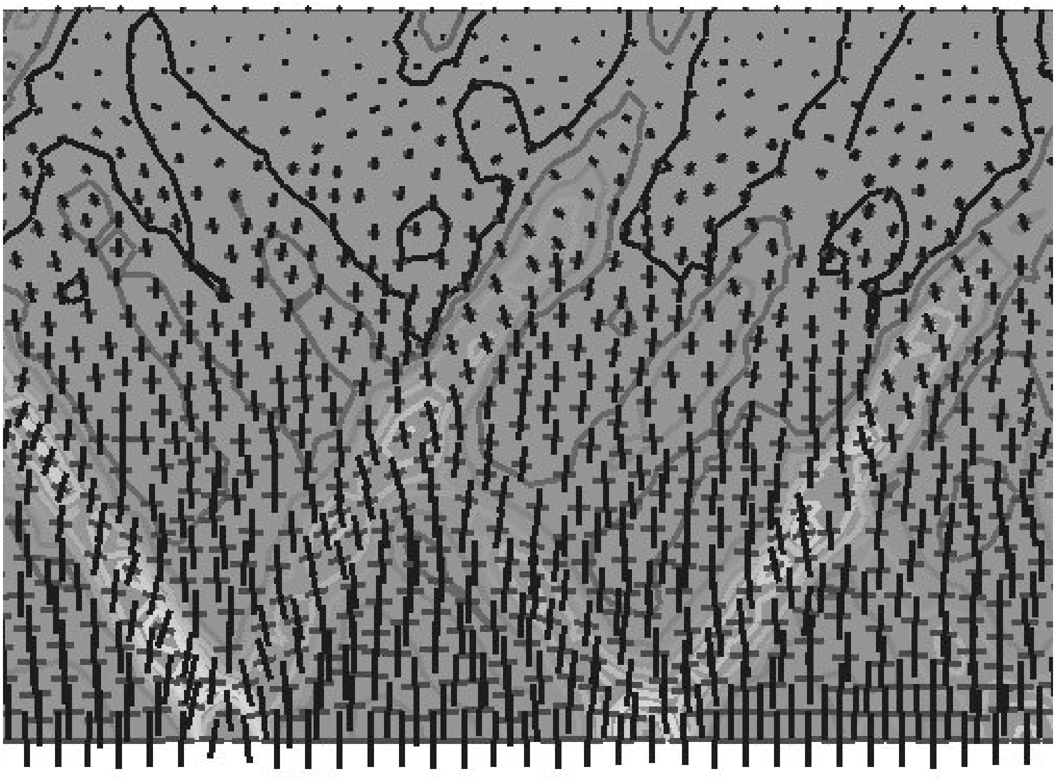

Figure 4.1.5 Result of finite element model of tectonic extension followed by erosion showing rotation of the stress state near the faults

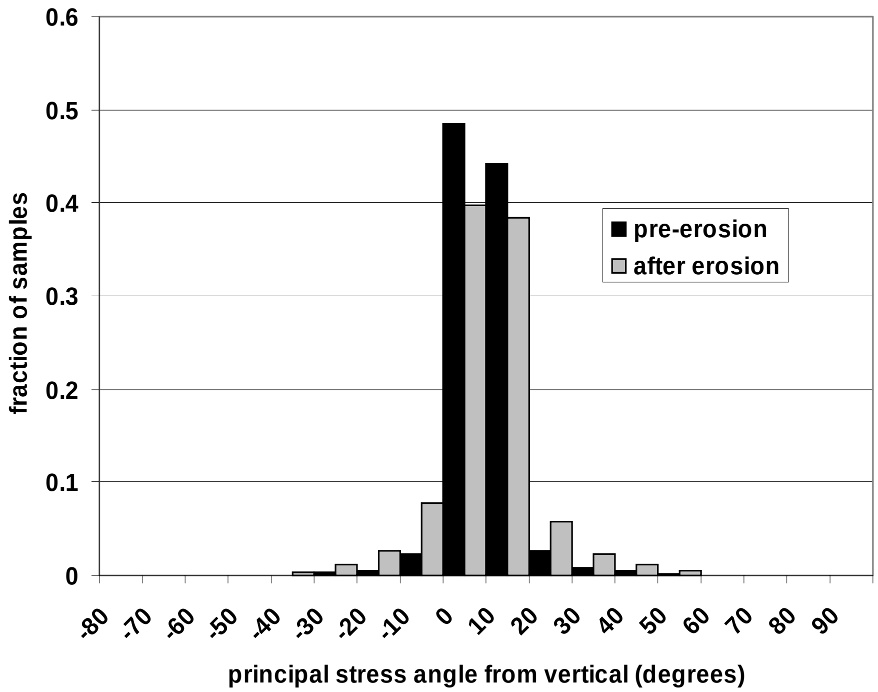

Figure 4.1.6 Result of finite element model of tectonic extension followed by erosion showing histograms of the plunge of the principal stress

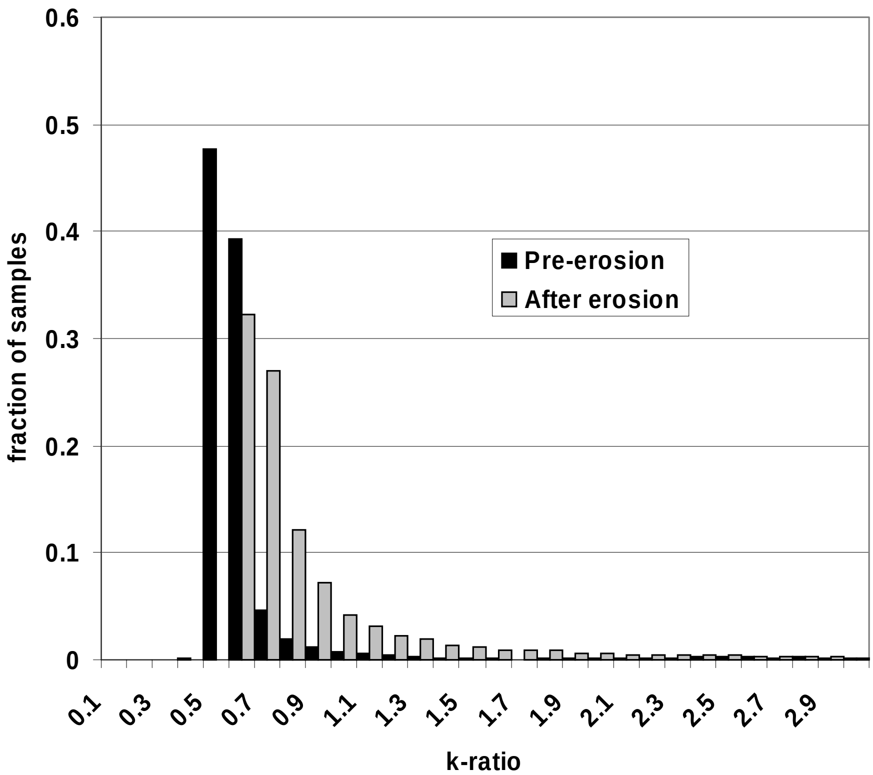

Figure 4.1.7 The distribution of k-ratios before and after erosion event in finite element model of tectonic extension followed by erosion

This example illustrates that the k-ratio may not be normally distributed but should have a minimum. The minimum will depend on the tectonic history and the material properties. As more tectonic events are imposed on the region, the k-ratios could be expected to become more normally distributed, as a normal distribution of properties can be considered to be the result of a number of independent random processes (Harr, 1977).

As a further example, the variability in the horizontal stress state induced in the area of a single mine shaft due to the most significant fault and dyke events was studied using the DIGS boundary element program. The sequence of dyke intrusions and faults is shown schematically in Figure 4.1.8. The numbers indicate the order in which the events were imposed, and do not necessarily indicate the real historical order. The final induced stress state is shown in Figure 4.1.9. Considerable rotations are observed and the stress state is enhanced and reduced at different places. Very high stresses are induced near intersections, but these may be numerical artefacts. This example serves to illustrate how variable the stress state may be and that the design of an excavation such as a longwall stope must be able to take into account considerable variability within a short distance.

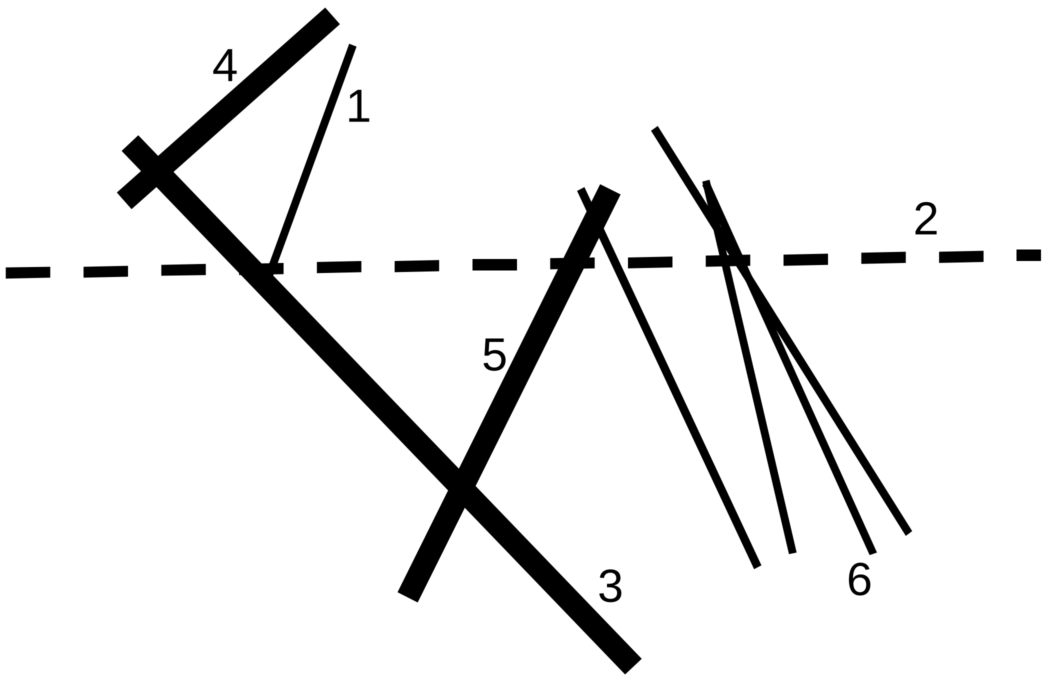

Figure 4.1.8 Schematic of plan of shaft geological structure showing sequence of structural events applied in the DIGS model
(Thick lines indicate dykes with an opening of 100 m, thin solid lines indicate dykes with an opening of 10 m and the dotted line indicates a fault with a slip of 200 m. The numbers indicate the analysis sequence)

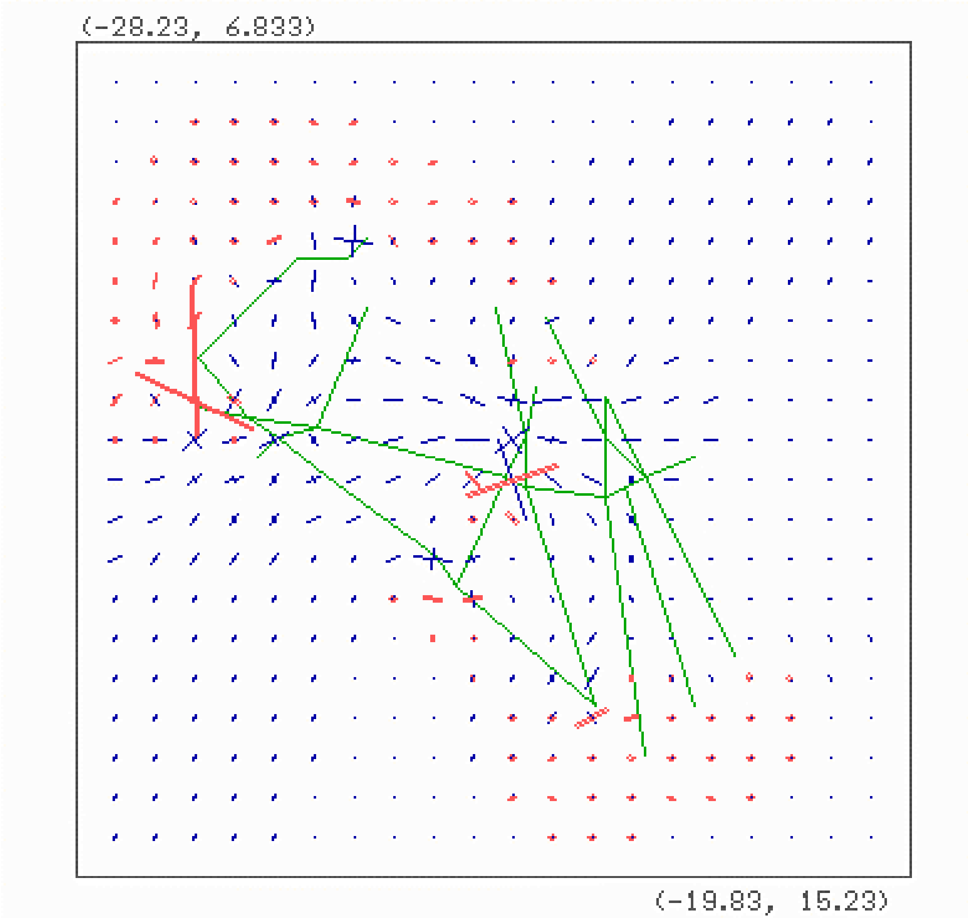

Figure 4.1.9 Results of DIGS model indicating the variability of the stress state induced by geological features over the extent of a single shaft

4.2 Quantification of the variability of the stress state in South Africa

A short study was done to quantify the variability of the stress state in South Africa from a set of published measurements. The measurements were collated by Stacey and Wesselloo (1998) as part of SIMRAC project GAP 511. No attempt was made to check the data and measurements were used as recorded in the spreadsheet created as part of the project. The measurements were collated based on the province where the measurements were taken. The measurements associated with Gauteng (Central gold mining region), Klerksdorp, the Free State gold mines, the North West platinum mines and the West Rand gold mines were studied. The number of measurements was limited in most regions ranging from seven to 55. This made it difficult to evaluate the statistical distribution of the measurements in most of the provinces as at least 30 measurements are required (Statistica, 1999).

The mean and standard deviation of the major k-ratio, the minor k-ratio and the bearing of the major k-ratio are shown in Table 4.2.1 for each region. The interpretation of these results in terms of the initial stress state is discussed in GAP 511 and in Sections 2.2 and 2.3. What can be determined from Table 4.2.1 are the high values of the standard deviations in all cases. The angle of the major horizontal stress is especially variable. There is a difference between the averages in each region. This suggests that the different loading histories in each region lead to a similar average stress.

Table 4.2.1 Mean and standard deviation of major k-ratio, minor k-ratio and bearing of different regions in South Africa

Region	Average			Standard Deviation		
	major ratio (kH)	minor ratio (kh)	bearing (degrees from N)	major ratio (kH)	minor ratio (kh)	bearing (degrees from N)
Central	1.05	0.58	98	0.28	0.16	61
Free State	0.80	0.60	109	0.17	0.21	64
Klerksdorp	0.99	0.65	112	0.31	0.26	41
Mpumulanga	1.06	0.35	82	0.45	0.95	48
North West	2.28	1.00	93	1.28	0.39	46
West Rand	1.13	0.63	95	0.32	0.19	60

Histograms of the major k-ratio are presented in Figure 4.2.1 for each of the regions. These show how few measurements have been made in the mining regions. The variation in the major k-ratio is small for the gold mining areas, but a wide range of k-values have been measured in the Bushveld. Most of the distributions differ from the bell-curve of the normal distribution. The ability of a distribution to fit the data can be measured by the Chi-squared goodness-of-fit test (Harr, 1977), but has not been considered in this study.

The histograms of the minor k-ratios are shown in Figure 4.2.2. These appear to be more like normal distributions, but extend more towards the higher values of the k-ratio. This is expected as there is a lower limit to the k-ratio defined by the elastic material properties or failure on fault systems. The ratio of horizontal to vertical stress will increase closure to the surface and so it may be expected that the distributions have a significant “tail”.

The variations of the bearing of the major principal stress are shown in Figure 4.2.3 for each of the mining regions. The limited data implies that it is very difficult to define a conclusive trend of the major stress. The directions of the stresses in the North West appears to be uniformly distributed, possibly due to the stresses being oriented along the curve of the Bushveld Complex as shown in Figure 2.3.3. Peaks can be expected to exist that relate to the major directions associated with the North West – South East trend and the North East – South West trend of stresses as mentioned in Sections 2.2 and 2.3.

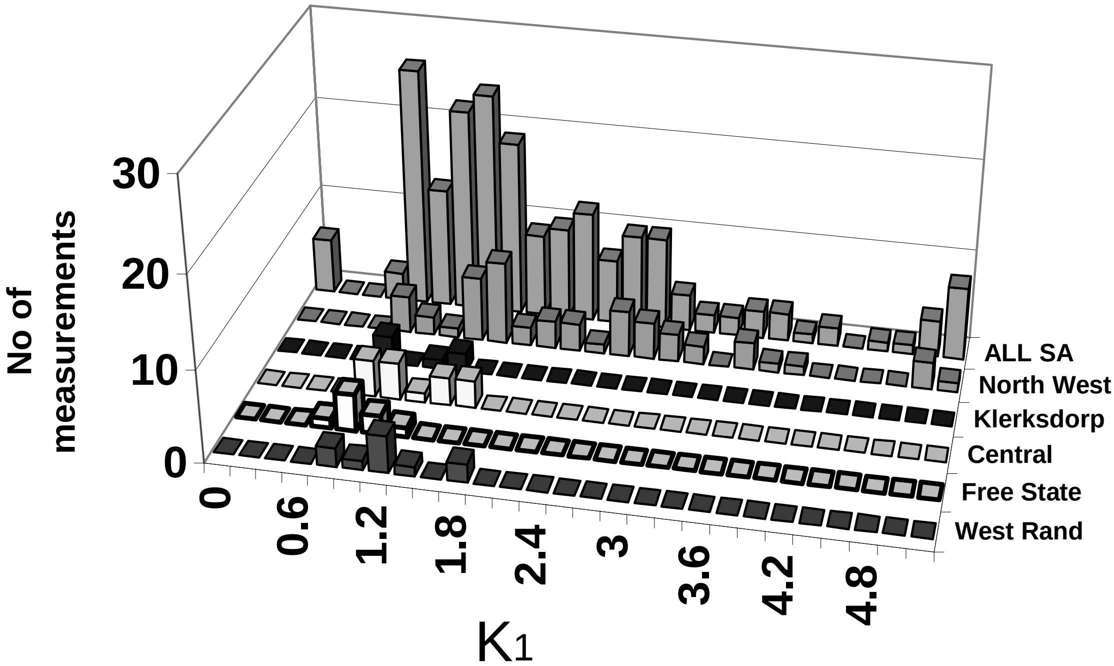

Figure 4.2.1 Variability of the major k-ratio for different regions in South Africa

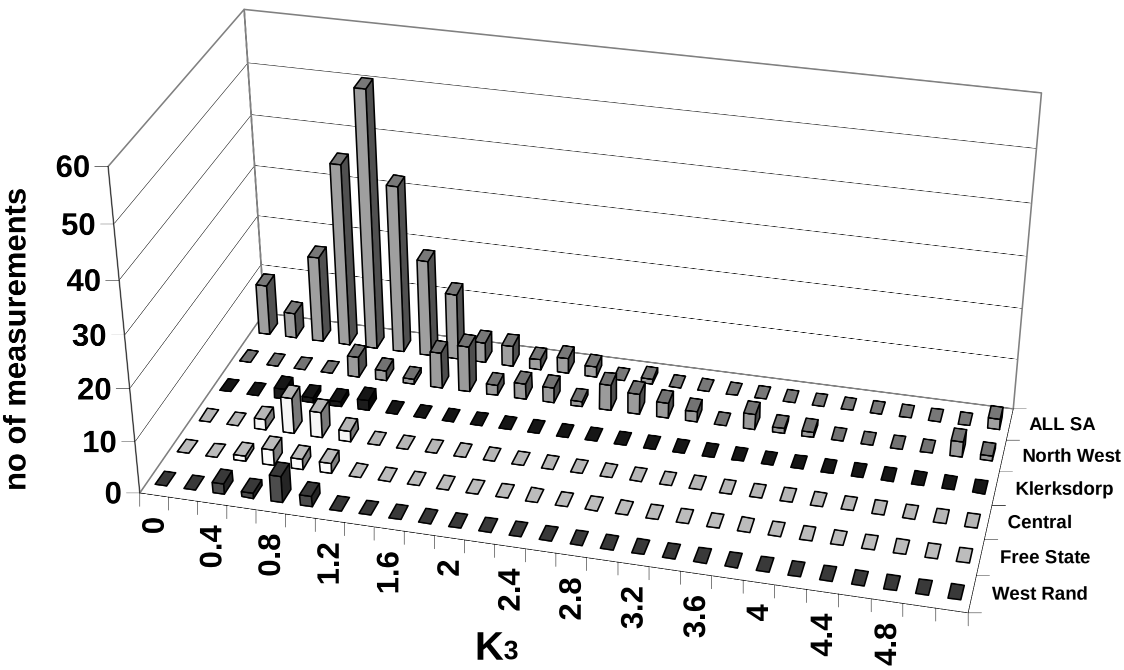

Figure 4.2.2 Variability of the minor k-ratio for different regions in South Africa

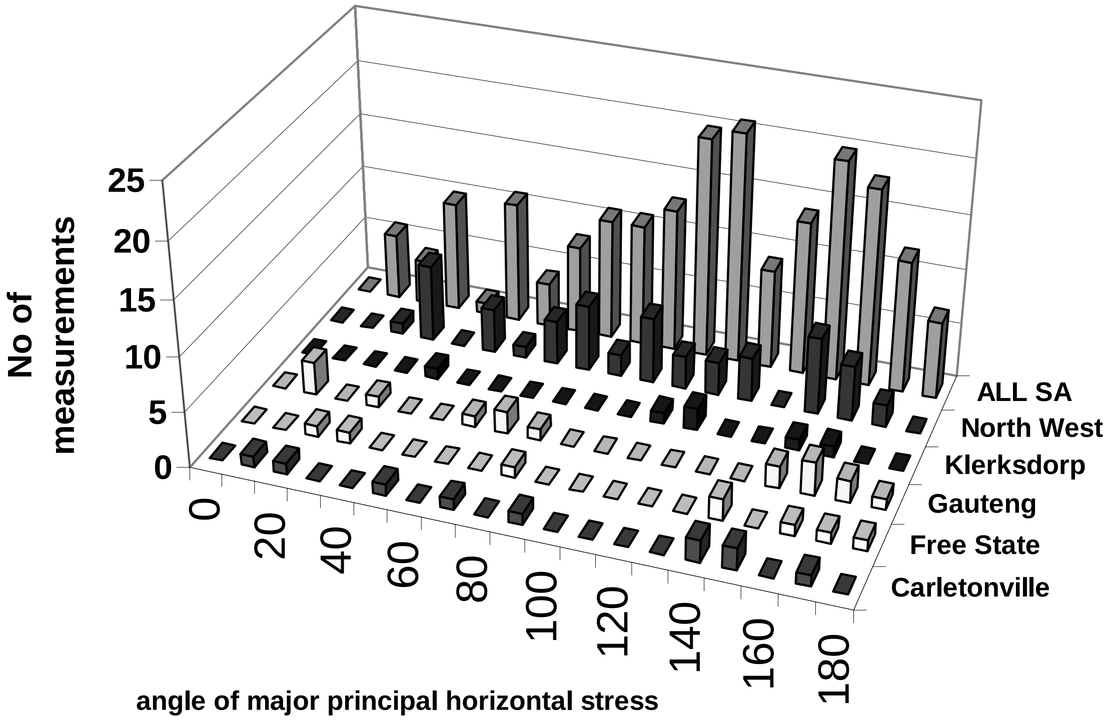

Figure 4.2.3 Variability of the bearing of the major principal horizontal stress for different mining regions in South Africa. Angle represents the angle of the stress clockwise from North

5 THREE-BOREHOLE STRESS MEASUREMENT TECHNIQUE

5.1 Development of new drilling and measuring techniques

The SIMRAC three borehole stress measurement technique was proposed as part of SIMRAC project GAP 220. The original idea was to use a percussion drilling technique to drill three parallel holes to provide the stress relief so that measurement of the deformation in the first hole during drilling of the third hole could then enable a number of measurements to be made in a single hole relatively inexpensively. SIMRAC funded developments of this idea as part of project GAP 314 (Stacey and Wesselloo, 1998). The technique was tested in the laboratory and underground as part of the project. The results suggested that the percussion drilling caused significant damage to the surface of the borehole, thus invalidating the assumption of elasticity that was required for back analysis. A cantilever based measuring device was built to determine the diametric change in four different directions, the minimum required for a least squares solution of the equations in the back analysis (Stacey, and Wesselloo, 1998).

The results of testing indicated that four diameter measurements were insufficient because of potential problems caused by a loss of signal underground, the point of a cantilever sitting on a pebble or drilling mud, or if the measuring point slipped into the depression formed by a pre-existing joint. Developments to the three-borehole technique for SIMRAC project COL 621 also confirmed the need for more measurements around the diameter of the hole. A technique using diamond core drilling was proposed for this project. The diamond drilling was expected to produce less damage to the borehole. The three-borehole technique itself could be validated without the additional influences of the percussion drilling. The diamond core drilling required modifications to the locator, in a similar manner to the coal technique. The borehole diameter selected was based on the B series of drill rod resulting in a borehole diameter of 60 mm. The locator, shown in Figure 5.1.1 is based on the inverted double tube concept. The fixed drill rod is placed into the first hole and the drill is moved sideways and is attached to the coupling on the second tube of the locator. The second tube contains bearings that support an axle that transmits the rotation of the drill rods to the bit situated at the other end of the rod. The axle had to be made hollow to permit passage of the drilling water. A slot was cut in the side of the first rod of the locator to allow drilling water and mud to return down the hole.

Figure 5.1.1 Locator developed for the diamond drilling method

A new measuring device had to be developed to enable the measurement of more than four diameters. A device containing a laser deformation meter was built and studied. The device, shown in Figure 5.1.2, contained a small motor to rotate the laser and scan the borehole sidewall. The device is able to provide measurements of up to eighty diameters. To check the calibration, two tubes were accurately machined in grey PVC and quartzite, respectively. Preliminary scans in the PVC tube showed that the laser-measuring unit was very sensitive to its environment. The outer housing slot and other parts that were located near the laser beam caused interference and altered the distance readings. Eventually, after many modifications, including the use of a prism instead of a mirror to rotate the beam through 90 degrees to scan the sidewall, stable measurements were possible. However, measurements using the quartzite tube were unsuccessful. From these measurements, it became clear that it was not feasible to use a laser distance measurement device to measure to micron accuracy under these conditions or with this configuration. The device was definitely unsuitable for use underground. This was found to be mainly because a laser unit requires a flat, uniform coloured target. The curved surface of the borehole and discontinuous surfaces from jointing generate too much stray light. In addition, because of the way that the laser measures the change in distance from the phase change between the source and incident laser beams, surface colour changes are displayed as a change in distance. A rock with different coloured grains will thus appear to have a surface roughness based on the reflectivity of the grains colours.

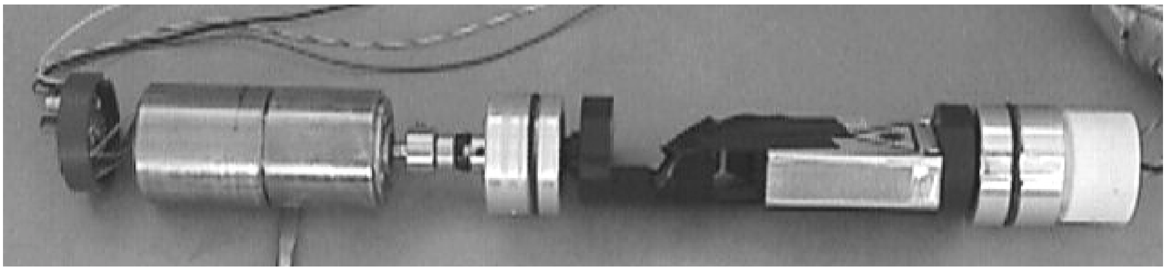

Figure 5.1.2 Laser measuring system

Subsequently, much work has been carried out on the development and manufacture of another measurement device. A measuring device using 16 alternating current linear voltage displacement transducers (LVDT's) was developed as shown in Figure 5.1.3. Most parts have been manufactured and assembled at CSIR Miningtek. Due to the small borehole diameter, the LVDT's were positioned alongside each other in eight sets of pairs. Each LVDT in the pair points in an opposite direction to measure the change across a single diameter as shown in Figure 5.1.4. Eight pairs were selected as being sufficient to provide enough redundancy and to limit the amount of drilling required for completely relieving the stresses.

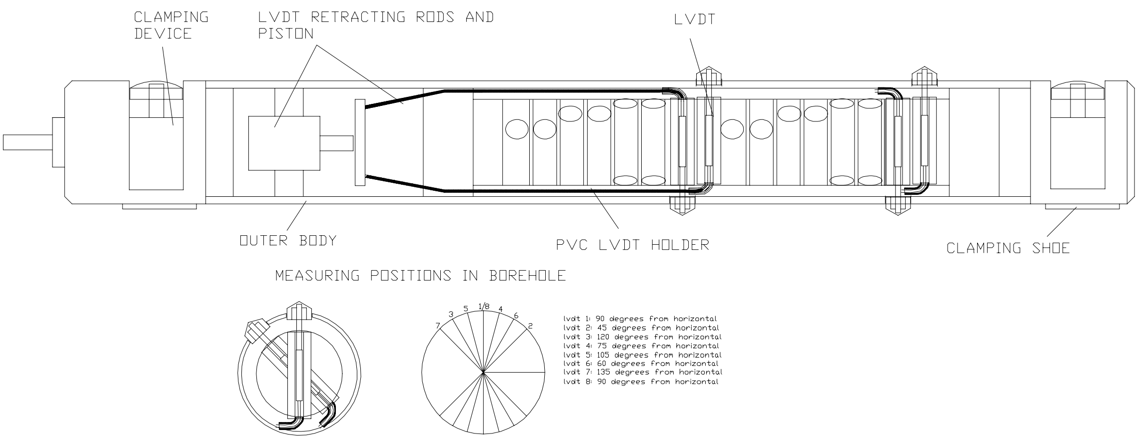

Figure 5.1.3 Schematic of new LVDT based measuring system

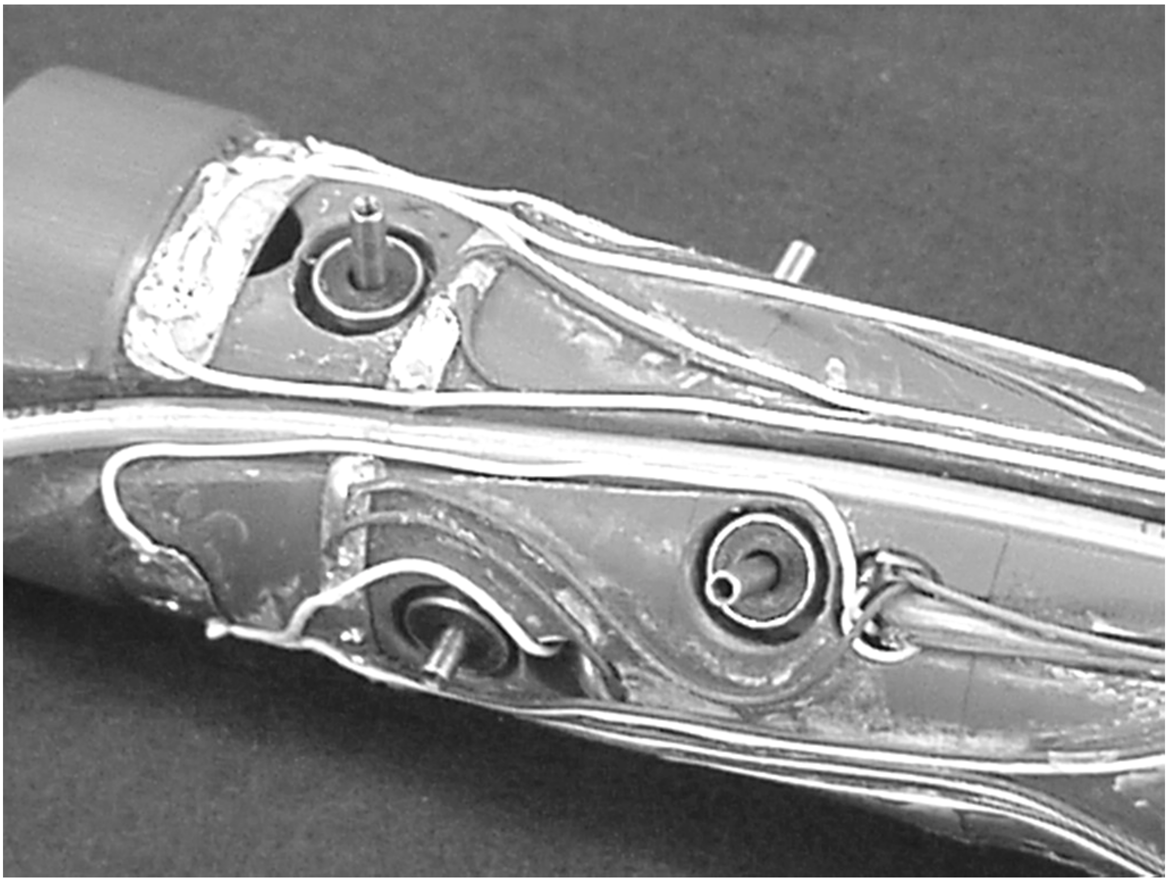

Figure 5.1.4 Photograph of the LVDTs assembled in pairs to measure diameters

For ease manufacture, the LVDT's are mounted in an inner plastic tube and surrounded by an aluminium tube for protection (see Figure 5.1.5). The aluminium tube is connected to two end pieces, each containing a small pneumatic piston. The pistons are extended under air pressure to fix the device into the hole.

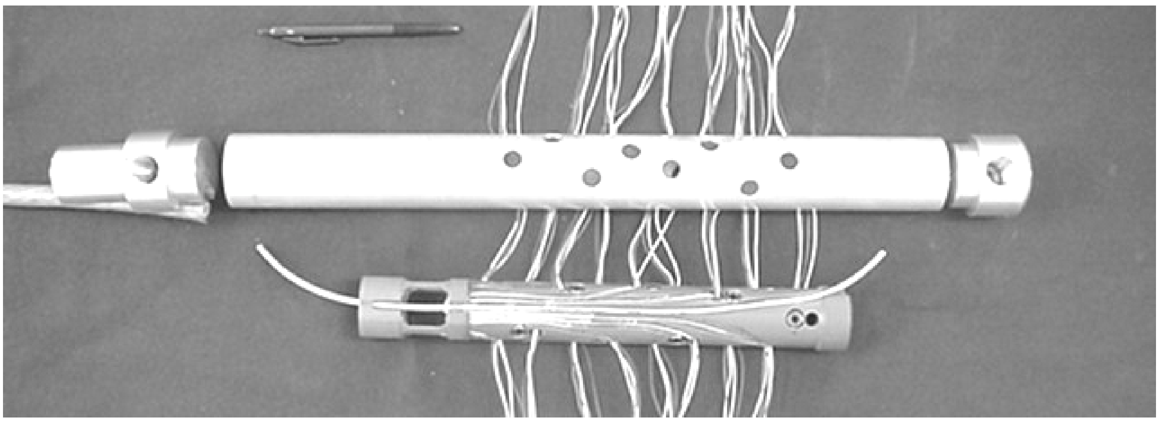

Figure 5.1.5 Photograph of the disassembled LVDT assembly showing the inner and outer tubes

The LVDT’s are spring loaded so that they tend to extend fully. A system was developed to connect the central pins by fine wires to another pneumatic piston to retract the pins when the device is being placed into position in the borehole. The LVDT’s were off-the-shelf components, but required some changes to be able to be used in the measurement device. The pin that passes through the LVDT was modified to allow for the attachment of the cable to retract the pin. The pin length was also changed. The LVDT’s are calibrated by the manufacturer, but the modifications meant that the calibration had to be checked again. The cable attachment made no difference to the calibration, but the length alteration caused some changes and new calibration values were obtained that are now used in the data analysis. Development, modification and calibration of the LVDT system took a considerable amount of time.

The LVDT’s require a power supply and a regulator to produce the analogue output. Experiments showed that the LVDT’s could interfere with each other if they were powered simultaneously from different supplies. A relay unit was developed (Figure 5.1.6) to be able to transfer the power from a single supply to any LVDT on command. A data acquisition unit was built (Figure 5.1.7) and programmed to switch through each LVDT in turn, allow it to warm up, settle, and then take a reading. This process takes approximately 40 seconds for all 16 LVDT’s.

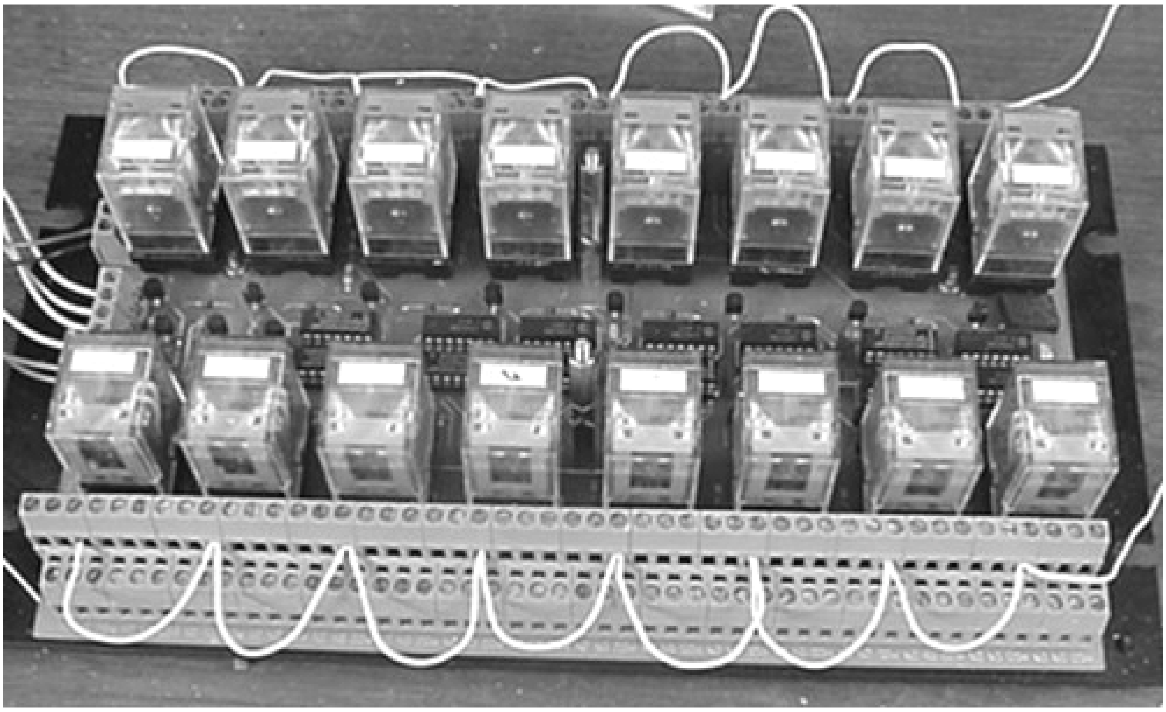

Figure 5.1.6 Photograph of the relay unit

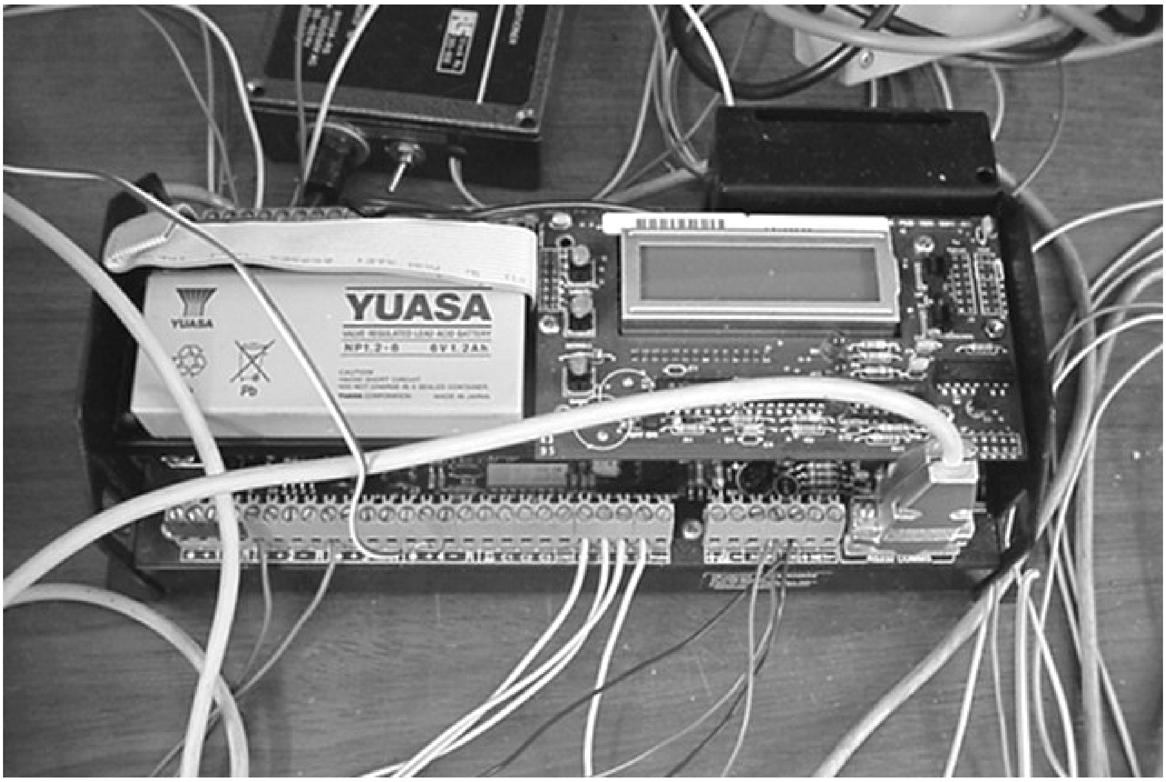

Figure 5.1.7 Photograph of the data acquisition unit

5.2 Underground testing and evaluation

The drill locator and the data acquisition unit were tested separately and together at the sites on Western Platinum Mine and Tau Tona Mine, as described below. A photograph of the drill set up at the Western Platinum site is shown in Figure 5.2.2. A photograph of the locator being used to drill the third hole is shown in Figure 5.2.3a. The photograph also indicates how the drilling water returns through the second hole. The return water will have very little impact on the measuring device.

Modifications were required to the locator to thicken the wall thickness and to remove stress concentrators from the central axle turning the bit. Experience indicated that the drill set up was crucial for good parallel holes. Inexperience caused the drillers to drill without the required accurate setup procedures and caused damage to the locators. A number of locators had to be built with modifications to cope with the problems identified underground. Due to differences in the tolerance between the first two holes, a slot was machined out of the side of the locator to ensure that it would never touch the measuring device. An angle iron was welded into the slot, with its apex pointing inwards, as shown in Figure 5.2.1, to provide rigidity.

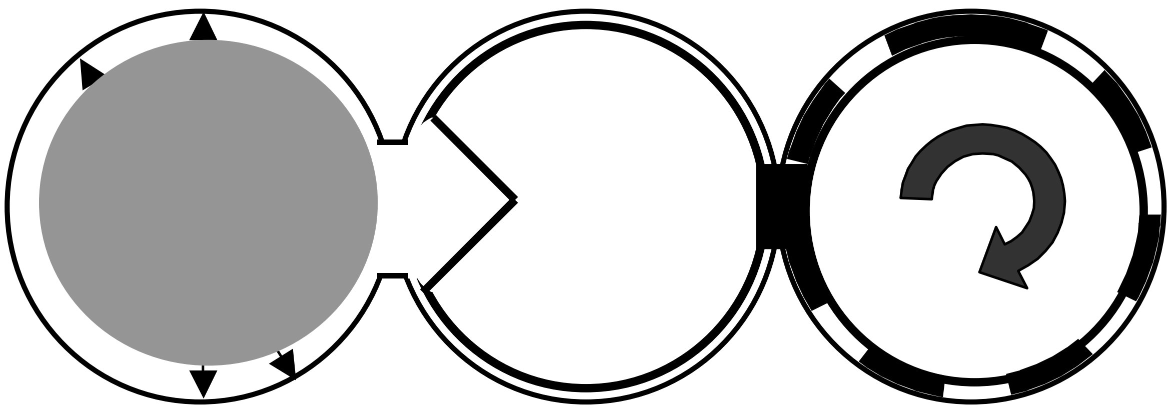

Figure 5.2.1 Schematic of three-borehole technique with measuring device and cut-away locator

The measuring device worked well the first time that it was used underground on Western Platinum Mine see Figure 5.2.2 and Figure 5.2.3. The measurements of the change in the borehole diameter during drilling alongside the device indicated that the readings were stable to within the three-micron resolution of the device. Unfortunately, the measurements had to be stopped on that shift due to malfunction of the drill without having drilled far enough to obtain a stable change in the deformation. Measurements shown in Table 5.2.1 indicate that changes in the order of five to eleven microns were measured.

Table 5.2.1 Diametric deformations measured at Western Platinum

Angle (degrees)	Deformation (mm)
52.5	0.0045
60	0.0118
75	-0.0060
90	-0.0052
105	-0.0057
120	0.0048
135	-0.1509

Subsequently, the air pipes were inadvertently removed from the haulage and drilling was delayed. Following this delay a temporary air supply was arranged, but the theft of fittings delayed the drilling for a number of shifts. At this stage, development of the haulage had to be continued and the site became unavailable. An orepass was blasted near the site and so the stress state would have been altered and could not be compared with the strain cell measurements done at the site (see section 6.1).

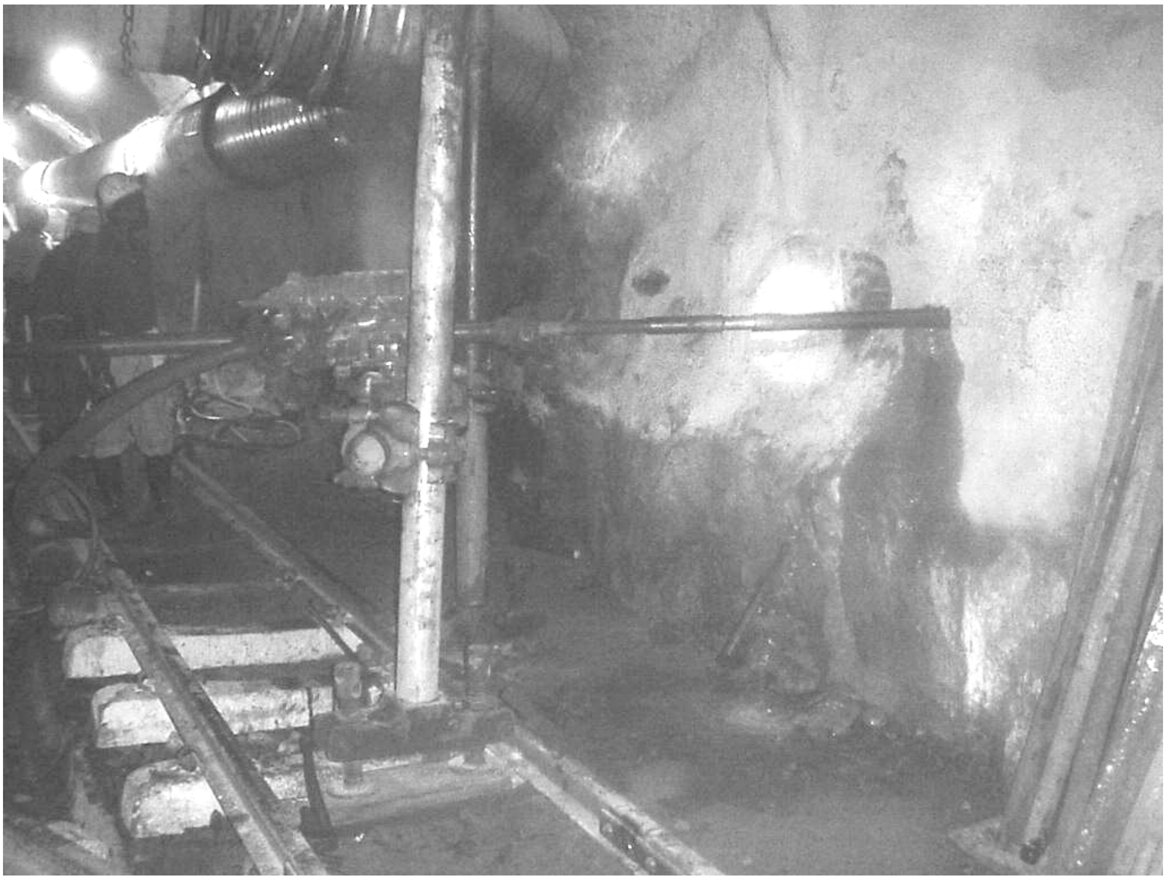

Figure 5.2.2 Photograph of site at Western Platinum Mine

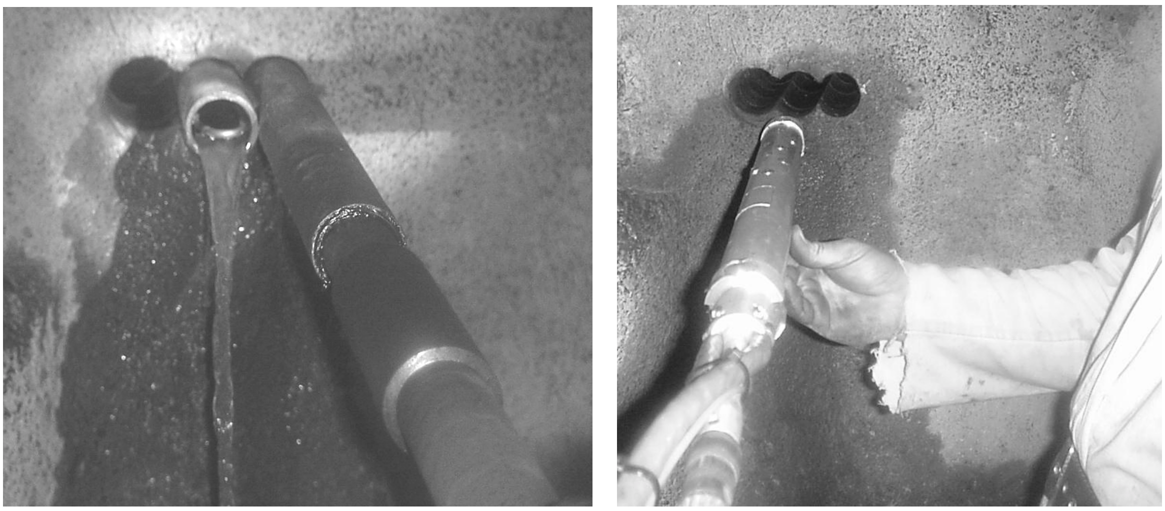

(a) (b)

Figure 5.2.3 Photograph of locator and measuring device

Figure 5.2.4 Photograph of data acquisition system underground

A third site was established on Impala Platinum Mine number 14 shaft, where stress measurements had been carried out as part of a consultancy project. A site was provided in a refuge bay. The site was established and the first two parallel holes were drilled within a week. Four tests were performed during a shift from 8 am to 4 pm. The test log is shown in Table 5.2.2. The first test was unsuccessful because the air pipe was cut by the locator and the pistons holding the measuring device in place retracted. Removal of the locator was difficult during the first few metres of drilling the third borehole. The three holes with the cables from the measuring device and drill rods attached to the locator are shown in Figure 5.2.5.

The next few tests produced results that appeared to be suitable for determining the stress state. The measuring device and the developed data acquisition system (shown in Figure 5.2.6) was stable enough to have no variation within one microvolt when there was no drilling being carried out and sensitive enough to measure the difference in borehole diameter when the rods were withdrawn. There did not appear to be any significant effect when the drilling water was turned on, indicating that the device was insensitive to the environmental conditions. During the test, some LVDT's went out of range, but no explanation could be provided for this problem. During the fourth test, it became apparent that the locator could not slide past the measuring device. It appeared that the locator had slipped into the indentation caused by a joint striking sub-parallel to the borehole and the locator had rotated to such an extent that the edge touched the measuring device, as shown in Figure 5.2.7.

Table 5.2.2 Activity log for tests at Impala Platinum Mine

Hour: Min	Activity	Test
0:00	testing logger and setting up	
1:02	insert logger with end at 3.050m	1
1:09	start drilling locator into position	1
1:10	water on	1
1:16	stopped to add rods	1
1:35	drilling started again	1
1:40	drilling into solid	1
1:42	end of feed	1
1:46	locator pulled out (locator traps aieline and deflates pist	1
1:53	drop pressure on locator	1
	3rd hole drilled to 3.050m	1
3:39	next test end of locator at 3.8m	2
3:40	drilling locator into position	2
3:47	drilling into solid starts at 3rd hole end	2
3:50	end of first 750mm	2
3:51	removing rods	2
4:01	core was not removed	2
4:04	start drilling in again	2
4:10	changing rods	2
4:15	drillling in again	2
4:16	3rd hole at 3.8m rods out	2
4:25	removing core from 1st 750mm	2
4:26	hole at 3.8m deep (equal to locator end) not rods in hol	2
4:29	start drilling in locator	2
4:34	drilling stopped 3rd hole at 4.550m	2
4:51	rods in at 4.550m push to end of hole	3
4:56	adding rods	3
5:08	hole drilled to 4.550m	3
5:12	no rods in for 3min stable readings	3
5:16	rods back in	3
5:21	start drilling	3
5:24	drill sticks slightly 750mm to go	3
5:26	drill stopped	3
5:29	removing rods	3
5:34	hole drilled to 5300 no rods	3
5:35	rods in locator moved to 5.850m	3
5:36	remove and repostion logger	3
5:37	logger shows out of ranges	4
5:38	remove and repostion logger	4
5:39	locator has rotated cannot get rods past	4
5:52	stop testing and pack up time approx 4pm	4

Figure 5.2.5 Photograph of drilling of third borehole past the measuring device during testing at Impala Platinum mine

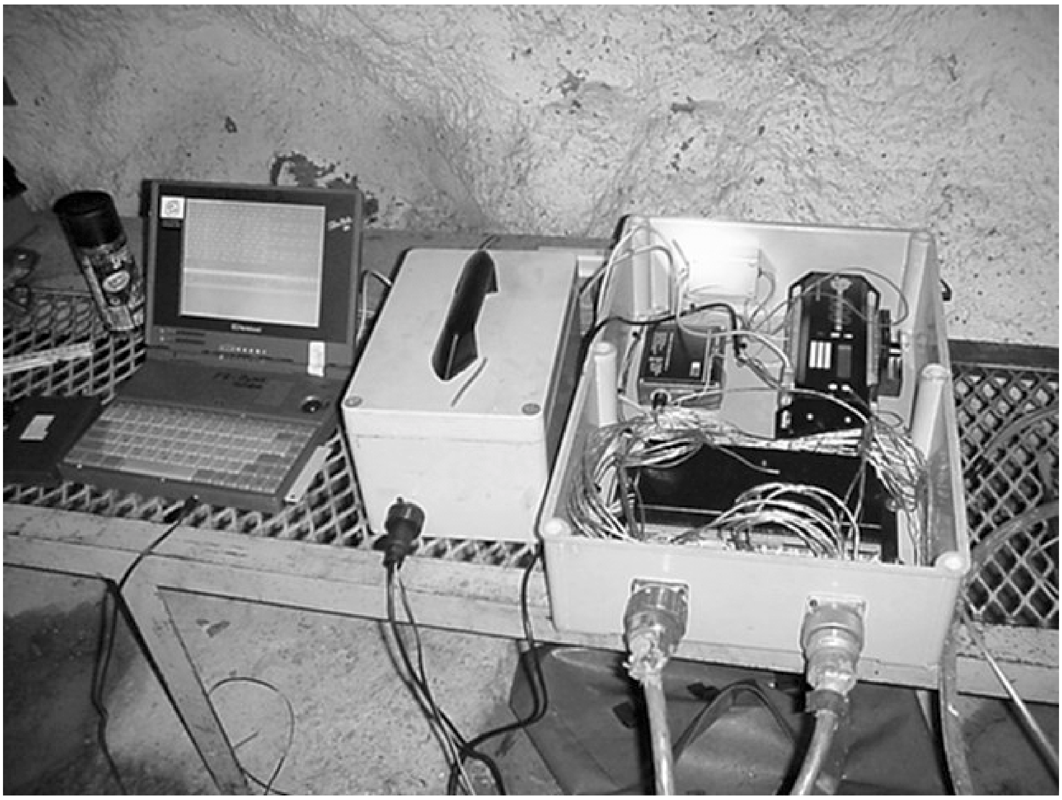

Figure 5.2.6 Data acquisition system in use on the site at Impala platinum mine

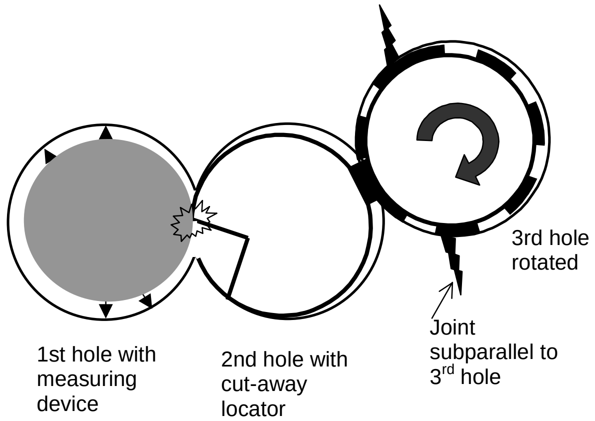

Figure 5.2.7 Schematic of three borehole technique showing how the locator was diverted by a joint aligned sub – parallel to the third borehole causing the locator to rotate and hit the measuring device (not to scale)

Plots of the measured change in borehole diameter for test 2 are shown in Figure 5.2.8. The results of the change in borehole deformation between the second and third hole are shown in Table 5.2.3. The vertical LVDT's measured a change in diameter of 39.6 microns. This is close to the expected values corresponding to the measured vertical stress of 35 MPa. However, the variation between the values for the LVDT's at the other angles is too great to calculate a complete stress tensor.

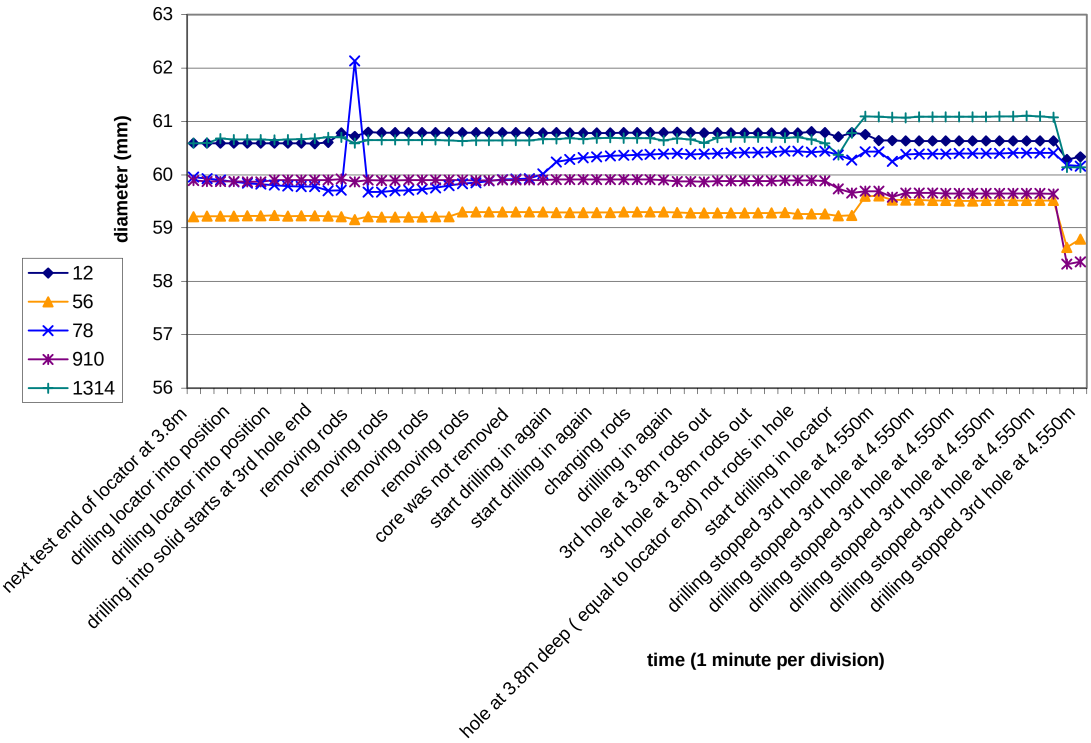

Figure 5.2.8 Diameter deformation measurements for test 2 at Impala platinum mine

Table 5.2.3 Diametric deformations measured at Impala Platinum in test 2

Angle (degrees)	Deformation (mm)
52.5	68.3879
60	72.2576
75	0.4540
90	0.0396
105	-0.2459
120	0.3027
135	0.4876

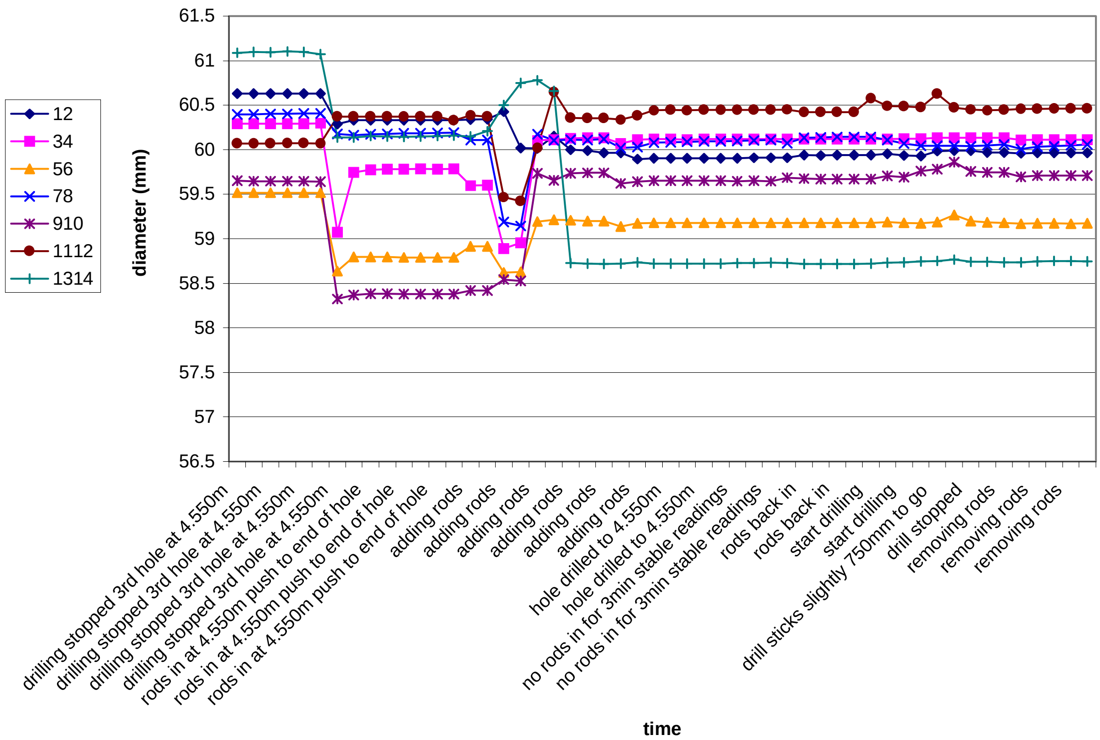

Figure 5.2.9 Diameter deformation measurements for test 3 at Impala platinum mine

Table 5.2.4 Diametric deformations measured at Impala Platinum in test 3.

Angle (degrees)	Deformation (mm)
52.5	-0.1798
60	0.3910
75	-0.3422
90	-0.6631
105	0.0621
120	-0.3465
135	-2.3399

6 CASE STUDIES OF STRESS VARIABILTY

6.1 Stress state near a fault

6.1.1 Site description

The first underground site was chosen to determine the stress state near a fault. The fault that was selected was on the Western Platinum Mine. The geological setting of the Mine is described by Farquhar (1986) and Langweider (2001). The Western Platinum Mine is situated in the Bushveld Complex, about 40 km East of Rustenburg. A site was provided by the mine on the Roland Shaft. The mine rearranged development operations so that a haulage was not used for tramming and so stress measurements could be made at various distances above and below the fault. The site is at a depth of 885 m. The stress state was considered to be close to virgin conditions, but an incline shaft was being developed nearby as indicated in the plan of the site in Figure 6.1.1. Stoping was being carried out at shallower depth with the closest stoping being about 400 m away to the South East.

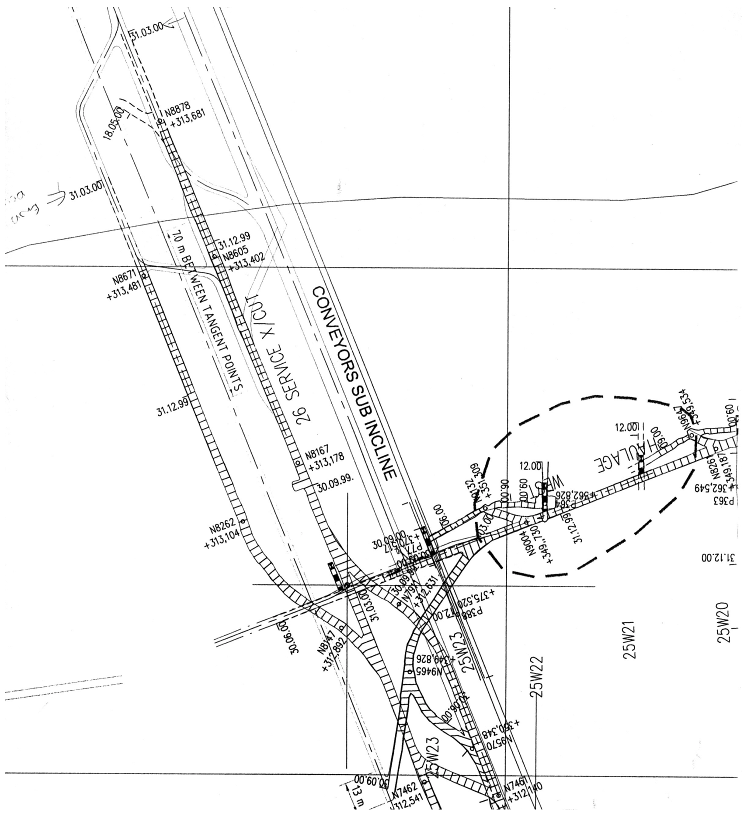

Figure 6.1.1 Plan of the site near a fault at Western Platinum Mine

The stresses were measured using the CSIR three-dimensional strain cell (Leeman, 1968) and analysed using the standard methodology (Vreede, 1981). A total of six boreholes were drilled and three cells overcored in each borehole. Some of the cells were unsuccessful due to breakage of the overcore on joints.

The fault is known on the mine as the “Modderlaag shear” and is essentially bedding parallel, dipping at between 10 degrees and 15 degrees to the North. A photograph of the shear is shown in Figure 6.1.2. The shear has undergone at least three phases of tectonic movement. The first phase was a compressive event that caused the shear to be formed as a reverse thrust fault with the direction of movement aligned towards the South-South West (160 degrees from North). The fault is filled with micaceous material that would have formed due to the high temperatures and circulating fluids commonly associated with thrust events. The slip on the fault cannot be determined as there are no suitable markers.

The second phase was a subsequent tectonic compression towards the North-North-West that caused reactivation of the shear as a normal fault. This event is confirmed by microstructral evidence associated with small shears that slay off into the hangingwall rocks. Steeply dipping normal faults, which strike to the NNE, formed. Lateral movements along these faults, and on a set of NNW trending faults caused intense deformation at the intersections of the fault sets.

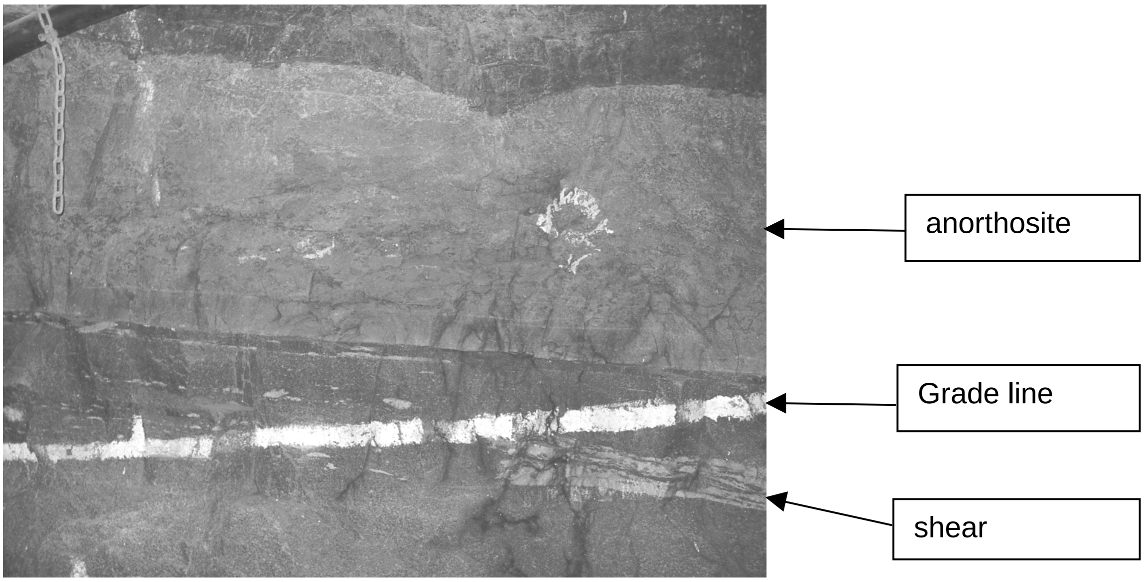

Figure 6.1.2 Photograph of the shear zone and the layer of pink Mottled Anorthosite.

These two compressional events were followed by a phase of relaxation that resulted in back slip along the shear and opened many of the steeply dipping joints. Secondary shears also formed during this event.

A photograph of a blast hole socket is shown in Figure 6.1.3. The socket is considerably elongated in a sub-horizontal direction. Blast sockets are observed to extend in the direction of the maximum compressive principal stress (Brost, 1970) and so the photograph confirms that the maximum compressive stress is aligned about ten degrees from the horizontal plane.

Figure 6.1.3 Photograph of borehole breakout in the vicinity of the tunnel

6.1.2 Analysis of results

The stresses measured in the six boreholes drilled at the site are shown in Table 6.1.1 in the West, South, Down co-ordinate system. The distance of the borehole collar from the shear is also shown in the Table. The results that did not pass the strain consistency checks are denoted as dubious readings. The mean value of the vertical stress is equal to 21.3 MPa, which is very close to the theoretical calculation of 23.8 MPa for the overburden stress. The standard deviation of 4.5 MPa is high due to the non-linear stress strain curves (see Appendix A) and the consequent variation in the selection of the relevant value of Young’s modulus.

Table 6.1.1 Stress state near Modderlaag shear in West, South Down coordinate system

distance to shear		borehole no	test	σWW	σDD	σSS	σWD	σDS	σSW	quality
30.9	North	4	1	28.83	16.17	14.51	-1.61	-0.17	0.92	
30.9	North	4	2	30.07	15.86	15.44	-1.78	-0.36	0.64	
4.4	North	2	1	20.57	23.19	14.05	-6.69	4.85	-0.32	dubious
4.4	North	2	2	41.76	25.1	18.22	0.93	-0.53	0.66	
0	North	3	1	8.01	18.03	10.46	-5.96	-3.54	4.35	
4.5	South	1	1	6.89	23.27	9.78	3.67	4.1	-0.13	
4.5	South	1	2	14.75	23.82	14.54	4.22	2.18	-0.29	
8.8	South	5	1	4.88	5.26	-1.33	-5.96	-0.77	4.2	dubious
8.8	South	5	2	18.31	26.76	12.38	-4.89	-3.02	4.55	
56.6	South	6	1	11.28	5.94	15.78	3.49	-1.58	1.53	dubious

Table 6.1.2 presents the direction and magnitude of the principal stresses for each of the measurements. A perspective view of the principal stresses, plotted using 3-D visualization software, is shown in Figure 6.1.4. The figure shows the view of the stresses relative to the fault, looking west along the strike of the fault. The haulages are also shown. It appears that the major stresses are aligned along the strike of the fault plane and that the intermediate and minor stresses are visible in the vertical plane shown in Figure 6.1.4. There is considerable variation in the directions of the minor and intermediate principal stresses.

Table 6.1.2 Principal stress state near Modderlaag shear. Bearing is clockwise in degrees from North and dip is in degrees and positive down from horizontal. An asterisk denotes a dubious reading

borehole no	test	σ1	σ1 bearing	σ1 dip	σ2	σ2 bearing	σ2 dip	σ3	σ3 bearing	σ3 dip
4	1	29.09	266	7	15.97	105	82	14.44	357	2
4	2	30.32	267	7	15.82	167	55	15.22	2	34
2	1*	29.73	294	51	16.96	54	22	11.13	158	30
2	2	41.82	88	3	25.09	212	84	18.16	358	5
3	1	22.91	229	54	9.57	18	32	4.02	117	15
1	1	25.1	37	72	9.05	159	10	5.79	252	15
1	2	25.81	64	67	14.84	328	3	12.46	236	23
5	1*	11.98	250	41	0.89	37	44	-4.07	144	17
5	2	30.25	240	59	17.3	63	31	9.91	332	1
6	1*	16.28	195	4	12.87	103	28	3.84	291	61

A view of the principal stresses looking down on the Modderlaag shear is shown in Figure 6.1.5. The figure confirms that the major principal stresses are aligned parallel to the strike of the fault. Further confirmation is shown in the plot of the most compressive horizontal compressive stress in Figure 6.1.6.

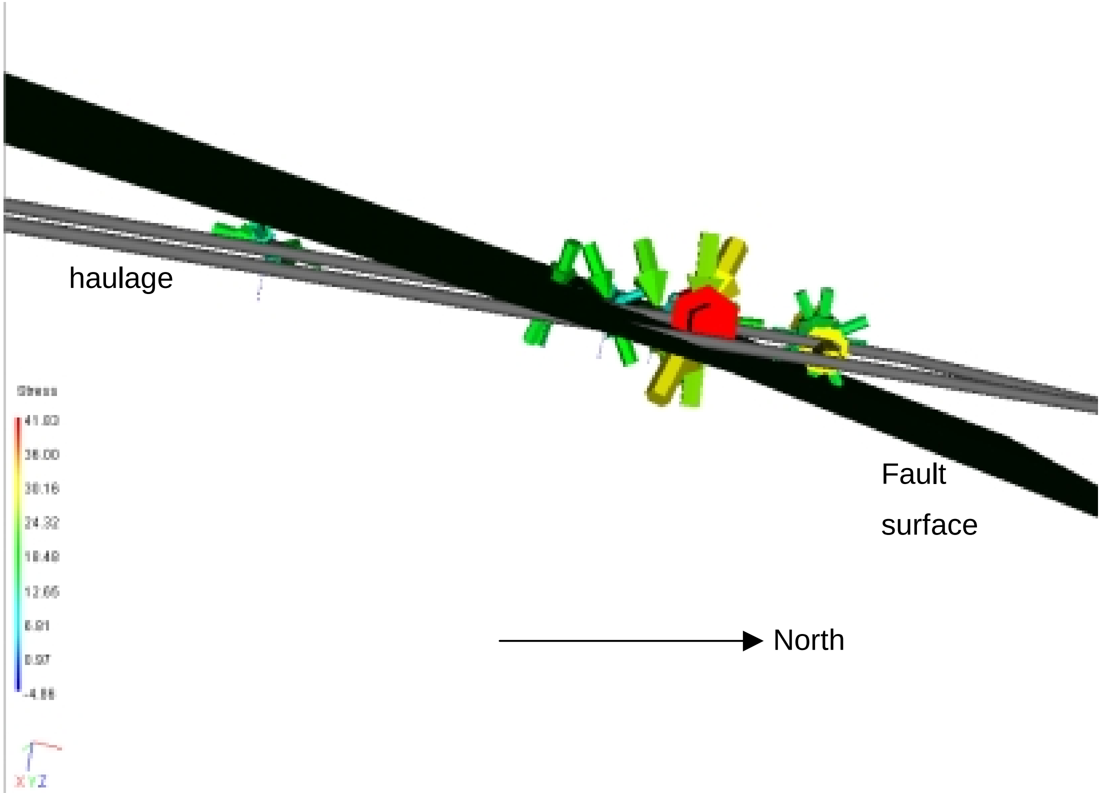

Figure 6.1.4 Perspective view of principal stresses near Modderlaag shear

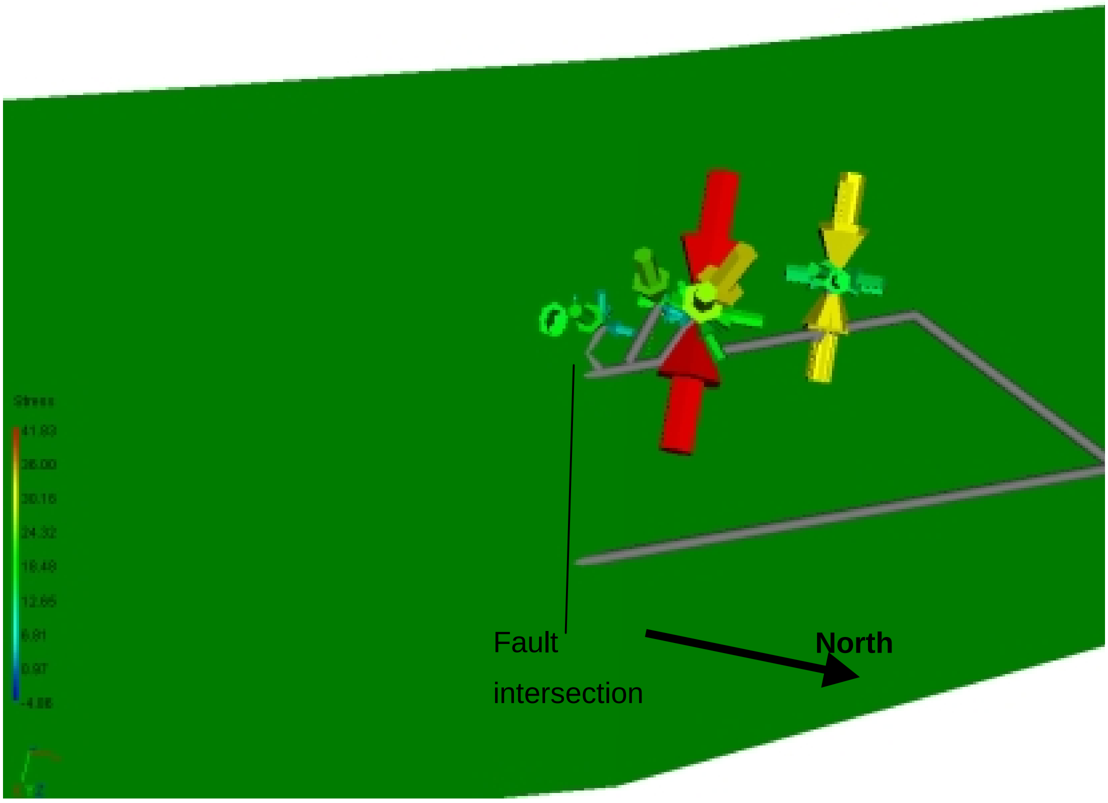

Figure 6.1.5 Vertical view of principal stresses relative to the Modderlaag shear

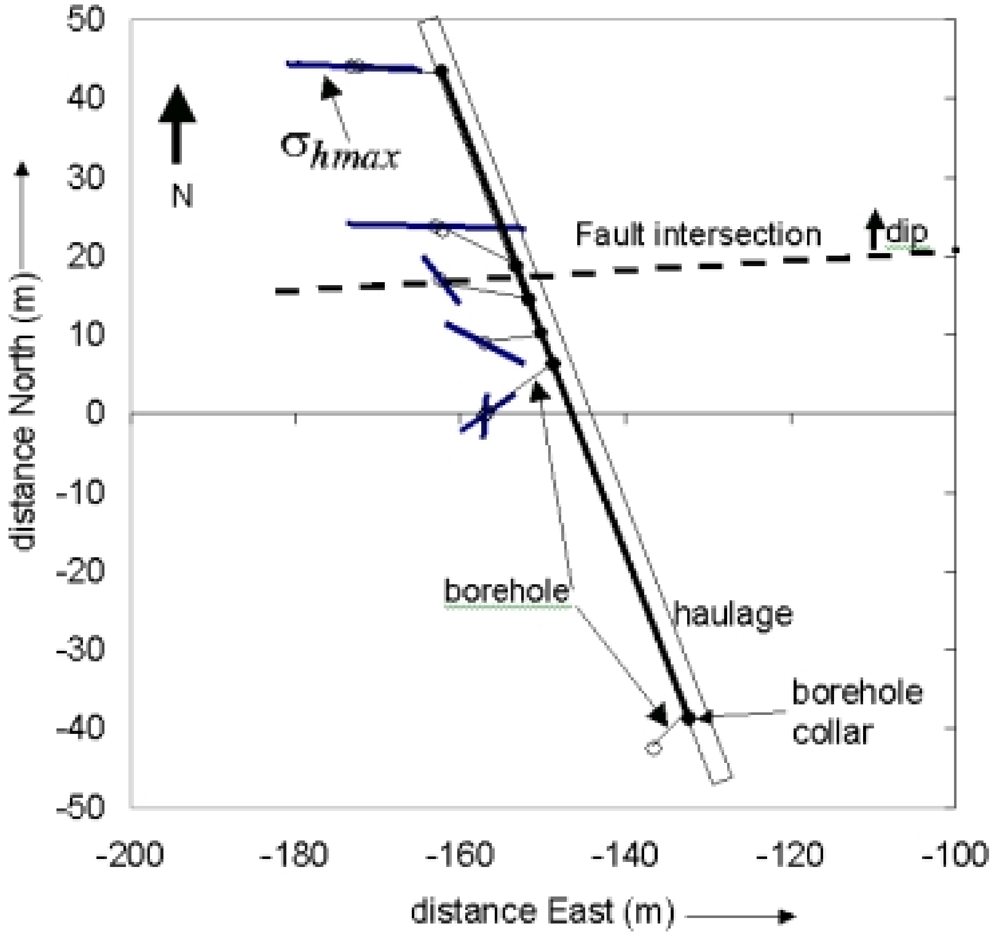

Figure 6.1.6 Plan view of the site showing the direction of the most compressive horizontal principal stresses (thick lines) relative to the boreholes (marked by a dot at the collar and a thin line), the shear plane intersection (dotted line) and haulage (thin rectangle)

6.2 Stress state near a dyke

6.2.1 Site description

A site was made available on Tau Tona Mine for stress measurements in a Dyke. The site that was suggested was in the waiting place, close to the station on the sub main shaft at 83 level. A plan of the site is shown in Figure 6.2.1. The figure shows the site at the intersection of the Speckled Dyke with the waiting place. Mr Shaun Murphy noted that previous experience of drilling at the site had been difficult due to the lack of air pressure. It was decided to use a modified electric powered surface drill. It was planned to perform

3-D strain cell readings in the dyke and in the host rock to evaluate how the dyke altered the stress state.

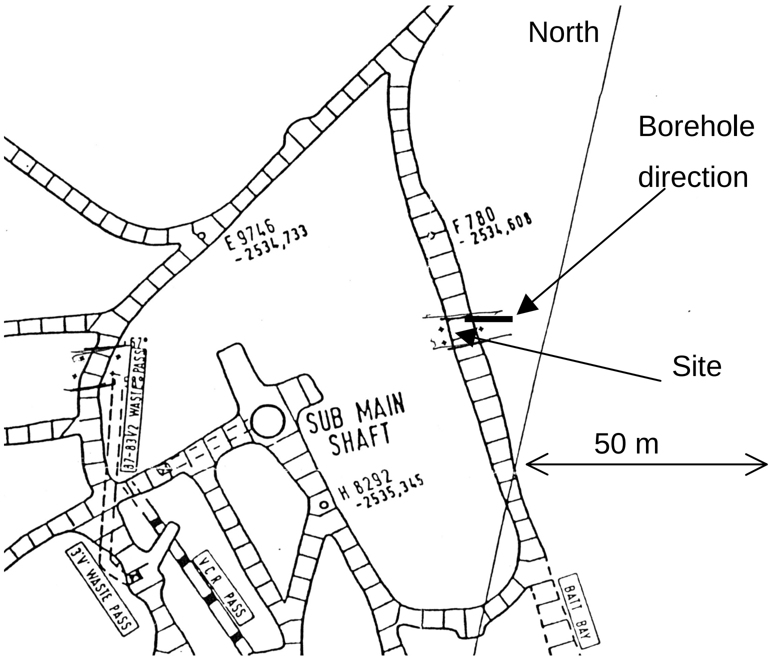

Figure 6.2.1 Plan of the site on 83 Level at Tau Tona

The dyke had been shotcreted and a number of sections of shotcrete were removed in order to find the dyke. The drill team had to undergo two weeks of induction training before work could commence. Once drilling was started, the core initially contained igneous rock and then changed to altered quartzite. Consideration of the plans and geological information from some distance away indicated that the dyke dipped at about 70^{o} to the North. This was confirmed later by the fault and dyke database (Szakmeister, 1998) that states that the Specked dyke dips at 75^{o} to the North with an azimuth of 165^{o} and a strike of 91^{o}. The dyke consists of a medium to coarse grained gabbroic rock and has a width of about 6 m and a throw ranging from 8 to 45 m (Szakmeister, 1998). Thus, the boreholes had initially entered the dyke but then exited through the dyke margin. The rock in the dyke margin was of poor quality and contained joints and veins at various angles. These caused the core to be extremely fragmented and prevented stress measurements immediately in the dyke margin. Further holes were drilled into the centre of the dyke, at angle of 70 degrees upwards and directed parallel to the strike of the dyke. The first two of these holes had quartz veins running sub-parallel to the borehole that caused the core to split longitudinally. Finally, a hole was drilled that was intersected occasionally by the veins, and the veins occurred at a more acute angle. Thus, the core could be obtained in reasonable sections.

Three CSIR strain cells were installed in sequence. The first two were unsuccessful due to the overcore breaking up along the quartz veins. The third cell was overcored, but the overcore broke off shortly after the drill passed the strain cell. This provided a first estimate of the stress state.

The site was closed and then re-established in September 2001 for testing of the locator drilling technique and to perform more strain cell measurements. A new policy of strict enforcement of safety regulations at the mine resulted in many delays for site establishment. The drill team had to undergo two weeks of induction training. Then risk assessments were required for the drill and the measurement technique. Risk assessments were performed and required some iterations to satisfy the mine's safety officer.

Drilling started in December and problems were experienced with the locomotives hitting and damaging the drill. The contractor also had management problems and was unable to properly supervise drilling. Finally, suitable core was obtained in early February 2002. A cell was installed, but the cable was cut overnight and the cell was lost. The cell was drilled out and a new cell installed. The overcore was unsuccessful due to the presence of quartz veins that caused the core to break up into small pieces.

6.2.2 Results

Of the eight cells installed and tested on the site at Tau Tona, only one of the test results passed the strain consistency tests. The values of the stresses in the West, South Down co-ordinate system are shown in Table 6.2.1. The principal stresses are shown in Table 6.2.2. The vertical stress is higher than the 62.1 MPa overburden stress expected for the depth of 2300 m. The stress may be increased in the shaft because of the surrounding mining. The stress state was input into the INSITU visualization utility to compare the principal stresses with the dyke position. The view looking west along the strike of the dyke is shown in Figure 6.2.2. The figure shows how the major principal stress is aligned at an angle to the dyke, as may be expected for a normal fault. This would be consistent with the observations of the faulting along the dyke margin. Thus, the stress state measured is related to the faulting, not the dyke. The normal faulting is confirmed by the fault and dyke database (Szakmeister, 1998), which states that the throw on the dyke is from 8 to 45 m.

Table 6.2.1 Stress state measured in the Speckled dyke on Tau Tona Mine in West, South Down coordinate system

test	σWW	σDD	σSS	σWD	σDS	σSW
1	56.84	87.8	38.85	-30.96	18.16	-8.66
stdev	1.22	1.81	1.19	0.96	0.89	0.71

Table 6.2.2 Principal stress state in Speckled dyke on Tau Tona Mine

σ1	σ1 bearing	σ1 dip	σ2	σ2 bearing	σ2 dip	σ3	σ3 bearing	σ3 dip
112.38	298	56	38.53	67	23	32.55	168	24

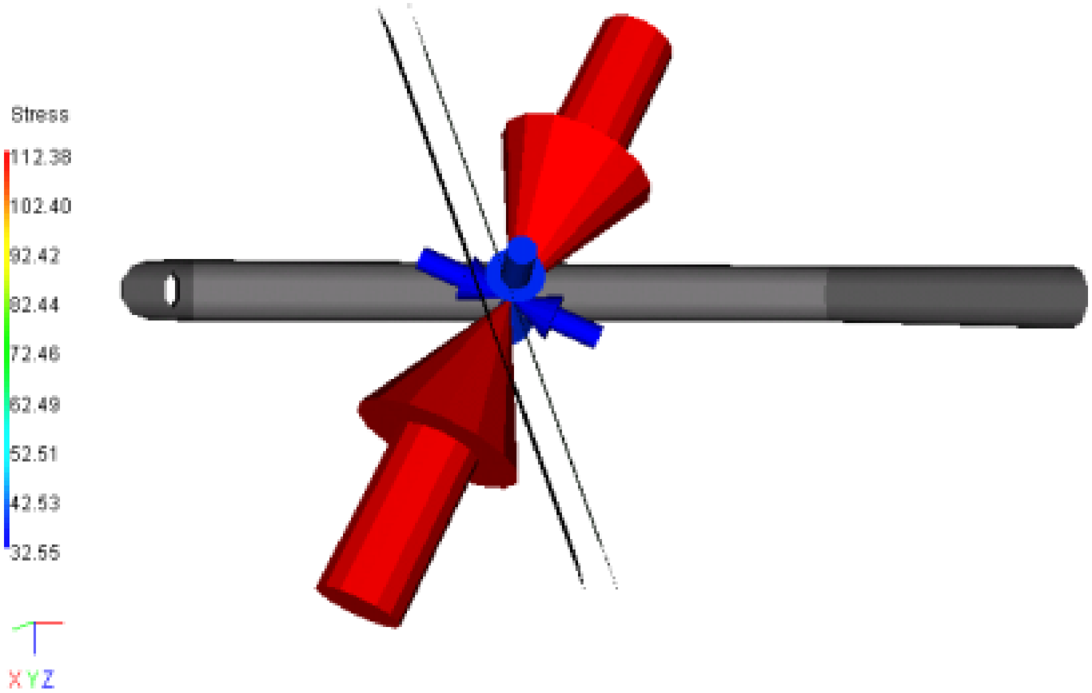

Figure 6.2.2 Visualization of the stress state measured at Tau Tona Mine looking west

The plan view of the stress state is shown in Figure 6.2.3. This confirms that the intermediate principal stress is directed along the strike of the dyke, and the minor stress is almost perpendicular to the dyke surface. These directions are expected for a normal fault as described in section 3.5. The stress was not measured outside the dyke and so no comparison can be made regarding the magnitude of the stresses outside and inside the dyke. A view of the stress state looking south–west is shown in Figure 6.2.4.

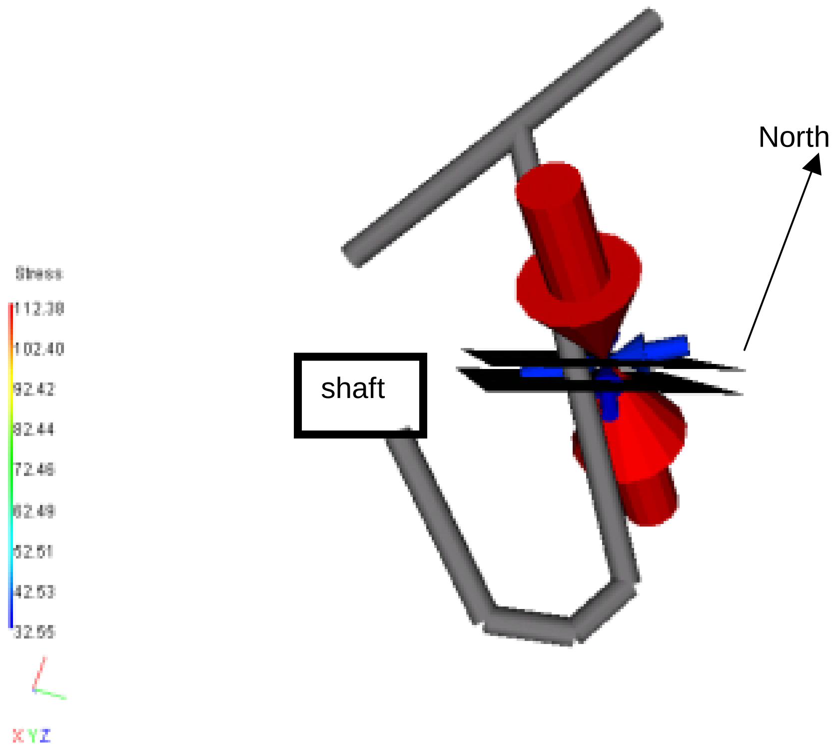

Figure 6.2.3 Visualization of the stress state measured at Tau Tona Mine in plan, looking down

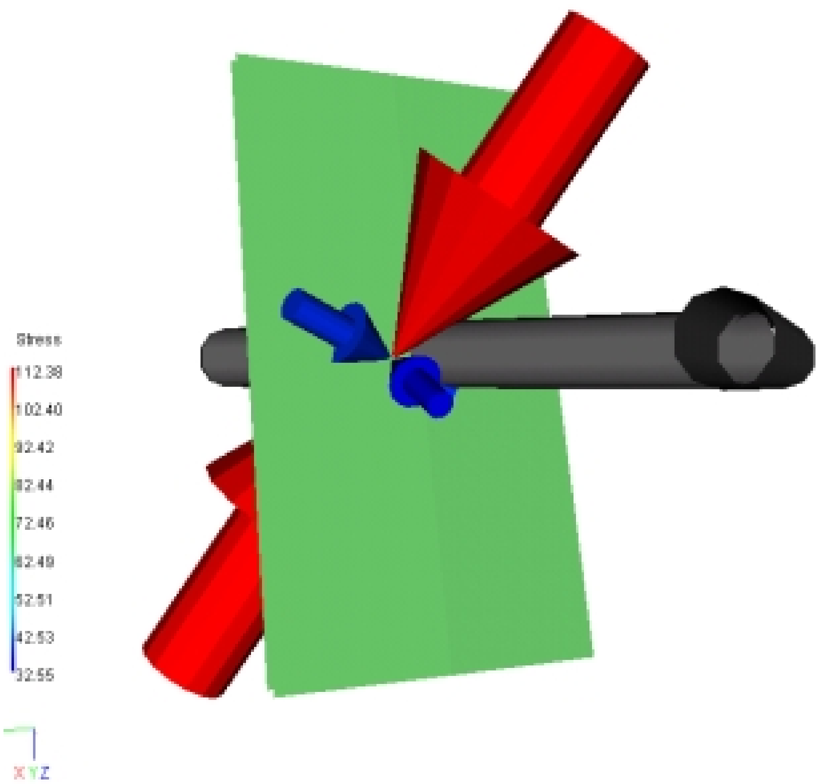

Figure 6.2.4 Visualization of the stress state measured at Tau Tona Mine looking South-West

7 CONTROLLING FACTORS, DENSITY AND METHODOLOGY

The main conclusion of the previous sections is that the stress state varies continuously throughout the rock mass. The stresses are measured at single points, but can be considerably different a few centimetres away. However, local geological conditions and a similar tectonic history should produce a stress state that is similar on average. The variability will depend on the scale of the region under consideration. Geological variability will increase as the size of the region increases. The average stress state will depend on where the mine and the measuring site is located in relation to the distance of the point to:

- the Witswaterand basin or the Bushveld Complex,
- large structural events e.g. thrust blocks, the Pilanesburg intrusive event etc,
- dyke intrusions and faults, and
- folds, layering and the distance to the surface.

To specify a required density of measurements to completely characterize the stress state in a mine or shaft would lead to a stress measurement programme that is both uneconomic and impractical. Measurements should be done in major geotechnical or structural regions and wherever crucial excavations will be sited. A more appropriate approach is to deal with the variability in terms of a risk-oriented design methodology as described subsequently.

A methodology is required to enable the rock engineer to design excavations in a manner that takes into account the variability of the stress state between the different sections of a mine. The application of risk analysis is becoming more common in geotechnical engineering where there are many unknowns and where some information can be obtained about the distribution of these unknowns. Risk is the product of the probability of failure and the consequences of failure (Xu *et al*, 2000). Formal methods are available to assist with the input of statistical distributions of input parameters and to determine the hazard or reliability of an excavation.

The first step is to define the criterion for failure. This can be limit state design value, which represents the probability that the factor of safety is less than unity i.e.

$$P_f = P[FS < 1]. \tag{7.1}$$

This method is most appropriate for pillar (Esterhuizen, 1993, Joughin *et al*, 2000) or tunnel designs. Alternatively, a serviceability state could be used (e.g. Lilly and Li, 2000) that, for example, limits a selected displacement δ to be less than a critical value δ_c i.e.

$$P_f = P[\delta < \delta_c]. \tag{7.2}$$

Once the criterion for the probability has been determined, the statistical distribution x_i of each of the *n* input parameters must be determined. In this case, it is the variability of the stress state. In the simplest analyses, the variability can be considered in terms of the variability of the major and the minor k-ratios. The analyses becomes more complex as more input variables are added. However, the plunge of the principal stress could also be considered as it is a parameter that has been shown in this study to be significantly altered by the geological and tectonic state. In factor of safety approaches, the variability of the initial stress state will results in variability of the applied loading on the excavation. There will also be variability in the ability of the system to resist the loading i.e. the rock mass strength distribution must also be taken into account.

Many rock engineers have been trying to cope with the variable stress by applying a number of different k-ratio values in their numerical modelling of excavations. This method is an informal way of attempting a Monte Carlo simulation to establish the design parameters (Harr, 1987). One method for determining the risk associated with the structure is to follow a formal Monte Carlo simulation procedure. The probability distributions of each input variable are sampled at random to provide a set of combinations of the input variables. Each set of input data is then applied in the design procedure or numerical analysis to obtain a distribution of output values of the failure criterion. This distribution can then be used to estimate the reliability or the probability of failure of the excavation. The number of analyses required can be calculated as

$$N = (h_{\alpha/2}^2 / (4\varepsilon^2))^m \tag{7.3}$$

for m input distributions (Harr, 1987). The value of $h_{\alpha/2}$ can be obtained from Table 7.1.1 depending on the required error fraction ε. However, for a proper simulation using a Monte Carlo approach millions of analyses may be required to determine to complete output probability distribution. Thus, performing a few numerical modelling exercises with some different k-ratios does not provide any confidence that the correct range of input values has been considered.

Table 7.1.1 Confidence coefficients for normal distribution (Harr, 1987)

Error value ε	Confidence Level %	$h_{\alpha/2}$
0.1	90	1.64
0.05	95	1.96
0.01	99	2.58
0.001	99.9	3.29
0.0006	99.994	4.0

A simpler approach that also leads to a formal design methodology based on a risk analysis of the excavation is to apply Rosenblueth's Point Estimate method (Harr, 1987). The method has been applied to pillar design (Esterhuizen, 1993, Joughin *et al*, 2000) and to the design of tunnels (Lilly and Li, 2000). The essentials of the point estimate methodology are given here and more details can be found in the book by Harr (1987).

The expected value $E[y^n]$ of the design criterion y^n is calculated by evaluating the design criterion at a small number of specific points in the input distributions. These point estimates for the input distribution are calculated at the points:

$$x_{i+} = \bar{x} + \sigma[x] \text{ and } x_{i-} = \bar{x} - \sigma[x] \tag{7.5}$$

where $\bar{x}$ is the mean and $\sigma[x]$ is the standard deviation of the distribution. All the permutations of the point estimates for each variable are entered into the design criterion $y(x_1,x_2,..x_N)$ so that the expected value of the design criterion can be determined as a weighted sum of the point estimates. For example in the case of n=2, the expected value is given by:

$$E[y] = p_{++}y_{++} + p_{-+}y_{-+} + p_{+-}y_{+-} + p_{--}y_{--} \tag{7.6}$$

where the weighting factors:

$$p_{++} = p_{-+} = p_{+-} = p_{--} = \tfrac{1}{4}, \qquad (7.7)$$

for this case. The variance of the distributions for the output design criterion can be determined from

$$V[y] = E[y^2] - (E[y])^2 \text{ where } E[y^2] = p_{++}y_{++}^2 + p_{-+}y_{-+}^2 + p_{+-}y_{+-}^2 + p_{--}y_{--}^2. \qquad (7.8)$$

The method can be extended to consider N variables, in which case there are 2^N terms in the expected value calculation and the values of the 2^N weighting functions $p_{???...N}$ can be obtained from Harr (1987). A computer programme using a matrix of permutations is suggested for N>3. If the input distributions are skew i.e. the variation is not symmetric about the mean, the moment of skewness β must be taken into account in the calculation of the weighting functions $p_{???...N}$. The probability of failure is then found by fitting a distribution to the expected values and the variance, and substituting in the failure criterion.

As a simple example to illustrate the Point Estimate Method for this project, the design of tunnels at a depth of 3000 m in a gold mine in the Klerksdorp region was selected. The design criterion to be used in this example is chosen to be the Rockwall Condition Factor (RCF) as defined in Jager and Ryder (1999). The RCF can be expressed as:

$$RCF = 3(\sigma_1 - \sigma_3)/F\sigma_c \qquad (7.9)$$

where σ_1 is the major principal stress, σ_3 is the minor principal stress, F is a factor assumed equal to unity for competent rock and σ_c is the unconfined compression strength of the rock. In this example, further assume that the major principal stress is vertical, and F = 1. In this case, equation (7.9) becomes

$$RCF = 3\sigma_v(1-k)/\sigma_c. \qquad (7.10)$$

The vertical stress at 3000 m is calculated be equal to 81 MPa and only the minor k-ratio is considered, in this example, for input into the equation. The mean $\bar{k}$ and the standard deviations *s[k]* of the minor k-ratio are obtained from the analysis of the GAP 511 database in Section 4.2 and are shown in Table 7.1.2. The mean $\bar{\sigma}_c$ and standard deviation $s[\sigma_c]$ of the unconfined compressive strength (UCS) that are assumed for the rock mass in this example are also given in Table 7.1.2.

Table 7.1.2 Values of means and standard deviation of k-ratio and unconfined strength assumed for the minor k-ratio and UCS in the example

Variable	minor k-ratio (kh)	UCS (MPa)
Mean	0.65	180
Std Dev.	0.26	30

The calculation of the point estimates and the expected values are shown in Table 7.1.3. The values for the k-ratio are determined from $\bar{k} \pm s[k]$ and the corresponding strengths are found from $\bar{\sigma}_c \pm s[\sigma_c]$. These values are substituted into equation 7.10 to get the point estimates of the RCF.

Table 7.1.3 Calculation of Point estimates for example

term	kh	UCS	k	σc	RCF	RCF*p	RCF^2*p
1	+	+	0.91	210.00	0.10	0.03	0.00
2	+	-	0.91	150.00	0.15	0.04	0.01
3	-	+	0.39	210.00	0.71	0.18	0.12
4	-	-	0.39	150.00	0.99	0.25	0.24
					Σ=	0.49	0.38

The point estimates are multiplied by the weighting functions (all equal to 0.25) and summed as in equation 7.6. The expected values and the variances are found from equations 7.6 and 7.8, respectively and are shown in Table 7.1.4.

Table 7.1.4 Expected values and variance for the RCF in the example

Expected value	0.49
Variance	0.14
Std Deviation	0.37

To calculate the probability of failure, it is necessary to reconsider the RCF criteria. Jager and Ryder (1999) state that if the RCF < 0.7 then the rock conditions are excellent. If the RCF > 1.0 the conditions are poor. Fitting a cumulative distribution to the mean and standard deviation given in Table 7.1.4, using a program e.g. Excel or a table of the distribution, allows the calculation of the probability that the RCF *is less than* a given value. This provides the reliability R of the RCF for the given conditions (Harr, 1987). The probability of failure is the probability that the RCF *exceeds* some value and so:

$$Pf = 1 - R \tag{7.8}$$

The simplest distribution to fit, given just the mean and standard deviation, is the normal distribution and the results of this fit are shown in Table 7.1.5. Thus, the probability that the rock conditions in the tunnel will be excellent is 72% and the probability that they will be poor is 9%. Lilly (1999) considers that the Beta distribution is the most flexible distribution for fitting the results of the point estimate method. However, the minimum and maximum value of the distribution are required for this method.

Table 7.1.5 Calculated probabilities of failure.

condition	condition factor C	R (RCF<C)	Pf = (1-R)
excellent	0.70	0.72	0.28
poor	1.00	0.91	0.09

The methodology for undertaking a set of stress measurements on a mine is summarized in the flowchart of Figure 7.1.1. The flow chart of Figure 7.1.2 shows how the stress measurement programme is integrated into the risk based design methodology. This section has presented the broad outlines of a probabilistic approach to dealing with the variability of the primitive stress. Consideration still needs to be given to selection of the appropriate confidence levels and to determine what level of risk is acceptable in order that such a method can become a standard design methodology.

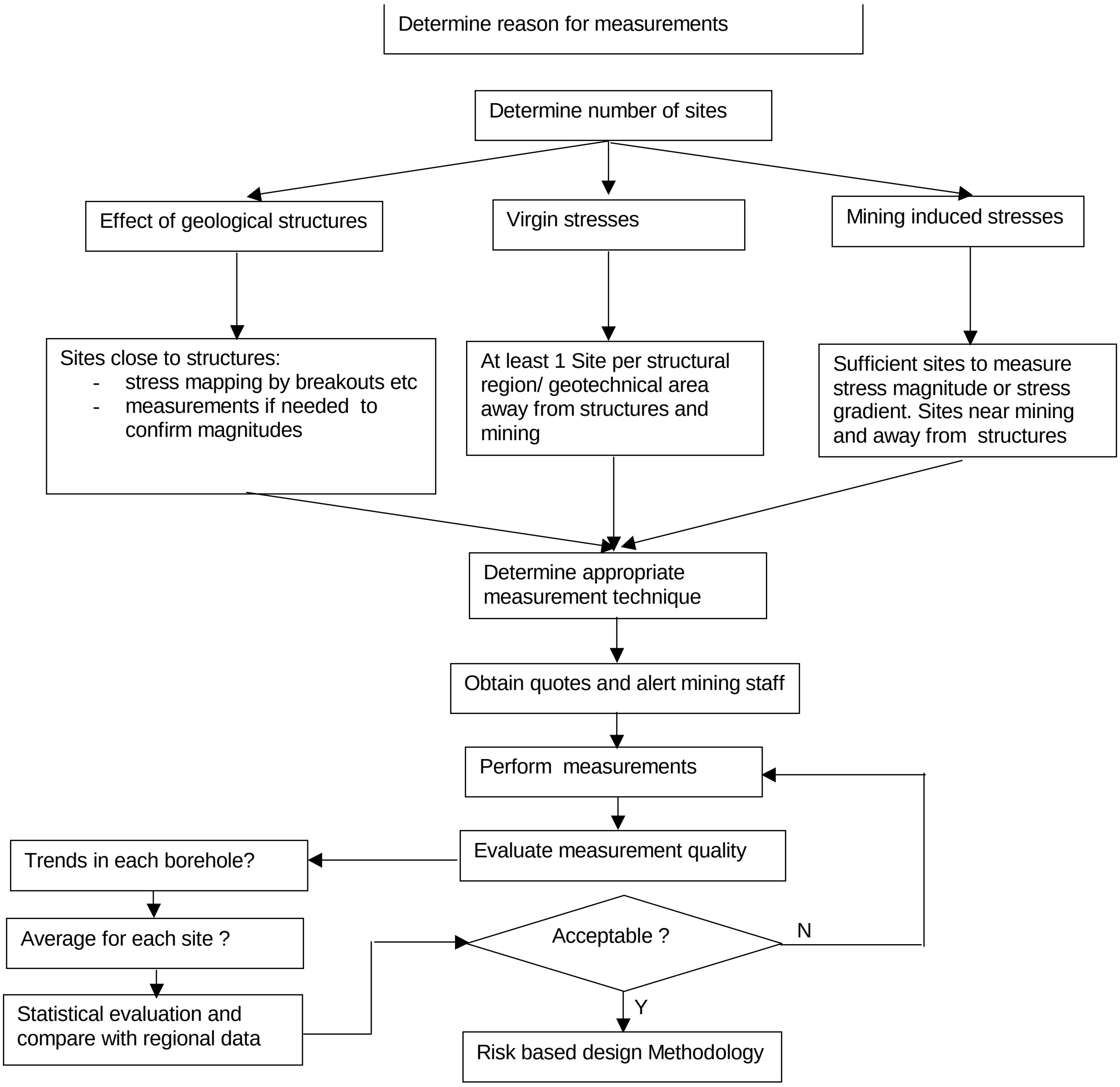

Figure 7.1.1 Flowchart of methodology for stress measurement programme

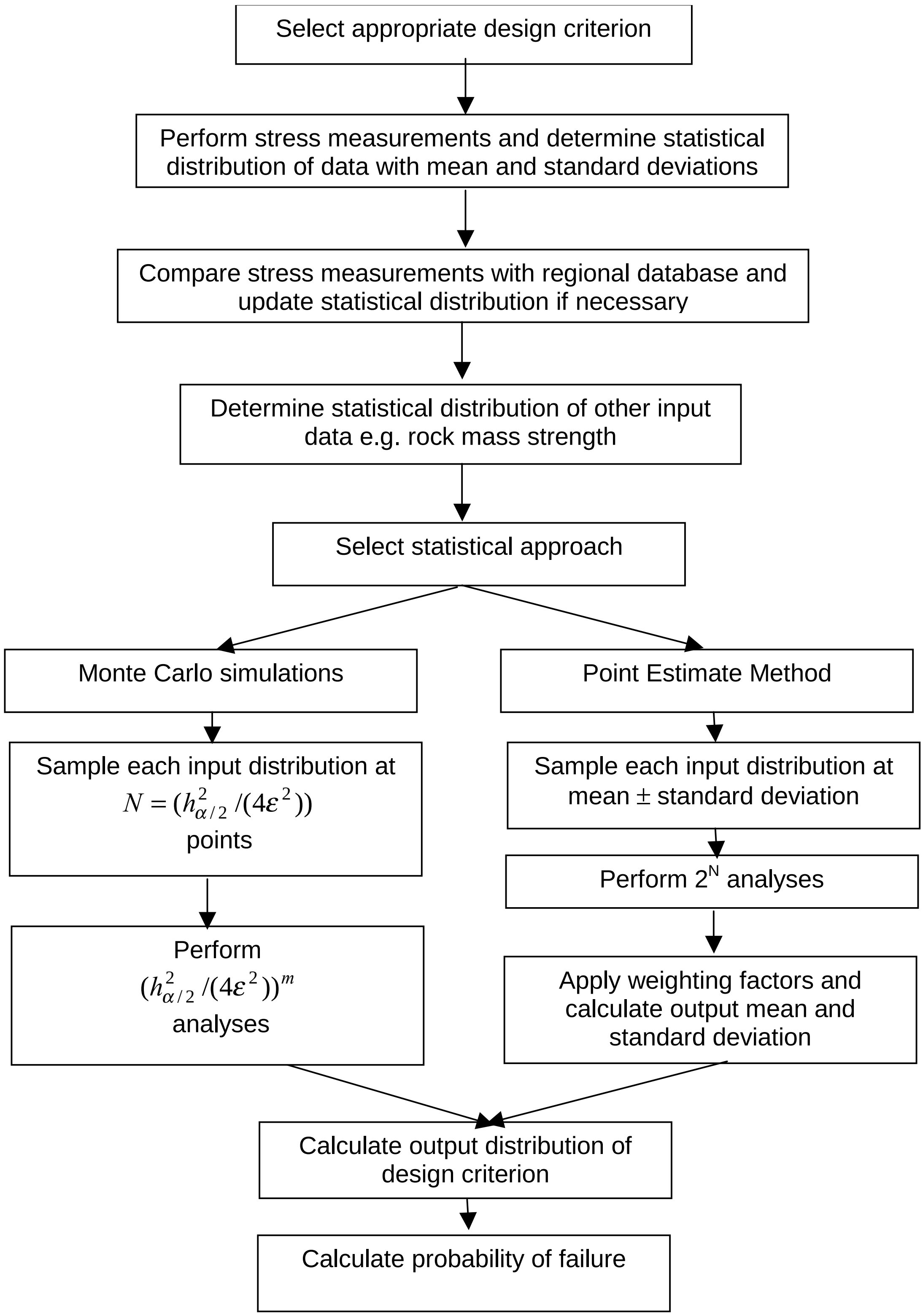

Figure 7.1.2 Flowchart of methodology for risk based design methodology incorporating variability of the stress state

8 CONCLUSIONS

The primitive stress state is an important input into the design of underground excavations. However, it is well known that the stress state varies considerably from place to place. The aim of this project was to determine the main causes of the variability to be able to understand how to consider the stress state in the context of designing safer mine excavations.

Furthering the *understanding* is addressed in the first section of the report in a review of the literature on the stress state in South Africa and its application in mine design. The section emphasized the importance of considering the correct magnitude and directions of the *in situ* stress state in the design of mine excavations. Descriptive summaries of the stress state in the gold and platinum mines were also provided. A literature survey of the causes of the initial stress state and the effects that various geological structures have on the distribution of stresses is also presented.

In the review, theoretical studies were compared with published observations and measurements. The review showed that the tectonic history is the main influence on the primitive stress state. A number of figures are presented to illustrate the effect of typical geological structures. The vertical component of the stress state is induced by the weight of the overburden, but the horizontal stress state is not well constrained and depends on the geological setting. Folds and surface topography cause rotations of the stress state. Faulting causes the major stress state to rotate towards being parallel to the fault surface. The final stress state depends on whether the tectonic loading causes normal, reverse or thrust faulting. Dykes can act like faults if the contact is sheared, but may also contain residual stresses that are significantly different to the surrounding stresses. Thus, the stress state varies continuously and a single measurement cannot be considered to be representative of the complete primitive stress state within a mine or mining region.

The problem of *quantifying* the variability was addressed by firstly re-evaluating the stress measurement database to determine statistical trends and variation between the major mining regions. Methods are presented for the correct determination of the average and standard deviation of a number of stress tensors. The data provided in SIMRAC project GAP 511 was analysed and indicated considerable variability in the major and minor k-ratios and the horizontal stress directions. The values of the standard deviation tend to be relatively low within each of the separate regions, but large for the whole country, highlighting how the different tectonic environment in each region constrains the average primitive stresses. Thus, on average the stress measurements taken within a mining region are relatively consistent. The stress state associated with the Bushveld Complex is more difficult to average as the stresses are aligned relative to the curve of the outcrop. In this case, the averages must be determined over a smaller region where the outcrop direction is more or less constant.

Secondly, improvements were made to the SIMRAC three-borehole technique. The use of percussion drilling in the original design for the three-borehole method meant that the drilling could be performed economically by non-specialised drill crews with standard equipment. However, the measurement accuracy required for the stresses in hard rock implied that damage to the rock surrounding the borehole led to overestimates of the deformation. It was decided to prove the technique using diamond drilling. A new measuring device was required that could measure more diameters and so provide redundant readings for the least squares estimate of the stress state. Three different measuring techniques were tested and the final method uses a set of 16 linear voltage differential transducers to obtain eight diametric regions. Underground testing proved that the drilling technique was practical as long as the drill was set up accurately. Testing was undertaken at sites on Western Platinum Mine, Impala Platinum Mine and Tau Tona Mine. Some problems remain when the ground is considerably faulted as the locator may alter alignment. The current design can be difficult to retract and hence slows down the drilling process. The measuring device was shown to be able to measure the borehole deformation to micron accuracy in underground tests. The measurements that appeared to be successful indicated that some of the borehole deformations were in the correct order of magnitude, but that errors due to the locator hitting the measuring device were significantly large. It was impossible to select sufficient appropriate deformation measurements. Unfortunately, the testing of the measurement technique had already been considerably delayed by difficulties with the underground sites and further measurements could not be obtained within the remaining project duration.

A statistical method was used to determine the stress state using combinations of the eight borehole diameters and to identify outliers due to sensors resting on flakes or pebbles in the borehole. Even with the ability to determine the erroneous readings, the three-hole method was found to be highly sensitive to such variations in the borehole diameter. The method is not very sensitive to changes in the stress component aligned parallel to the line connecting the centres of the three holes. The method will not be economic in lower stress regions where the CSIR and CSIRO strain cells operate well and only require a single hole for a full three dimensional stress tensor. The benefit of the method would be that only the measuring device needs to be purchased and can be used many times, whereas the strain cells are discarded after use. The three borehole technique as developed does appear to be a step towards a device that is able to make stress measurements in highly stressed ground where strain cells cannot be used due to discing of the overcore. More testing is needed and some modifications to the locator may be required. Other hole configurations methods must be considered as drilling the third hole in a straight line has a very small effect on the first hole and so minute deformations must be measured. A method can be envisaged in which the locator design is altered to permit the measurements to be made with only two holes. This would significantly reduce the amount of drilling required and increase the magnitude of the deformations being measured. In all tests, it was drilling of the third hole that caused problems. The third hole requires considerable accuracy of alignments and errors build up with increasing number of holes. The project has made significant advances towards the ultimate goal of developing an indirect measurement technique that can determine the stress field over a wide area easily and economically, but the current approach would need further development.

The stress measurement database is focused on the virgin stress conditions away from the disturbance by geological features and very few local measurements are available to determine the effect of geological structures on the stress state. Stress measurements were undertaken at two sites where the effect of a dyke and a fault could be measured directly. The stress state surrounding the Modderlaag thrust fault on the Western Platinum Mine was measured using CSIR strain cells from six boreholes varying in distance up to 50 m from the fault intersections. The stress state appears to be most affected by the subsequent tectonic activity and the major principal stresses are aligned in an East-West direction, sub-parallel to the outcrop of the Bushveld Complex, and perpendicular to the approximately North- South trending dyke sets. Numerous attempts were made to measure the stresses in and near the Speckled Dyke on Tau Tona mine. The measurements were hampered by the faulted nature of the dyke and the presence of quartz veins at many different angles. The single reliable stress measurement indicated that the principal stress was oriented at an angle to the dyke, consistent with the activation of the dyke contact as a normal fault. The three-borehole drilling technique was successfully tested at the site, but no stress measurements could be made within the project duration due to delays in drilling.

Finally, *dealing* with the variable stress distribution is the most important task from the point of view of the rock engineer. This requires the incorporation of statistical distributions into standard design procedures. In the final section, a literature investigation was performed to determine the optimum number of measurements for a reliable stress measurement. It would appear that ten measurements are required in a single borehole to be able to statistically prove that the mean value is representative. This number of measurements is common overseas, but would be uneconomical in mining conditions. Three measurements should therefore be used at each point. Thirty to fifty average stress tensors would be required to determine a stress field. However, analysis of the stress database suggests that the stress state does have a representative mean value within a similar tectonic environment or geotechnical region. Thus, the number of measurements required to determine an average stress state would depend on the geological variability of the mine and where a mine is located in relation to the Bushveld Complex or Witwatersrand basin, the presence of large structural events such as thrust blocks, the Pilanesburg, and the relationship to dykes and faults.

The basis of a design methodology is presented that permits the formal application of variable *in situ* stress conditions in rock engineering designs within the context of risk based design procedures. The methodology describes the point estimate method for selecting the appropriate combinations of values of the stress state for input into analytical design formulas or numerical modelling exercises to determine the probability distribution of the failure criterion as a function of the variable stress state. A simple example is given to illustrate the technique. The application of probabilistic design methods is becoming more popular, but consideration still needs to be given to selection of the appropriate confidence levels and to determine what level of risk is acceptable.

References

Adams, D. J. 1995. Develop criteria for designing mining layouts at depth so as to reduce seismicity and enhance worker safety. *SIMRAC final project report GAP 034.*

Adams, D.J. and Geyser, D., 1999. Preconditioning of 43 hangingwall haulage at Kloof no 4 shaft. *SARES 99*. (ed. Hagan, T.O.) SAIMM.

Almen, J.O. and Black, P.H., 1963. *Residual stresses and fatigue in metals,* McGraw Hill.

Amadei, B. and Pan, E., 1992. Gravitational stresses in anisotropic rock masses with inclined strata. *Int. J. Rock. Mechanics Min. Science. & Geomech*. Abstr. vol 29 No 3, 225-236.

Amadei, B., 1984. In-situ stress measurements in anisotropic rock. *Int. J. Rock. Mechanics Min. Science and Geomech*. Abstr. vol 21 No 6, 327-338.

Amadei, B., Swolfs, H.S., and Savage, W., 1988. Gravity-induced stresses in stratified rock masses. *Rock Mechanics and Rock engineering,* vol 21, 1-20.

Brace, W.F. and Kohlstedt, D.L., 1980. Limits on lithospheric stress imposed by laboratory experiments. *J. Geophys*. Res. vol 85, 6248-6252.

Brady, B.H.G. and Brown, E.T., 1993. Rock Mechanics for underground mining. *2. ed Chapman and Hall London.*

Briggs, D.J., 1982. Mechanical properties of quartzites and associated rock types, *COMRO Report No. 13/83.*

Brown, E.H. and Hoek, E., 1978. Trends in relationships between measured in-situ stresses and depth. *Int. J. Rock. Mechanics Min. Sci. Geomech Abstr. 15,* 211-215

Brown, E.T., Leijon, B.A., and Hustrulid, W.A., 1986. Stress distribution within an artificially loaded block Pro*c. Int symp on rock stress and rock stress measurement*, Stockholm Centek, Lulea (ed. O. Stephansson), 429-440.

Burov, E. and Poliakov, A. 2001. Erosion and rheology controls and synrift and postrift evolution: Veryfing old and new ideas using a fully coupled numerical model. *J. Geophys. Res.* 106. B8. 16461-16481.

Carlsson, A. and Christiansson, R., 1986. Rock stresses and geological structures in the Forsmark area *Proc. Int symp on rock stress and rock stress measurement,* Stockholm Centek, Lulea (ed. O. Stephansson), 457-466.

Coetzer, S. J., 1986. Report on the measurement of rock stresses at Durban Deep gold mine. Report GIS 1154. *Geophysical Instrumentation Pty Ltd*.

Cook, N.G.W. 1976. Methods of acquiring and utilizing geotechnical data for the design and construction of workings in rock. *Proc. Symp. Exploration for Rock Eng.* Johannesburg. 1-13.

Cornet, F.H., 1993. Stresses in rock and rock masses, *Comprehensive rock engineering* vol 3, Pergamon, 297-324.

Crouch, S.L. and Starfield, A.M., 1983. *Boundary element methods in solid mechanics,* George Allen, London

Day, A.P. and Godden, S.J. 2000. The design of panel pillars on Lonmin's platinum mines. *SANIRE Symposium 2000*. SANIRE.

De Marr, and Holder., 1994. An overview of rock engineering problems Rustenburg Platinum mines Limited (Rustenburg Section). *Xvth CMMI Conf. Johannesburg. SAIMM*. 1, 149-157.

Dede,T. and Handley,M.F., 1997. Bracket pillar design charts. *SIMRAC interim project report*. Project No. GAP 223.

Delaney, P.T., Pollard, D.D., Ziony, J.I., and Mckee, E.H., 1986. Field relations between dikes and joints: Emplacement processes and paleaostress analysis. *J. Geophys.* Res. vol 91, 4920-4938.

Durrheim, R.,J., Roberts, M.C.K., Haile, A.T., Hagan, T.O., Jager, A.J. Handley, M.F., Spottiswoode, S.M., and Ortlepp, W.D. 1998. Factors influencing the severity of rockburst damage in South African gold Mines. *J. SAIMM*. 53-57.

Dyke, C.G., Hyett, A.J. and Hudson, J.A. 1988. A preliminary assessment of correct reduction of field measurement data: scalars, vectors and tensors. *2nd Int Symp. Field measurements in Geomechanics.* (Sakurai (ed). Balkema. Rotterdam.

Dyskin, A.V., Germanovich, L.N., Jewell, R.J., Joer, H., Krasinski, J.S., Lee, K.K., Roegiers, J.C., Sahouryeh, E., and Ustinov, K.B., 1995. Some experimental results on three-dimensional crack propagation in compression. *Mechanics of Jointed and Faulted Rock*, Rossmanith (ed.) Vienna, Austria, pp. 91-96.

Farquhar, J., 1986. The western Platinum Mine. *Mineral Deposits of South Africa* (Anhausser and Maske, eds.) Geology. Soc. South Africa. Johannesburg.

Gale, W.J., 1986. The application of stress measurements to the optimisation of coal mine roadway drivage in the Illawarra coal measures. *Proc. Int. Symp. rock stress and stress measurements.* (Stephansson O. ed.). Centek. Lulea. 551-560.

Gay N., 1975. In-situ stress measurements in South Africa, *Tectonophysics* 447-459.

Gay, N. and Jager, A.J., 1986. The influence of geological features on problems of rock mechanics in Witwatersrand mines. *Mineral Deposits of South Africa* (Anhaeusser, Maske eds.) *Geol. Soc. South. Africa.* 753-772.

Gay, N., (1986). Mining in the vicinity of geological structures - an evaluation of the problem, *Mining in the vicinity of geological and hazardous structures,* SAIMM, 1-32.

Gay, N.C. and van der Heever, P.K., 1980. *In situ* stress measurements in the Klerksdorp district, *COMRO IR-74.*

Gay, N.C., 1979. The state of stress in a large Dyke on E.R.P.M., Boksburg, South Africa*. Int. J. Rock. Mechanics. Min. Science. Geomech Abstr.16, 179-185.*

Gay, N.C., 1980. The state of stress in the plates. Dynamics of plate interiors, *Geodynamics series, Vol 1, American Geophysical Union*.

Gay, N.C., Spencer, D., van Wyk, J.J., and van der Heever, P.K., 1984. The control of geological and mining parameters in the Klerksdorp gold mining district. *Proc. 1st Int. Congress on Rockbursts and Seismicity in Mines*, Johannesburg, SAIMM, 107-120.

Gray, W.M and Toews, N.A. 1973. Analysis of variance applied to data obtained by means of a six-element borehole deformation gauge fro stress measurements. *Proc 15th US Rock Mech. Symp.* Rapid city. 323-356.

Guangyu, L., Shiwei, B., and Jiguang, L., 1986. Twenty years of experience on in-situ measurements in China. Proc. Int. Symp. *Rock stress and stress measurements.* (Stephansson O. ed.). Centek. Lulea. 79-88.

Haile A.T. and Jager, A.J. 1995. Rock Mass condition, behaviour and seismicity in mines of the bushveld igneous complex. *SIMRAC project report.* Project GAP 027. SIMRAC.

Haile,A., Wojno, L., and Jager, A.J. 1995. Strata control in tunnels and an evaluation of support units and systems currently used with a view to improving the effectiveness of support, stability and safety of tunnels*. SIMRAC Final Report Project GAP 026.*

Handley, M.F. 1987. A study of the effect of mining induced stresses on a fault ahead of an advancing longwall face in a deep level gold mine. *MSc Thesis. University of the Witwatersrand.*

Handy, M., 1989. Deformation regimes and the rheological evolution of fault zones in the lithosphere: the effects of pressure, temperature, grain size and temperature. *Tectonophysics, 163*, 119-152.

Hansen, K. and Mount, V. S. 1990. Smoothing and extrapolation of crustal stress orientation measurements. *J. Geophys. Res.* 95. B2. 1155-1165.

Harr, M. 1977 The mechanics of particulate media – a probabilistic approach. McGraw Hill.

Harr, M.E. 1987. *Reliability based design in civil engineering*. McGraw-Hill. 290pp.

Haxby, W.F. and Turcotte, D.L., 1976. Stresses induced by the addition or removal of overburden and associated thermal effects. *Geology.* 181.

Hemp,D. 1994. The classification of dykes and faults on South African Gold Mines. *SIMRAC interim Report*. Project GAP 034. SIMRAC.

Herget, G., 1986. Changes of ground stress with depth in the Canadian shield. *In Proc. Int symp on rock stress and rock stress measurement,* Stockholm Centek, Lulea (ed. O . Stephansson) 61-68.

Hobbs, B.E., Winthrop, D.M., Williams, P.F., 1976. *An outline of structural geology*. Wiley International.

Hyett, A.J., Dyke, C. G., and Hudson, J.A., 1986. A critical examination of basic concepts associated with the existence and measurements of *in situ* stress. *Proc. Int. Symp. Rock stress and stress measurements.* (Stephansson O. ed.). Centek. Lulea. 387-398.

Jaeger, J.C. and Cook, N.G.W., 1979. *Fundamantals of rock mechanics.* Chapman and Hall, London.

Jager, A.J. and Ryder, J.A. 1999. *A handbook on rock engineering*. SIMRAC. Johannesburg.

Jeffery, G.D., 1975. Structural discontinuities in the Witwatersrand group on the E.R.P.M. mine. *MSc thesis*, University of the Witwatersrand.

Joughin, W.C., Swart A.H. and Wesselloo, J. 2000. Risk based chromitite pillar design. *SANIRE Symposium 2000*. SANIRE.

Kirsten, H.A.D., 1976. Selected Aspects of rock stress measurements in South Africa. *Proc. Symp. Exploration in Rock Engineering.* Johannesburg. Balkema. 55-65.

Lan L. and Huddleston P.J. 1992. Finite-element models of buckle folds in non-linear materials*. Tectonophysics*, 199,1-12.

Lan, L. and Wang, R., 1987. Finite-element analysis of an overturned fold using viscous-fluid model. *Tectonophysics*, 139, 309-314.

Lang, P.A., Thompson, P.M., and Ng, L.K.W., 1986. The effect of residual stress and drill hole size on the insitu stress determined by overcoring. *Proc. Int. Symp. Rock stress and stress measurements.* (Stephansson O. ed.). Centek. Lulea. 687- 692.

Langwieder, G. 2001. Geological history of Western Platinum Mine. *Western Platinum Mine internal report.*

Leary, P.C., 1985. Near-surface stress and displacement in a layered elastic crust. *J. Geophys Res.* 1901-1910.

Leeman, E.R., 1964a. The measurement of stress in rock; Parts I and II, *J.SAIMM*, Vol 65, 45-114.

Leeman, E.R., 1964b. The measurement of stress in rock; Part III, *J.SAIMM*. vol 65, 254-284.

Leijon, B.A., 1986. Application of the LUT triaxial overcoring technique in Swedish mines. *Proc. Int. Symp*. Rock stress and stress measurements. (Stephansson O. ed.). Centek. Lulea. 569-582.

Leijon, B.A. 1989. Relevance of pointwize rock stress data-an analysis of overcoring data.

Lilly, P. 2000. Probability and risk in Geomechanics. *Course notes* Snowden Mining Industry Consultants.

Lilly, P. and Li, J., 2000. Estimating excavation reliability from displacement modelling. *Int. J. Rock. Mech. Min Sci*. 37. 1261-1265.

Malan D.F. 1998. An investigation into the identification and modelling of time-dependant behaviour of deep level excavations in hard rock. *PhD thesis, University of the Witwatersrand,* Johannesburg.

Malan D.F. and Basson, E.R.P. 1998. Ultra-deep mining: the increased potential for squeezing conditions. *J. SAIMM*. 353-363.

Mandl, G., 1988. Mechanics of tectonic faulting: *Models and basic concepts. Elsevier*, Amsterdam.

Martin, C.D. and Chandler, N.A., 1993. Stress heterogeneity and geological structures, Int. J. Rock. Mechanics. *Min. Sci & Geomech*. Abstr. vol 30, 993-999.

Martin, C.D. and Maybee, W.G., 2000. The strength of hard rock pillars. *Int. J. Rock Mech. Min. Sci.* 37. 1239-1246.

Martna, J. and Hanssen, L., 1986. High horizontal stresses around the vites headrace tunnels no.2 and 3, Sweden. *Proc. Int. Symp. Rock stress and stress measurements.* (Stephansson O. ed.). Centek. Lulea. 605-614.

McCarthy, T.S., Charlesworth, E.G., and Stanistreet, I.G., 1989. Post-transvaal structural features of the northern portion of the Witwatersrand basin, Trans. *Geol. Soc. South Africa*. vol 89, 311-323.

McCarthy, T.S., McCullum, Myers, R.E., and Linton, P., 1990. Stress states along the northern margin of the Witwatersrand basin during Klipsriviersberg volcanism, Trans. *Geol. Soc. South Africa.* vol 89, 311-323.

McCrutchen, W.R., 1982. Some elements of a theory for in-situ stress. *Int J. Rock Mechanics. Min Sci & Geomech*. Abstr. vol 19, 201-203.

McGarr, A. and Gay, N.C., 1978. State of stress in the earth's crust. Ann, Rev. *Earth Planet Science.* vol 6, 405-436.

Mills, K.W., Pender, M.J., and Depledge, D., 1986. Measurement of insitu stress in coal. *Proc. Int. Symp. Rock stress and stress measurements.* (Stephansson O. ed.). Centek. Lulea. 543-550.

More O'Ferrall, R., 1986. Procedure for mining in the vicinity of faults and dykes in the Klerksdorp area. *Mining in the vicinity of geological and hazardous structures.* SAIMM.

Mühlhaus, H.B., Hobbs, B.E., and Ord, A., 1994. The role of axial constraints on theevolution of folds in single layers, *Computer methods and advances in geomechanics*, Siriwardane, and Zaman (eds) Balkema, Rotterdam, 223-231.

Mullar and Pollard 1986

Muller, O.H. and Pollard, D.D., 1977. The stress state near Spanish Peaks, Colorado determined from a dike pattern. *Pure and Applied Geophys*. vol 115, 69-86.

Murphy S. 2000. Personal communication.

Ortlepp, W.D., 1997. Rock fracture and rock bursts. SAIMM.

Ortlepp, W.D., Spencer, D., and Faure, M., 1986. Problems associated with major geological structures in the Orange Free State, *Mining in the vicinity of geological and hazardous structures*. SAIMM.

Papanasatiou., 2000. Formation stability after hydraulic fracturing. Int. J. um. *Meth. Analyt. Meth. Geomech. 23*, 1927-1944.

Peacock, D.C.P. and Marrett. R., 2000 Strain and stress: Reply. *J. Struct Geol*. 1369-1378.

Pollard, D.D. and Segal, P., 1987. Theoretical displacements and stresses near fractures in rock, in Fracture mechanics of rock, Atkinson, K.K. (ed), *Academic Press*, London, 277-347.

Potgieter, C.J. and Roering, C., 1984. The influence of geology on the mechanisms of mining-associated seismicity in the Klerksdorp gold-field. *Proc. 1st Int. Congress on Rockbursts and Seismicity in Mines*, Johannesburg, SAIMM. 45-50.

Price, N.J., 1966. Fault and Joint developments in brittle and semi-brittle rock. *Pergammon,* London

Rapson., 1970. Virgin rock stresses. *Chamber of mines information circular*, 28/70.

Richardson, A.M., Brown, S.M., Hustrulid, W.A., and Richardson, D.L., 1986. An interpretation of highly scattered stress measurements in foliated Gneiss. Proc. *Int symp on rock stress and rock stress measurement*, Stockholm Centek, Lulea (ed. O. Stephansson), 441-447.

Roberts, D.P., Sellers, E.J., and Sevume, C., 1999. Numerical modelling of fracture zone development and support interaction for a deep level tunnel in a stratified rockmass. *SARES 99*. SANIRE. Johannesburg.

Rummel, F., 1986. Stresses and tectonics of the upper continental crust - a review. Proc. *Int symp on rock stress and rock stress measurement,* Stockholm Centek, Lulea (ed. O. Stephansson), 177-186.

Ryder, J.A., 1988. Excess shear stress in the assessment of geologically hazardous situations, *J. South African. Inst. Min. Metall*., vol 88, 27-39.

Savage, W., Amadei, B., and. Swolfs, H.S., 1986. Influence of rock fabric on gravity-induced stresses. *Proc. Int symp on rock stress and rock stress measurement,* Stockholm Centek, Lulea (ed. O. Stephansson), 99-110.

Schwietzer J.K.and Berlenbach, J. 1995. Geological controls on rockmass behaviour associated with platinum and chromitite excavations, Rustenberg Layered Suite, Bushveld Igneous Complex pilot study. CSIR Miningtek Report No 97-0101.

Schweitzer J.K. and Johnson, R. 1987. Geotechnical classification of deep and ultra deep Witwatersrand mining areas, South Africa*. Mineralium Deposita*. 32. 335-348.

Seiki, T., Aydan, O., and Kawamota, T., .The relationship between geological features and the state of stress of the earth's crust in central Japan. *Rock Stress*. (Sugawara & Obara eds) Balkema. Rotterdam, 385-390.

Sellers, E., 1995. Modelling of the influence of geology on the in-situ stress state, *SIMRAC Interim Project report, GAP029*, CSIR Division of mining technology.

Sellers, E.J., Berlenbach, J., Schweitzer, J., 1998. Fracturing around deep level stopes: Comparison of numerical simulation with underground observations. *Mechanics of Jointed and Faulted Rock 3,* Rossmanith (ed), Balkema, Rotterdam.

Szakmeister, R. 1998. Fault and Dyke Database. *CSIR Miningtek Internal report.*

Smallbone, P.R., James, J.V., and Isaac, A.K., 1993. In-situ stress measurements and use in the design of a deep gold mine. *Innovative Mine design for the 21st century*, Bawden and Archibald (eds) Balkema, Rotterdam, 653-658.

Stacey, R. and Wesselloo, J., 1998. Evaluation and upgrading of stress measurement data. *SIMRAC Report for Project GAP 511.*

Stacey, T.R. , 1998. Reliable, practical technique for in-situ rock stress measurements in deep gold mines. SIMRAC project Report, GAP 314.

Stacey, T.R. and Wesseloo, J. 1998. *In situ* stresses in mining areas in South Africa. *J. SAIMM.* 365-369.

Sugawara, K., 1977. Measuring rock stress and rock engineering in Japan. *Rock Stress.* (Sugawara & Obara eds) Balkema. Rotterdam, 15-25.

Su, S. Stephansson, O. 1999. Effect of a fault on *in situ* stresses studied by the distinct element method. *Int. J. Rock. Mech. Min. Sci.* 38. 1051-1056.

Tankard, A.J., 1982. Crustal evolution of Southern Africa; 3*.8 Billion years of earth history.* Springer-Verlag, New York.

Truswell, J.F., 1970. An introduction to the historical geology of South Africa. *Purnell,* London.

Tucker, H., 1968. The thermal conductivity. *J. of Mine Vent. Soc. of South Africa,* 79-82.

Vermaak, C.F. and Von Gruenewalt, G., 1986. Introduction to the bushveld complex. *Mineral Deposits of South Africa (Anhausser and Maske, eds.) Geol. Soc. South Africa.* Johannesburg.

Vreede, F.A., 1981. Critical study of the method of calculating virgin rock stresses from measurement results of the csir triaxial strain cell. *CSIR Report Me1679* Pretoria

Vreede, F.A., 1982. Interpretation of virgin stress measurements with regard to large caverns. *ISRM symposium*. Aachen. 1121-1126.

Warren, W.E. and Smith, C.W., 1985. Insitu stress estimates form hydraulic fracturing and direct observation of crack orientation. *J. Geophys.* Res. vol 90 6829-6839.

Weertman, J., 1980. The stopping of a rising liquid-filled crack in the Earth's crust by a freely slipping horizontal joint, *J. Geophys. Res*., vol 85, 967-976.

Weertman, J., 1980. The stopping of a rising, liquid filled crack in the earth's crust by a freely slipping horizontal joint. *J. Geophys*. Res. vol 85, 967-976.

Weijermars, R., 1992. Progressive deformation in anisotropic rocks. *J. Struct Geol.* 723-742.

Wiles,T.D. and Kaiser, P. K. 1990. A new approach for statistical treatment of stress tensors. *CANMET symp: stresses in underground structures*. Ottawa. 62-76.

Witlox, H.W.M., 1986. Finite element simulation of basal extension faulting within a sedimentary overburden. *Numerical methods in geomechanics* - European conference, Stuttgart. vol 2, 765.

Yin, Z-M. and Rogers, G.C., 1995. Rotation of the principal stress directions due to earthquake faulting and its seismological implications. *Bull. Seis. Soc. America.* 85. 1513-1517.

York, G., Canbulat, I., Kabaeya, K., Le Bron, k., Watson, B.P., Williams, S.B. 1998. Develop guidelines for the design of pillar systems. *SIMRAC final report GAP 334.*

Appendix A

Rock test results